The cross-regulation of autophagy and necroptosis

Inaugural dissertation

for the attainment of the title of doctor
in the Faculty of Mathematics and Natural Sciences
at the Heinrich Heine University Düsseldorf

presented by

Wenxian Wu
from Henan, China

Düsseldorf, July 2019

from the institute for Molecular Medicine I
at the Heinrich Heine University Düsseldorf

Published by permission of the
Faculty of Mathematics and Natural Sciences at
Heinrich Heine University Düsseldorf

Supervisor: Prof. Dr. Björn Stork
Co-supervisor: Prof. Dr. Peter Proksch

Date of the oral examination: 16.09.2019

Table of Contents

Acknowledgement

First of all, but most importantly I would like to take this opportunity to express my sincere appreciation to my supervisor Prof. Dr. Björn Stork who gave me the precious opportunity to study in Germany. He is a very motivated, considerate and knowledgeable mentor who always gives me some constructive suggestions in my study, and meanwhile he is like a big brother who also provides huge help for my family that I will keep in my mind forever. What I can learn and experience here is inexhaustible wealth in my whole life.

I would like to thank Prof. Dr. Sebastian Wesselborg who supports me to study in Institut für Molekulare Medizin I of Heinrich-Heine Universität. Also thank him for his powerful drill that makes me have a beautiful kitchen.

I also thank my second advisor Prof. Dr. Peter Proksch for his support for my PhD study and carefully reading and evaluating my thesis.

Thank Prof. Dr. Du Feng for giving me support and encouragement to study in Germany.

Thank Prof. Dr. JiaHuai Han for kindly providing plasmids and cell lines, and thank Prof. Dr. Sudan He for kindly providing plasmids.

Especially, thank Dr. Niklas Berleth and Jana Deitersen for carefully reading my PhD dissertation and considerately taking care in my study and life.

Thank all of the members of our lab (current and previous) who make me have a colorful life in Germany: David Schlütermann; Fabian Stuhldreier; Philip Böhler; Jan Cox; Sabine Seggewiß; Yadong Sun; Selina Dangeleit; Dr. Christoph Peter; Dr. Nora Wallot-Hieke; Dr. Antje Löffler; Dr. Stefan Drießen; Dr. Maria Jose Mendiburo; Dr. Katharina Schmitz; Dr. Gudrun Totzke.

Thank my chinese friends in Düsseldorf for your accompanying and supporting.

At last, I would like to thank my family: my parents, my wife and my son for your understanding and great supporting that makes me become motivated. I love you forever!

Abbreviation

ACACA/ACC	Acetyl-CoA carboxylase alpha
ACD	Accidental cell death
AMP	Adenosine monophosphate
AMPK	AMP-activated protein kinase
Apaf-1	Apoptotic protease activating factor-1
ATG	Autophagy-related
ATP	Adenosine triphosphate
Baf A_1	Bafilomycin A_1
Bcl-2	B cell lymphoma 2
BECN1	Beclin 1
BH-3	Bcl-2 homology 3
BR	Brace region
CaMKK2	Ca^{2+}/calmodulin dependent protein kinase kinase 2
c-FLIP	Cellular FADD-like interleukin 1β-converting enzyme-inhibitory protein
cIAP	Cellular inhibitor of apoptosis protein
CMA	Chaperon-mediated autophagy
CYLD	Cylindromatosis
DAI	DNA-dependent activator of IFN-regulatory factors
DD	Death domain
DED	Death effector domain
DFCP1	Double FYVE domain-containing protein 1
DISC	Death-inducing signaling complex
DR	Death receptor
DUBs	Deubiquitinases
EBSS	Earle's Balanced Salt Solution
ER	Endoplasmic reticulum
ESCRT	Endosomal sorting complexes required for transport
FADD	Fas-Associated Death Domain Protein
FasL	Fas ligand

FIP200	Focal adhesion kinase (FAK) family interacting protein of 200 kD
G	GSK872
GFP	Green fluorescent protein
4HBD	Four helical bundle domain
HMGB1	High-mobility group box 1
HSC70	Heat shock-cognate chaperone of 70 kDa
ID	Intermediate domain
IFN	Interferon
LIR	LC3-interacting region
IκB	Inhibitor of NF-κB
IKK	IκB kinase
LKB1	Liver Kinase B1
LPS	Lipopolysaccharide
LUBAC	Linear ubiquitin chain assembly complex
(MAP1)LC3	Microtubule-associated protein 1 light chain 3
MAPK	Mitogen-activated protein kinase
MCMV	Murine cytomegalovirus
MEF	Mouse embryonic fibroblast
MK2	MAPK-activated protein kinase 2
MLKL	Mixed lineage kinase domain-like
MOMP	Mitochondrial outer membrane permeabilization
MTOR	Mechanistic target of rapamycin
NAP1	Nucleosome assembly protein 1
NCCD	Nomenclature Committee on Cell Death
NEMO	NF-κB essential modulator
NF-κB	Nuclear factor κ light-chain enhancer of activated B cells
OTULIN	OTU deubiquitinase with linear linkage specificity
PINK1	PTEN-induced putative kinase protein 1
RPTOR	Regulatory associated protein of MTOR complex 1
PCD	Programmed cell death
PE	Phosphatidylethanolamine

PIK3C3	Phosphatidylinositol 3-kinase catalytic subunit type 3
PIK3R4	Phosphoinositide 3-kinase regulatory subunit 4
PIPs	Phosphatidylinositol phosphates
PLA	Proximity ligation assay
poly(I:C)	Polyinosinic:polycytidylic acid
PRRs	Pattern-recognition receptors
PtdIns	Phosphatidylinositol
PtdIns3K	Phosphoinositide 3-kinase
PtdIns3P	Phosphatidylinositol 3-Phosphate
Q	Q-VD-OPh
Q-VD-OPh	Quinolyl-Val-Asp-OPh
RCD	Regulated cell death
RHIM	C-terminal RIP homotypic interaction motif
RIPK1/3	Receptor-interacting protein 1/3
RPTOR	Regulatory associated protein of MTOR complex 1
S	Smac mimetics
Smac	Second mitochondria-derived activator of caspases
SNAP29	Synaptosomal-associated protein 29
SNARE	Soluble N-ethylmaleimide-sensitive factor attachment protein receptor
SPATA2	Spermatogenesis-associated protein 2
SQSTM1	Sequestosome-1
STK11	Serine/Threonine Kinase 11
STX17	Syntaxin 17
T	TNFα
TAB2/3	TAK1-binding proteins 2/3
TAK1	Transforming growth factor β-activated kinase 1
TANK	TRAF family member-associated NF-κB activator
tBid	Truncated Bid
TBK1	TANK-binding kinase 1
TIR	Toll/interleukin-1 receptor
TLR3/4	Toll-like receptor 3/4

TNFR1	TNF receptor 1
TNFR1-SC	TNFR1 signaling complex
TRADD	TNFR1-associated death domain (DD) protein
TRAF	Tumor necrosis factor receptor-associated factor
TRAIL	TNF-related apoptosis-inducing ligand
TRIF	TIR domain-containing adaptor-inducing interferon-β
TSC2	Tuberous sclerosis complex subunit 2
UBL	Ubiquitin-like
ULK1	Unc-51 like autophagy activating kinase 1
UV	Ultraviolet
UVRAG	UV radiation resistance associated gene
VAMP8	Vesicle-associated membrane protein 8
WIPIs	WD-repeat domain phosphoinositide-interacting proteins
Z	z-VAD-FMK
ZBD	Z-binding domain
ZBP1	Z-DNA binding protein 1
z-VAD-FMK	Carbobenzoxy-valyl-alanyl-aspartyl-[O-methyl]-fluoromethylketone

Amino acids

	single-letter	three-letter code
Alanine	A	Ala
Cysteine	C	Cys
Aspartic acid	D	Asp
Glutamic acid	E	Glu
Phenylalanine	F	Phe
Glycine	G	Gly
Histidine	H	His
Isoleucine	I	Ile
Lysine	K	Lys
Leucine	L	Leu
Methionine	M	Met
Asparagine	N	Asn
Proline	P	Pro
Glutamine	Q	Gln
Arginine	R	Arg
Serine	S	Ser
Threonine	T	Thr
Valine	V	Val
Tryptophan	W	Trp
Tyrosine	Y	Tyr

1. Summary

Autophagy, apoptosis and necroptosis are three well studied intracellular signaling pathways to modulate cell fate. Among them, apoptosis and necroptosis predominantly regulate cell death and extrinsic apoptosis shares the same upstream signal transduction with necroptosis. Apoptotic cell death is mediated by the activation of a family of cysteine proteases termed caspases. However, when the activity of caspase 8 is inhibited, apoptotic cell death can switch to necroptotic cell death that is controlled by the RIPK1-RIPK3-MLKL protein complex. Although under certain conditions autophagy can also cause cell death via degrading pro-survival proteins, in general autophagy represents a pro-survival pathway via degrading misfolded proteins, damaged organelles and invaded pathogens to maintain intracellular homeostasis. While the cross-regulation of apoptosis and autophagy is under investigation for many years, the crosstalk of necroptosis and autophagy is a new field and so far poorly understood due to limited research. Therefore, my thesis focused on the cross-regulation of necroptosis and autophagy to explore the underlying mechanisms, specifically on the two protein kinase complexes of RIPK1-RIPK3 and AMPK-ULK1 that represent the signaling nodes of necroptosis and autophagy, respectively.

In the first part of this thesis, it was shown that autophagy induced by amino acid starvation blocks necroptosis induction upon TNFα treatment in L929 cells. Since the Ser/Thr kinases ULK1 and RIPK1 represent the core of autophagy and necroptosis, respectively, and they are required for autophagy and necroptosis initiation, this part of my study focused on the ULK1-RIPK1 axis. The knockdown of ULK1 can enhance necroptotic cell death in L929 cells and necroptotic/apoptotic cell death in MEFs. Furthermore, ULK1 interacts with RIPK1 and restricts RIPK1 activity by direct phosphorylation at Ser 357. Moreover, ULK1-mediated phosphorylation of RIPK1 blocks the formation of complex II (RIPK1, FADD, caspase8 and/or RIPK3) and thereby cell death induced by TNFα.

In the second part of this thesis, it was demonstrated that necroptosis also cross-regulates autophagy in L929 cells. This cross-regulation is mediated by the AMPK-RIPK3 axis. In L929 cells, TNFα-induced necroptosis inhibited LC3-II degradation by lysosomes. Meanwhile, TNFα-induced necroptosis also promotes autophagy via activating early pro-autophagic proteins, e.g., the phosphorylation of ULK1 at Ser 555, Beclin1 at Ser 91 and AMPK at Thr 172/Thr 183, or the formation of ATG14 puncta. This work identified necroptosis-related RIPK3 as a new regulator of autophagy. RIPK3 interacts with AMPK and directly phosphorylates it at Thr 172/Thr 183 to control AMPK activity and hence regulate autophagy.

In summary, autophagy plays a pro-survival role in cell death mediated by TNFα since autophagy deficiency enhances TNFα-induced cell death. More importantly, this work provides new evidence for the cross-regulation between autophagy and necroptosis/apoptosis induced by TNFα and identifies mechanistic details, which might potentially provide novel therapeutic targets in the future. A scheme of the cross-regulatory mechanisms between autophagy and necroptosis/apoptosis identified in this thesis is shown in figure 1. Since my study mainly focuses on necroptosis and autophagy, a short introduction to these pathways is provided. In order to understand necroptosis, apoptosis will also be introduced briefly.

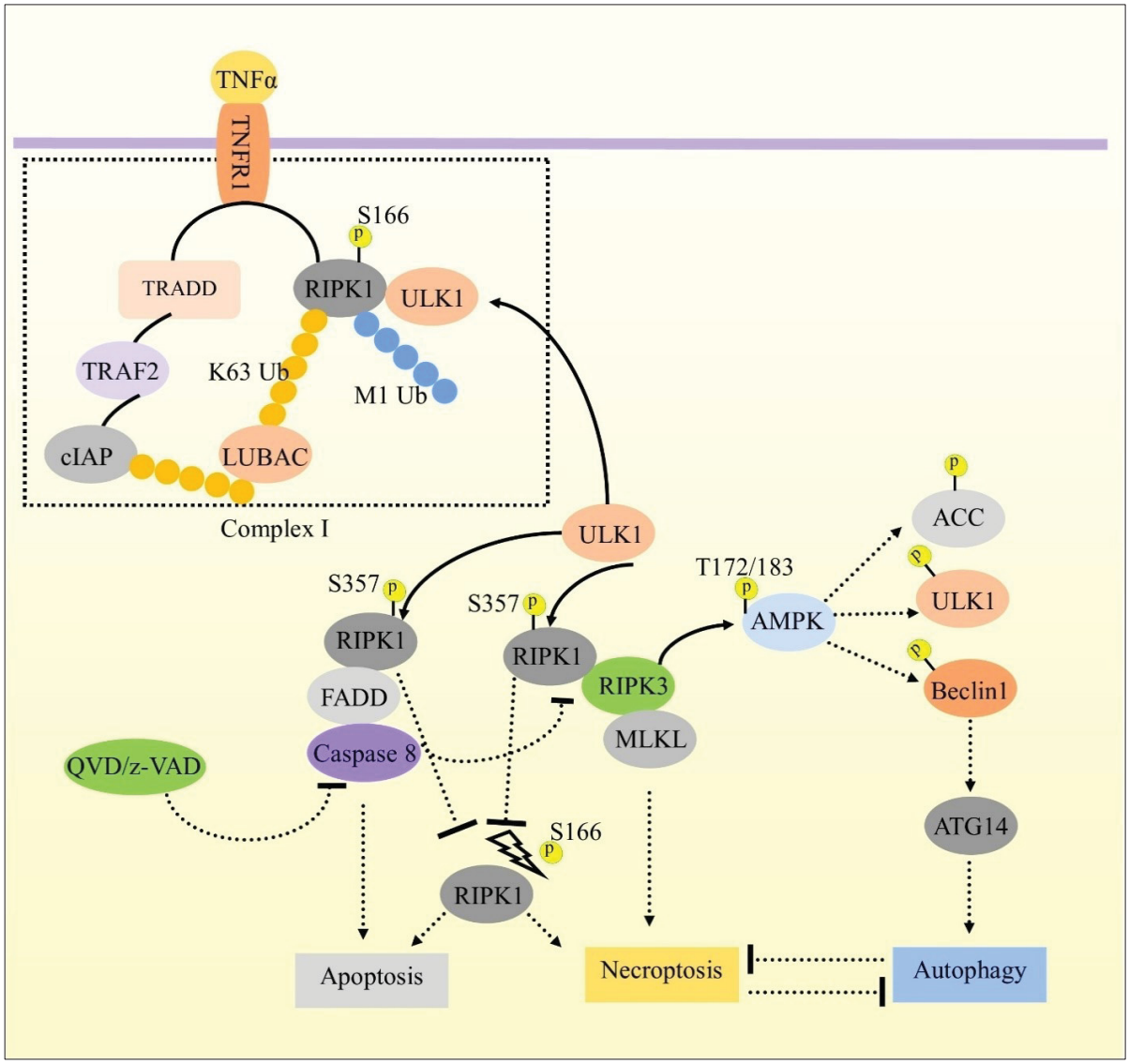

Figure 1. Summary of the cross-regulatory mechanisms of autophagy and necroptosis. Upon TNF stimulation, the autophagy-initiating kinase ULK1 phosphorylates the apoptosis/necroptosis-regulatory kinase RIPK1 at Ser 357 in the cytosol to inhibit RIPK1 activity and cytotoxic complex IIb/necrosome formation, thereby blocking apoptosis and necroptosis-mediated cell death. In turn, the pro-necroptotic protein RIPK3 can control AMPK activity via direct phosphorylation of AMPK at Thr 172/Thr 183 upon TNF stimulation to regulate autophagy.

2. Introduction

2.1 Regulated cell death

Cell death critically maintains developmental and immune homeostasis in multicellular organisms through removing damaged and infected cells. In human bodies, billions of cells undergo programmed cell death efficiently and silently each day and are replaced by new healthy cells to maintain the homeostasis and prevent diseases (Grootjans et al., 2017; Kolb et al., 2017). In 1973, three different types of cell death were classified into types I, II, and III by Schweichel and Merker depended on the morphology and structure of tissue and cells upon stimuli (Schweichel and Merker, 1973). The three different types of cell death correspond to apoptosis, autophagy and necrosis, respectively (Grootjans et al., 2017; Tang et al., 2019). Long time ago, necrosis was only considered as an unregulated type of cell death, however recent evidence has shown that necrotic cell death is indeed regulated under certain conditions, especially after the identification of the regulated necrosis inhibitor necrostatin-1 (Degterev et al., 2005). In the last two decades, cell death-related research is advanced and new classification methods have also been re-defined and re-interpreted by the Nomenclature Committee on Cell Death (NCCD). Nowadays, cell death can be basically classified into accidental cell death (ACD) and regulated cell death (RCD) (Galluzzi et al., 2015; Galluzzi et al., 2018; Galluzzi et al., 2012; Kroemer et al., 2005; Kroemer et al., 2009). Regulated cell death (RCD) is also known as programmed cell death (PCD) only under physiological conditions like shaping of organs during development etc. (Pasparakis and Vandenabeele, 2015; Tang et al., 2019). ACD can be triggered by severe physical attack (e.g., high pressures, high temperatures, or osmotic forces), chemical (e.g., extreme pH variations), or mechanical stress (e.g., shear forces), which occur beyond any regulated mechanisms (Galluzzi et al., 2018). In contrast, RCD involves a dedicated molecular machinery that can be modulated (Galluzzi et al., 2018). According to different molecular regulatory processes, RCD can be additionally divided into different subtypes: apoptosis, necroptosis, pyropotosis, ferroptosis, autophagy-dependent cell death, entotic cell death, alkaliptosis, netotic cell death, parthanatos, lysosome-dependent cell death, immunogenic cell death, and oxeiptosis (Galluzzi et al., 2018; Tang et al., 2019).

2.2 Apoptosis – a quiet and clean cell death in the body

Apoptosis (derived from Ancient Greek ἀπόπτωσις meaning "falling off" of leaves from a tree) named and defined by John Kerr, Andrew Wyllie, and Alastair Currie in 1972 (Kerr et al., 1972), is the most

common form of programmed cell death. It is accompanied by particular morphological features including cell shrinkage, membrane blebbing, chromatin condensation, DNA fragmentation, and eventually the formation of membrane-bound 'apoptotic bodies'. The apoptotic bodies containing intracellular components are ultimately engulfed and digested by phagocytes. This process is called efferocytosis (He and Wang, 2018; Nagata, 2018). Since apoptotic bodies contain considerable intracellular damage-associated molecular patterns (DAMPs) like DNA, RNA, high-mobility group box 1 (HMGB1), ATP, IL-1b and others, efferocytosis prevents unexpected immune responses (Green et al., 2009). In the past decades, many groups have identified a family of cysteine proteases called caspases involved in apoptosis. Based on their distinct functions, the caspase protein family can be further divided into three subfamilies: initiator caspases (caspase 2, 8, 9 and 10 (human)), executioner caspases (caspase 3, 6, and 7), and inflammatory caspases (caspase 1, 4, and 5 in human; caspase 1 and 11 in mice) (Galluzzi et al., 2016; Kolb et al., 2017; McIlwain et al., 2013, 2015; Taylor et al., 2008). Apoptosis can be triggered by death receptors (DRs) in the extrinsic pathway or by mitochondrial outer membrane permeabilization (MOMP) in the intrinsic pathway (He and Wang, 2018; Kolb et al., 2017).

2.2.1 The extrinsic pathway of apoptosis

The extrinsic apoptotic pathway is induced by death ligands of the TNF (tumor necrosis factor) family (FasL, Fas ligand, also known as CD95L; TNFα, tumor necrosis factor α; TRAIL, TNF-related apoptosis-inducing ligand, also known as TNFSF10) in combination with their corresponding death receptors (Fas, also known as APO-1 or CD95; TNFR1, TNF receptor 1, also known as TNFRSF1A or CD120a; and TRAIL-R1 (DR4) or TRAIL-R2 (DR5)) (Nagata, 1997, 2018; Schulze-Osthoff et al., 1998; Vincenz, 2001). Subsequently, the activation of caspase 8 facilitates apoptosis that can be inhibited by specific caspase inhibitors. However, under certain conditions such as the treatment with cellular inhibitor of apoptosis protein (cIAP) antagonists in combination with blocked caspase 8 activity, the death ligands can induce necroptotic cell death. Hence, necroptosis and apoptosis derive from the same upstream stimulation. Compared to TNFα, FasL and TRAIL induce stronger apoptosis, whereas TNFα mainly activates gene transcription. The details of the TNFα signaling pathway are described in section 2.3.

The binding of the death ligands FasL or TRAIL to their corresponding receptors Fas or TRAIL-R induces the trimerization of Fas or TRAIL-R. The trimerized receptors directly recruit the adaptor Fas-Associated Death Domain Protein (FADD) via their death domains (DDs). Subsequently, caspase 8 is recruited to

FADD via their death effector domains (DEDs) and forms the death-inducing signaling complex (DISC) with FADD and the death receptors (Reed et al., 2004; Walczak, 2013), where caspase 8 is activated by self-cleavage. Active caspase 8 cleaves and activates the downstream executioner caspase 3, 6, and 7 to induce apoptosis independent of receptor-interacting protein 1 (RIPK1). However, FasL and TRAIL stimulation combined with cIAP antagonists can lead to the recruitment of RIPK1 and the formation of a complex containing RIPK1, FADD and caspase 8, which induces caspase 8-mediated apoptosis depended on RIPK1 kinase activity (Pasparakis and Vandenabeele, 2015). In contrast, if activation of caspase 8 is inhibited by caspase inhibitors like Q-VD-OPh or z-VAD-FMK, apoptotic cell death can switch to necroptotic cell death. In this process, cellular Fas-associated DD-like interleukin 1β-converting enzyme-inhibitory protein (cFLIP) can negatively regulate DR-mediated cell death. Specifically, long splicer of cFLIP ($cFLIP_L$) contains two N-terminal tandem death effector domains (DEDs) and a C-terminal region. The C-terminus resembles the enzyme segment of caspases but lacks a catalytic cysteine residue critical for the cleavage between DED and p18 domains that is necessary to activate apoptosis (Barnhart et al., 2003; Riley et al., 2015; Tibbetts et al., 2003), whereas shorter splicers of cFLIP (short cFLIP, $cFLIP_S$; and Raji cFLIP, $cFLIP_R$) only have the tandem DEDs at the N-terminal regions, but not the pseudo-caspase domain at the C-terminal region. Thereby, all of cFLIP splicers can form a heterodimer with procaspase 8 at the DISC via their DEDs and hence prevent its dimerization that is required for self-cleavage and subsequent apoptotic activity (Riley et al., 2015; Walczak, 2013). Only $cFLIP_L$ but not $cFLIP_S$ or $cFLIP_R$ is able to induce the conformational changes in procaspase 8 that is required for processing between the p18 and p12 subunits and for creating its active site (active non-apoptotic protease) (Riley et al., 2015). So, $cFLIP_L$ can keep active, not apoptotic caspase 8 in the heterodimer, thus not only inhibiting caspase 8-mediated apoptosis but also necroptosis by enabling the cleavage of RIPK1 and RIPK3 (Feng et al., 2007; Oberst et al., 2011; Pop et al., 2011). Consequently, mice carrying the deletion of cFLIP die at embryonic day 10.5 (E10.5) due to aberrant apoptotic and necroptotic cell death (Dillon et al., 2012).

2.2.2 The intrinsic pathway of apoptosis

This intrinsic apoptosis pathway is activated by various intracellular signals (e.g., developmental signals, DNA damage, unfolded protein aggregation, hypoxia, etc.) (Kolb et al., 2017; Tait and Green, 2010), causing mitochondrial outer membrane permeabilization (MOMP) and resulting in the release of mitochondrial pro-apoptotic proteins into the cytoplasm such as cytochrome *c*, normally locating in the inner mitochondrial membrane (IMM) (Nagata, 2018). The cytosolic cytochrome *c* then forms a complex with the adaptor apoptotic protease activating factor-1 (Apaf-1), termed apoptosome (Yuan et al., 2010).

The formation of the apoptosome leads to the recruitment and activation of initiator caspase 9 and subsequent cleavage of downstream executioners caspase 3, 6, and 7 (Li et al., 1997; McIlwain et al., 2013). This process is strictly controlled by Bcl-2 family proteins, which consist of three subfamilies: pro-apoptotic BH3-only members (Bim, Bid, Puma, Noxa, Hrk, Bmf, and Bad), pro-apoptotic effector molecules (Bax and Bak), and anti-apoptotic Bcl-2 family proteins (Bcl-2, Bcl-xL, etc.) (Czabotar et al., 2014; Nagata, 2018; Warren et al., 2019). In healthy cells, Bax/Bak preferentially locate in the cytosol and are controlled by anti-apoptotic Bcl-2 proteins (Westphal et al., 2011). Upon apoptotic stimuli, BH3-only proteins are upregulated to directly induce Bax/Bak oligomerization or to indirectly antagonize the anti-apoptotic Bcl-2 family proteins. The Bax/Bak oligomer translocates to mitochondria to stimulate the release of cytochrome *c* (Nagata, 2018). Another pro-apoptotic mitochondrial protein is second mitochondria-derived activator of caspases (Smac, also known as Diablo), which can interact with IAPs to induce auto-degradation of IAPs by activating their intrinsic E3 ubiquitin ligase activity (Yang and Du, 2004) and hence promotes the formation of RIPK1, FADD and caspase 8 complex to facilitate apoptosis (Riley et al., 2015). In addition, the activation of the extrinsic apoptosis signaling pathway can also facilitate the intrinsic apoptosis pathway through caspase 8-mediated cleavage of Bid (Li et al., 1998). The truncated Bid (tBid) translocates from the cytosol to mitochondria and results in the release of cytochrome *c*.

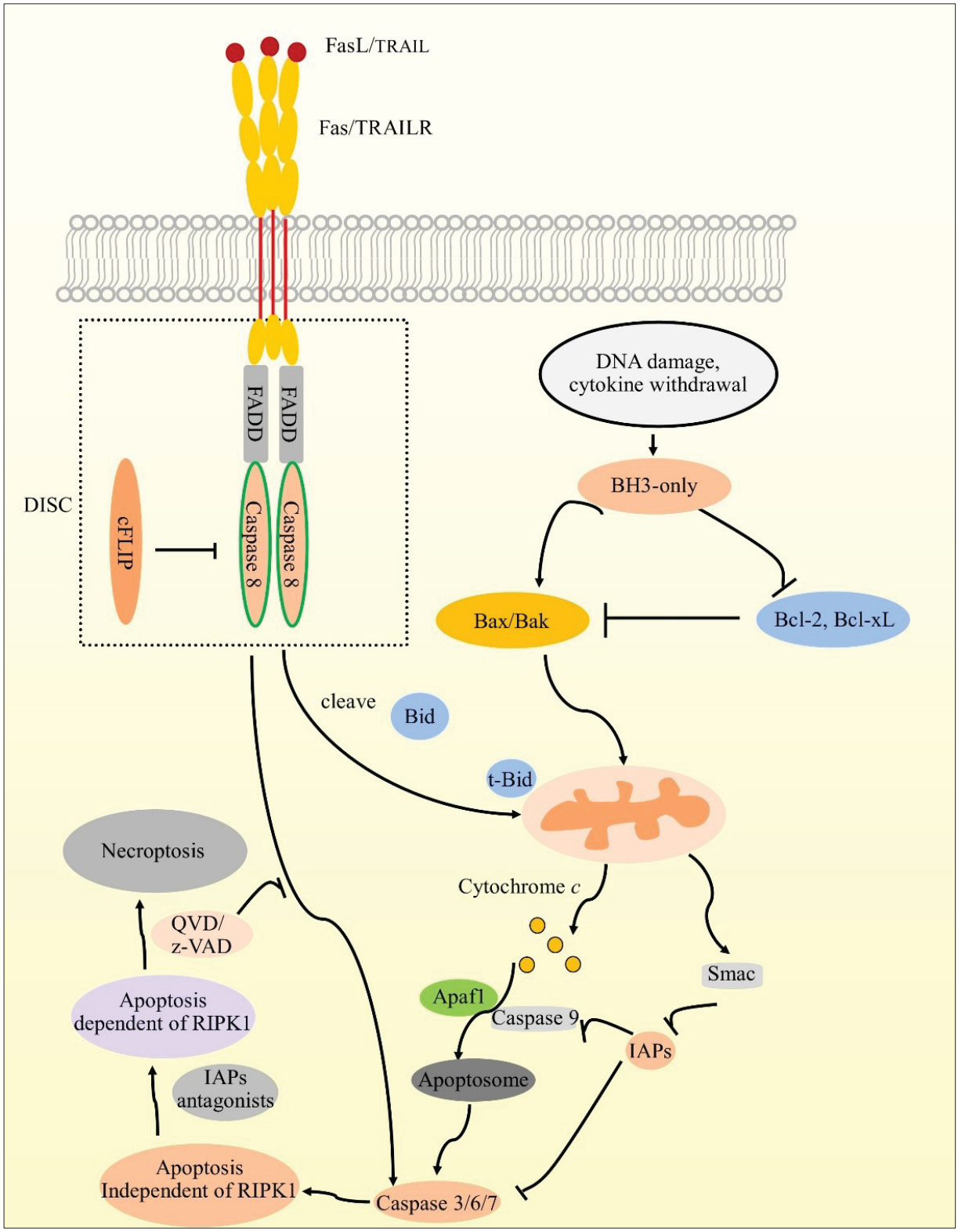

Figure 2. The extrinsic and intrinsic apoptosis pathways. For the extrinsic pathway, the activation of death receptors (Fas and TRAIL-R) results in the recruitment of FADD. FADD can further recruit caspase 8 and forms the death-inducing signaling complex (DISC), which causes the activation of caspase 8. Active caspase 8 cleaves and activates the downstream caspases 3/6/7 and thereby induces apoptosis. Intrinsic

apoptosis pathway is triggered by cytokine withdrawal or DNA damage, which causes the upregulation of BH3-only proteins. BH3-only proteins directly (or indirectly via antagonizing anti-apoptotic Bcl-2 proteins) induce Bax/Bak oligomerization, which causes the subsequent translocation from the cytosol to the mitochondria and pore formation in the mitochondrial outer membrane. The mitochondrial outer membrane permeabilization (MOMP) leads to the release of cytochrome c and Smac to the cytosol. Cytochrome c together with APAF-1 forms the apoptosome complex, where caspase 9 is recruited and activated. In turn, active caspase 9 cleaves caspases 3/6/7 and induces apoptosis. Moreover, the extrinsic apoptosis pathway can enhance intrinsic apoptosis via cleaving Bid. Truncated Bid translocates to mitochondria and promotes the release of pro-apoptotic proteins. Of note, FasL and TRAIL can directly induce apoptosis, which is independent of RIPK1. Combined with IAPs antagonists, RIPK1 can be recruited to the DISC and induce RIPK-dependent apoptosis. During this process, the absence of caspase 8 activity can lead to necroptosis.

2.3 Necroptosis – an inflammatory cell death pathway by the rupture of plasma membrane

The necrotic cell death induced by TNFα was firstly reported by Linda R Gooding's group in 1988 (Laster et al., 1988). At that time, necrosis was thought to be uncontrolled, whereas necrotic cell death triggered by TNFα/FasL had proved to be indeed under regulation in 2005, termed necroptosis (Degterev et al., 2005). Subsequent studies have shown that the protein complex RIPK1, RIPK3 and MLKL modulates necroptotic cell death induced by TNF family cytokines such as TNFα, FasL and TRAIL (Degterev et al., 2008; He et al., 2009; Sun et al., 2012). Necroptosis displays similar morphological features to necrosis, e.g., cell swelling, swelling of cellular organelles and rupture of plasma membrane that leads to the release of damage-associated molecular patterns (DAMPs) and thereby inflammatory reactions (Annibaldi and Meier, 2018; Yatim et al., 2015). Necroptosis triggered by death receptors (DRs) is similar to apoptosis, but the inactivity of caspase 8 is required. In addition to DRs (TNFR1, Fas and TRAIL-R), other stimuli can also initiate necroptosis such as the activation of toll-like receptors (e.g., toll-like receptors 3 and 4 (TLR3 and TLR4)), nucleic acid sensors (e.g., Z-DNA binding protein 1 (ZBP1, also known as DAI), etc. (Tang et al., 2019). So far, the activation mediated by death receptors, especially TNFR1 is the best studied mechanism.

Similar to the extrinsic apoptosis pathway, the binding of TNFα to its death receptor TNFR1 induces its trimerization and initiates the formation of TNFR1 signaling complex (TNFR1-SC) or complex I of TNFR1 signaling (Peltzer et al., 2016), resulting in the recruitment of RIPK1 and adaptor protein TNFR1-associated death domain (DD) protein (TRADD) to the TNFR1 mediated by their dead domains (DDs) (Micheau and Tschopp, 2003). Subsequently, TRADD recruits TNF receptor-associated factor 2/5

(TRAF2/5) by its N-terminal domain (Micheau and Tschopp, 2003; Peltzer et al., 2016). Next, the E3 ubiquitin ligases cIAP1/2 are recruited to TRAF2 mediated by the TRAF2-TRAF1 heterocomplex (Rothe et al., 1995), leading to ubiquitination of several components of complex I, especially RIPK1 and cIAPs themselves (Bertrand et al., 2008; Dynek et al., 2010; Varfolomeev et al., 2008; Yang et al., 2000). The ubiquitin chains in complex I generated by cIAP1/2 allow the recruitment of linear ubiquitin chain assembly complex (LUBAC) that consists of the central catalytic component HOIL-1 interacting protein (HOIP) together with the accessory proteins heme-oxidized IRP2 ubiquitin ligase-1 (HOIL-1) and SHANK associated RH domain interactor (SHARPIN) (Peltzer et al., 2016). LUBAC exclusively catalyzes the generation of linear (also known as M1-linked) ubiquitin chains on several components of complex I, including RIPK1, NF-κB essential modulator (NEMO), TRADD, and TNFR1 (Haas et al., 2009; Peltzer et al., 2016). LUBAC and cIAPs cooperatively generate ubiquitin chains of various linkage types (K63, K48 and K11 by cIAPs; linear by LUBAC; and cross-branched chains) on RIPK1 and other components of complex I (Bertrand et al., 2008; Dynek et al., 2010; Mahoney et al., 2008; Varfolomeev et al., 2008). These ubiquitin chains in combination with the branched ubiquitin chains provide scaffolds to recruit different downstream kinase complexes, such as transforming growth factor β-activated kinase 1 (TAK1)/TAK1-binding proteins 2/3 (TAB2/TAB3) (TAK/TAB complex) (Ori et al., 2013) and IκB kinase α/β (IKK α/β)/NEMO (IKK complex) (Rahighi et al., 2009). Recruitment of these kinase complexes ultimately results in the activation of nuclear factor κ light-chain enhancer of activated B cells (NF-κB) and mitogen-activated protein kinase (MAPK) signaling and the production of cytokines and pro-survival proteins, such as cFLIP, Bcl-2, cIAPs etc., which also explains why cell death cannot be induced upon TNFα stimulation in healthy cells.

Upon disruption of pro-survival signals from complex I by stress (e.g., poly-ubiquitin chains of RIPK1 are inhibited by cIAP antagonists or removed by the deubiquitinase cylindromatosis (CYLD) (Wang et al., 2008), or the phosphorylation of RIPK1 and the activity of NF-κB signaling is affected through disturbing TAK1, IKK, MAPK-activated protein kinase 2 (MK2) or TANK-binding kinase 1 (TBK1) kinases activities (Peltzer and Walczak, 2019)), TNFα can induce the formation of the secondary cytotoxic complex (termed complex II) that contains TRADD, RIPK1, FADD, Caspase 8/10 (human specific), cFLIP, and RIPK3. The cFLIP generates a heterodimer with caspase 8 in complex II to inhibit the release of activated caspase 8 and results in the inhibition of apoptosis. Moreover, the caspase 8/cFLIP$_L$ heterodimer can also cleave RIPK1 and RIPK3 in complex II to prevent necroptosis. However, when the stimulation of gene activation is reduced or blocked, cFLIP levels are downregulated so that fully activated caspase 8 is

completely released into the cytosol and leads to apoptosis. If caspase 8 activity is completely absent or inhibited by pharmacological compounds (e.g. Q-VD-OPh or z-VAD-FMK) (He et al., 2009) or in certain physiological conditions (e.g. viral infections) (Cho et al., 2009), RIPK1 can interact and activate RIPK3 and form an amyloid-like signaling complex called necrosome to induce necroptosis (Li et al., 2012). This necroptosis depends on RIPK1 and RIPK3 kinase activities. Activated RIPK3 further recruits and phosphorylates the downstream executioner mixed lineage kinase domain-like (MLKL). So far, there are several models to explain how MLKL translocates into the plasma membrane to execute necroptosis, but the most common one is that phosphorylated MLKL possesses a different conformation, leading to its oligomerization and recruitment to the plasma membrane where it generates pores, finally inducing membrane rupture and necroptosis (Grootjans et al., 2017).

2.3.1 RIPK1 – the central regulator of cell death

RIPK1 is a member of the serine/threonine protein kinases family, which contains four domains: an N-terminal kinase domain (KD), an intermediate domain (ID), a C-terminal RIP homotypic interaction motif (RHIM) and a death domain (DD) (Ofengeim and Yuan, 2013). RIPK1 is the core regulator of apoptotic or necroptotic cell death. Stimulation of TNFR1 by TNFα immediately ignites a series of signaling cascades from complex I, including ubiquitination and phosphorylation, particularly on RIPK1. Although TNFα mainly has pro-inflammation functions through complex I, destabilization of complex I via disturbing the ubiquitination and/or phosphorylation of RIPK1 can result in the formation of cytotoxic complex (complex II). The complex II in turn determines cellular responses (apoptosis or necroptosis). Hence, it is important to keep the stabilization of RIPK1 in complex I by various checkpoints.

Of note, RIPK1 scaffolding function plays an important role in protection. This may be more surprising since RIPK1 mostly demonstrates its pro-cell death function in cells dependent on its kinase activity (Peltzer and Walczak, 2019). However, Genetic ablation of *ripk1* causes postnatal lethality which cannot be prevented by deficiency of Caspase 8, FADD, RIPK3 or MLKL (Dillon et al., 2014; Rickard et al., 2014b). By contrast, *Ripk1*$^{-/-}$*Ripk3*$^{-/-}$*Caspase 8*$^{-/-}$ and *Ripk1*$^{-/-}$*Ripk3*$^{-/-}$*Fadd*$^{-/-}$ mice can survive and mature normally, demonstrating that RIPK1 can block aberrant cell death induced by FADD-caspase 8 and RIPK3-MLKL signaling pathways in mice (Dillon et al., 2014; Rickard et al., 2014b). The inhibitory function of RIPK1 on FADD-caspase 8 and RIPK3-MLKL signaling pathways in mice is independent of RIPK1 kinase activity since

RIPK1 kinase dead knock-in mice mature normally (Berger et al., 2014; Kaiser et al., 2014; Newton et al., 2014).

2.3.2 RIPK1 ubiquitination in complex I

Currently, there are three important ubiquitin E3 ligases (cIAP1, cIAP2, and LUBAC) to modify and stabilize RIPK1 in complex I. Upon TNFα stimulation, RIPK1 is promptly ubiquitinated by cIAP1/2 with K63, K48 and K11 ubiquitin (Ub) linkage types, which provide scaffolds to recruit the ubiquitin-binding proteins TAB2/3 and their associated kinase TAK1 (Witt and Vucic, 2017). Of note, TAB2/3 specifically binds to K63 linked Ub chains (Shan et al., 2018; Witt and Vucic, 2017). The Ub chains by cIAP1/2 are required to stabilize complex I and the deprivation of cIAP1/2 results in the loss of RIPK1 ubiquitination and thereby the inactivation of NF-κB signaling (Varfolomeev et al., 2008). In addition, cIAPs also participate in preventing cells death through inhibiting complex II formation as the absence of cIAP1/2 by genetic ablation or antagonists renders cells sensitive to TNF-induced cell death (Annibaldi et al., 2018; Varfolomeev et al., 2008). In addition, the absence of cIAP1/2 also spontaneously causes formation of a complex termed ripoptosome that includes RIPK1, FADD, caspase 8 and RIPK3 and is similar to complex II, but independent of TNF stimulation (Pasparakis and Vandenabeele, 2015). Although formation of the ripoptosome complex alone is not sufficient to induce cell death, it constitutes a potential threat under certain conditions (e.g., combination with other stimuli such as TNF).

In vivo the importance of cIAPs in TNF-induced cell death has been also displayed by many reports in the past two decades. Although single deprivation of cIAP1, cIAP2, or XIAP is not lethal to mice (Conte et al., 2006; Conze et al., 2005; Moulin et al., 2012), deletion of cIAP1 with cIAP2 or XIAP causes mid-embryonic lethality (Moulin et al., 2012). In contrast, *Xiap*$^{-/-}$*cIap2*$^{-/-}$ mice are viable (Moulin et al., 2012). The lethality of cIAP1 and cIAP2 double knockout mice is rescued to birth by deletion of TNFR1, and single knockout of RIPK1 or RIPK3 delays embryonic lethality in cIAP1/cIAP2 double knockout mice (Moulin et al., 2012). However, another study demonstrates the completely opposite phenotype that XIAP/cIAP1 null mice are viable and display a dramatical upregulation of cIAP2 protein (Heard et al., 2015). The differential expression of cIAP2 observed in diverse mouse strains (low cIAP2 expression in the lethal strain (Moulin et al., 2012) and high cIAP2 expression in the viable strain (Heard et al., 2015)) indicates that cIAP2 expression regulates aberrant cell death upon deletion of cIAP1 and XIAP.

In addition to cIAPs, the ubiquitin E3 ligase complex LUBAC consisting of the catalytic component HOIP with the two regulatory proteins HOIL-1 and SHARPIN generates linear ubiquitin chains on RIPK1 and other components of the TNFR1 signaling complex. The catalytic function of HOIP to produce linear ubiquitin chains on substrates requires the combination with either one or both complex members HOIL-1 and SHARPIN by their ubiquitin-like (UBL) domains (Fujita et al., 2018; Ikeda et al., 2011). Linear-linked Ub chains on NEMO, a key adaptor of the IKK, induce homodimerization of the IKKβ. This results in the activation of IKK by *trans* autophosphorylation and subsequent activation of NF-κB signaling pathway (Fujita et al., 2014), in which the phosphorylation of IKK by TAK1 also plays an crucial role (Kanayama et al., 2004; Wang et al., 2001). Another key function of LUBAC is the involvement in the regulation of TNFR1-triggerred cell death. LUBAC-catalyzed linear ubiquitin chains on RIPK1 are required to prevent TNF-induced cell death. Similar to the deprivation of IAPs, deletion of HOIP also results in aberrant endothelial cell death, defective vascularization and early embryonic lethality at (E)10.5 (Peltzer et al., 2014). HOIP-deficient cells are sensitive to cell death induced by both TNF and lymphotoxin-α (LT-α), and display aberrant complex II formation (Peltzer et al., 2014). However, these phenotypes can be prevented by ablation of TNFR1 (Peltzer et al., 2014). In addition, mice with Sharpin^{cpdm} (chronic proliferative dermatitis mice) mutation demonstrate spontaneous inflammation in multiple organs and cells from Sharpin^{cpdm} mice are also very sensitive to TNF stimulation (Rickard et al., 2014a). The phenotypes are almost reversed in *Sharpin$^{m/m}$Caspase8$^{+/-}$Ripk3$^{-/-}$* (Rickard et al., 2014a) or *Sharpin$^{m/m}$Ripk1$^{K45A/K45A}$* mice (Berger et al., 2014). Intriguingly, deletion of HOIL-1, another component of the LUBAC complex is not lethal to mice and does not show any inflammatory responses in some reports (Rodgers et al., 2014; Tokunaga et al., 2009). However, a recent report demonstrates that the deletion of HOIL-1 results in embryonic lethality at E10.5 by aberrant TNF-mediated cell death (Peltzer et al., 2018). In summary, these ubiquitin E3 ligases are required to restrict RIPK1-mediated cell death.

2.3.3 RIPK1 de-ubiquitination in complex I

As shown above, the ubiquitination has a profound effect on NF-κB signaling and TNF-mediated cell death. In order to keep the dynamic equilibrium of ubiquitination, various deubiquitinating enzymes (DUBs) are also involved in the regulation of TNFα stimulation. So far, the three DUBs cylindromatosis (CYLD), TNFα-induced protein 3 (TNFAIP3, also known as A20) and OTU deubiquitinase with linear linkage specificity (OTULIN) are the best studied. CYLD can be recruited to the TNFR1- and NOD2-associated signaling complexes by directly binding to HOIP (Draber et al., 2015) or indirectly by a linker spermatogenesis-associated protein 2 (SPATA2) (Elliott et al., 2016; Kupka et al., 2016; Schlicher et al.,

2016; Wagner et al., 2016). Once CYLD is recruited to the membrane-associated complex, it can affect NF-κB activation and cell death by removing K63 and linear poly-ubiquitin chains on components of TNFR1- and NOD2-associated complexes (Kupka et al., 2016). Previous reports showed that A20 has a similar function on the regulation of NF-κB activation by removing K63 and K48 linked ubiquitin chains of RIPK1 and other components of the TFNR1 signaling complex (Komander and Barford, 2008; Tokunaga et al., 2012; Wertz et al., 2004). However, recent studies display completely different roles of A20 in the regulation of cell death upon TNFα since A20 can be recruited to linear ubiquitin chains by its C-terminal zinc-finger 7 (ZF7) domain and prevents the linear ubiquitin chains from cleavage by CYLD and hence inhibit TNF-induced death (Draber et al., 2015). Of note, A20 still plays a negative role in gene activation through competitively binding to linear Ub chains with these factors required for gene activation (Draber et al., 2015). In addition, OTULIN cannot be recruited to complex I, but is also very important to regulate NF-κB activation and cell death by regulating the activity of LUBAC in the cytosol and hence affecting the linear Ub chains of other components of complex I (Draber et al., 2015). For example, a recent finding shows that OTULIN can activate LUBAC via removing the linear poly-ubiquitin chains from LUBAC itself to promote NF-κB activation and prevent cell death upon TNFα stimulation (Heger et al., 2018).

2.3.4 RIPK1 phosphorylation in complex I

Upon TNFα stimulation, E3 ubiquitin ligases like cIAPs and LUBAC are recruited to the complex of TNFR1 signaling to ubiquitinate RIPK1 and other components, which reinforces complex I and blocks the formation of cytotoxic complex II. In addition to ubiquitination of RIPK1, several serine/threonine kinases also play crucial roles in regulation of RIPK1 activity, e.g., TAK/TAB complex (TAK1/TAB2/TAB3) and IKK complex (IKKα/IKKβ/NEMO), which are recruited to complex I by K63 Ub chains and linear Ub chains, respectively (Witt and Vucic, 2017). Previously, it was thought that TAK/TAB complex only inhibited TNF-mediated cell death via gene activation and cFLIP production (Jaco et al., 2017). However, a recent finding shows that TAK1 can directly phosphorylate RIPK1 at Ser 320 (mouse)/Ser 321 (human) to block its autophosphorylation at Ser 166 and thus its activity (Geng et al., 2017). At the same time, three other groups also report that p38/MK2, the downstream kinase of TAK1 can inhibit RIPK1 activity through the direct phosphorylation of RIPK1 at Ser 320 and Ser 335 (Dondelinger et al., 2017; Jaco et al., 2017; Menon et al., 2017). Although p38/MK2 is not recruited to complex I, it serves as the safeguard in the cytosol to limit RIPK1 activity and hence the cytotoxic complex II formation. IKK can inhibit complex II formation via NF-κB activation and the direct phosphorylation of RIPK1 (Annibaldi et al., 2018). Recently, two groups report that the TANK-binding kinase 1 (TBK1) and IKKε can be recruited to complex I by the

interaction between NEMO and the adaptors TRAF family member-associated NF-κB activator (TANK) and nucleosome assembly protein 1 (NAP1), where TBK1 directly phosphorylates RIPK1 at Thr 189 (human)/Thr 190 (mouse) to inhibit RIPK1 activity (Lafont et al., 2018; Xu et al., 2018). Additionally, TBK1 deficiency leads to the sensitivity to TNFα-mediated apoptosis and necroptosis. The importance of TBK1 is also shown in mice, since *Tbk1*$^{-/-}$ mice die between E13.5 and E14.5 while the phenotype can be completely rescued by RIPK1 kinase-dead D138N mutation (Xu et al., 2018).

2.3.5 RIPK3 – the key to open the door of necroptosis

Activation of RIPK3 is required for initiating necroptosis in the absence of caspase 8 (Cho et al., 2009; He et al., 2009; Zhang et al., 2009). Similar to RIPK1, RIPK3 also harbors an N-terminal kinase domain (KD), an intermediate domain (ID) and a C-terminal RIP homotypic interaction motif (RHIM). The only difference is that RIPK3 lacks the C-terminal death domain (DD) (Grootjans et al., 2017). RIPK3 is activated by the interaction with RIPK1 via RHIM domains, which leads to the formation of an amyloid-like signaling complex (termed necrosome). Activated RIPK3 results in its autophosphorylation at Ser 227 (human) (Sun et al., 2012) or at Thr 231 and Ser 232 (mouse) (Chen et al., 2013), which are necessary to recruit and further activate the downstream executioner MLKL via the phosphorylation of Thr 357 and Ser 358 (human) or Ser 345, Ser 347, Thr 349 and Ser 352 (mouse) (Murphy et al., 2013; Wang et al., 2014; Xie et al., 2013). Phosphorylated MLKL exhibits a changed conformation and exposes its four-helical bundle domain, which can be translocated to plasma membrane and cause membrane rupture (Hildebrand et al., 2014; Murphy et al., 2013).

In addition to RIPK1, other adaptor proteins containing RHIM domains can also directly activate RIPK3 to induce necroptosis through their corresponding RHIM-mediated interaction, e.g., TIR domain-containing adaptor-inducing interferon-β (TRIF) (He et al., 2011) and ZBP1 (Upton et al., 2012). TRIF is a downstream adaptor of TLR3 and TLR4, belonging to the family of pattern-recognition receptors (PRRs). Diverse TLRs are sensitive to different ligands through their extracellular N-terminal leucine-rich repeats domains. For example, TLR3 recognizes viral double-strand RNA (dsRNA) or synthetic analog of dsRNA poly(I:C) (Alexopoulou et al., 2001), whereas TLR4 is sensitive to lipopolysaccharide (LPS) of Gram-negative bacteria (Hoshino et al., 1999). Upon the activation of TLR3 or TLR4, TRIF interacts with RIPK3 via their RHIM domains and subsequently induces necroptosis in the absence of caspase 8 (He et al., 2011). However, RIPK1 is dispensable for TLR3-mediated necroptosis in mouse fibroblast cells, which indicates

that RIPK3 is directly activated by the interaction with TRIF (Kaiser et al., 2013). In contrast, RIPK1 kinase activity is essential for TLR4-mediated necroptosis in macrophages (He et al., 2011; Kaiser et al., 2013). ZBP1 is necessary for RIPK3-mediated necroptosis upon infection by murine cytomegalovirus (MCMV) or influenza A virus. Previously, ZBP1 was identified as a sensor of dsDNA only (Takaoka et al., 2007), but a recent finding shows that endogenous RNA can also activate ZBP1 via binding to its Z-binding domain (ZBD) (Maelfait et al., 2017). Activated ZBP1 then interacts with RIPK3 via their RHIM domains to induce necroptosis.

2.3.6 MLKL – the executioner of necroptosis

Currently, MLKL is known as the sole executioner of canonical necroptosis, which consists of an N-terminal four helical bundle domain (4HBD), two-helix linker (the "brace" helices, also known as brace region, BR) and a C-terminal pseudokinase domain (KD), lacking the catalytic residues and hence its kinase function (Murphy et al., 2013; Murphy et al., 2014). Although phosphorylation of MLKL by RIPK3 is a key step to execute necroptosis, the mechanism how phosphorylated MLKL precisely translocates to the plasma membrane and ruptures it is still largely debated. Normally, it is thought that the phosphorylation of MLKL is required for inducing its structural change and exposing its four-helical bundle domain, which results in brace region-mediated oligomerization and translocation to the plasma membrane (Grootjans et al., 2017). In this process, some reports propose that oligomerized MLKL binds to phosphatidylinositol phosphates (PIPs) of the plasma membrane by its positively charged residues and directly permeabilizes the plasma membrane, which is demonstrated by the observation that wildtypic MLKL, but not a mutant lacking the positively charged residues, can induce the leakage of PIP-containing liposomes *in vitro* (Dondelinger et al., 2014; Hildebrand et al., 2014; Wang et al., 2014). Later, another group proposed that the recruitment of MLKL to the plasma membrane is a stepwise activity. Firstly, MLKL oligomerization mediated by the brace region is required. Then, the oligomer is translocated to phosphorylated inositol polar head groups of PIP phospholipids on the plasma membrane through its 4HBD. However, this is a low-affinity binding. Next, high-affinity PIP binding regions of MLKL are exposed through 4HBD rolling over, which is 'probably' responsible for the membrane rupture since the downstream steps of PIP binding were not addressed in this study (Quarato et al., 2016). Anyway, the exact mechanisms how MLKL ruptures the plasma membrane is controversial and many possibilities exist based on the direct pore formation or indirect ion channels on the plasma membranes (Grootjans et al., 2017). Since MLKL can rapture plasma membranes and induce cell death, it is crucial for normal cells to have regulators to surveil the aberrant accumulation of phosphorylated MLKL and to prevent cell death.

Indeed, the endosomal sorting complexes required for transport (ESCRT)-III accumulates at MLKL-damaged sites on the membrane to prevent membrane rupture and cell death. ESCRT-III facilitates the shedding of MLKL-damaged plasma membrane from intact cells when MLKL activation is not strong enough (Gong et al., 2017). Alternatively, phosphorylated MLKL can also be removed from the membrane by endocytosis. In this process, the lipid raft-associated proteins flotillin-1 and flotillin-2 are required. Subsequently, the phosphorylated MLKL is degraded in lysosomes (Fan et al., 2019). Thereby, phosphorylated MLKL cannot induce necroptosis on the membrane until they conquer the checkpoints. In addition to MLKL, a recent finding shows that RIPK3 can also induce myocardial necroptosis mediated by the activity of Ca^{2+}-calmodulin-dependent protein kinase (CaMKII) rather than MLKL (Zhang et al., 2016).

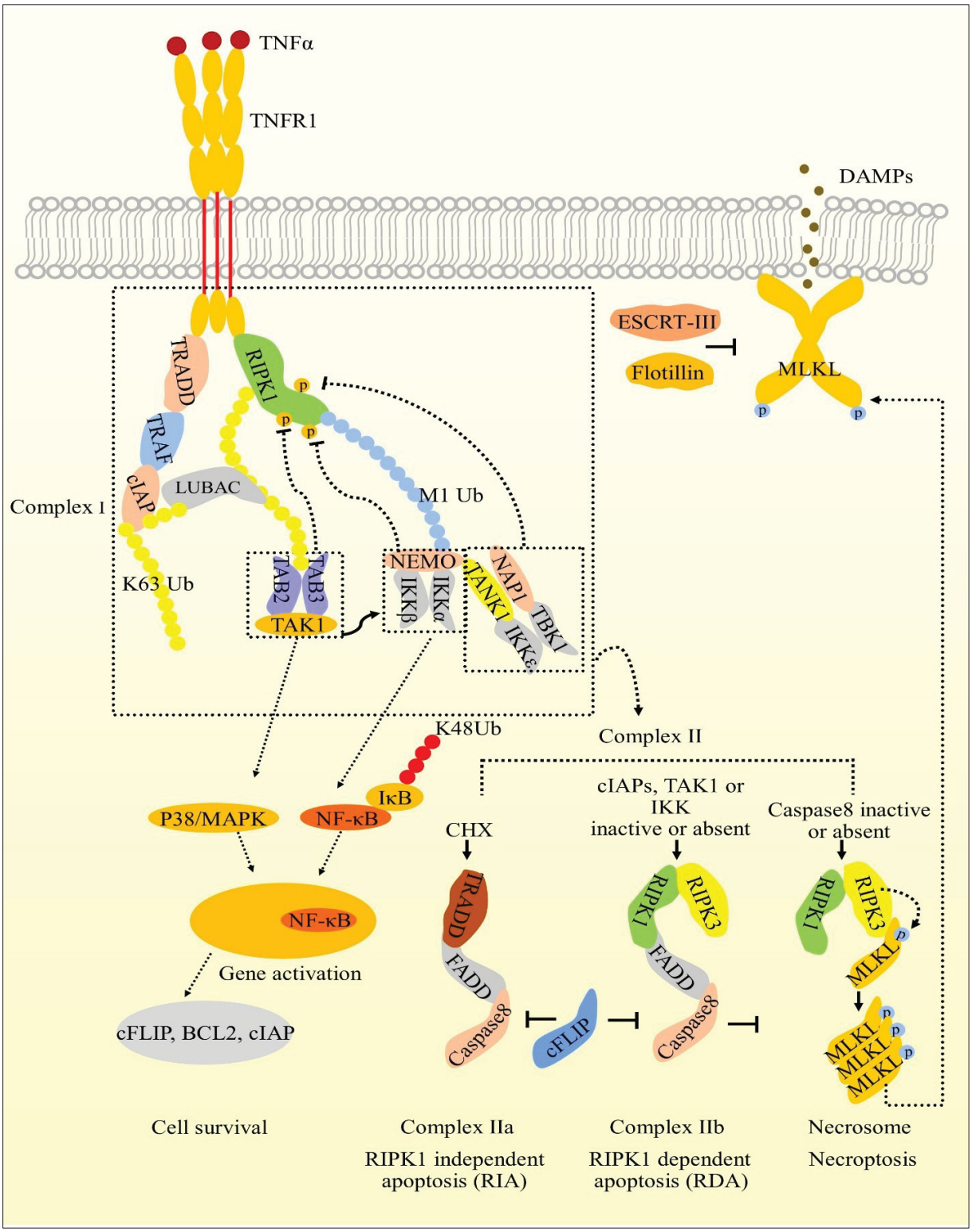

Figure 3. The induction of necroptosis by TNFα. Upon TNF stimulation, TNF receptor 1 (TNFR1) trimerizes and forms the TNFR1 signaling complex (TNFR1-SC or complex I). Then, the adaptor protein TRADD and the kinase RIPK1 are recruited to TFNR1. Subsequently, TRADD recruits TRAF2/5. In turn, TRAF2 enables the recruitment of the E3 ubiquitin ligases cIAP1/2, resulting in poly-ubiquitination of RIPK1 and other components of complex I. The ubiquitin chains in complex I cause the recruitment of LUBAC that exclusively generates linear ubiquitin chains on RIPK1 and other components of complex I. Ubiquitin chains generated by cIAP and LUBAC further recruit downstream kinases, i.e. TAB/TAK complex (preferably linked to K63 Ub) and the

IKK complex (preferably linked to linear Ub), which leads to downstream gene activation. Additionally, TBK1/IKKε can be recruited to complex I via the interaction between NEMO and TANK1/NAP1. The ubiquitin chains on complex I stabilize itself and directly inhibit RIPK1 activity. In addition, the phosphorylation mediated by TAK1, IKK, and/or TBK1 in complex I inhibits RIPK1 activity and blocks the formation of the cytotoxic complex II. Thereby, the ubiquitination and phosphorylation of complex I can inhibit cytotoxic complex II formation and activate downstream gene activation and promote cell survival. However, under certain conditions, i.e. when the pro-survival signal from complex I is disturbed, the secondary cytotoxic complex II can be formed. For example, cycloheximide (CHX) treatment can downregulate cFLIP levels to cause complex IIa formation (TRADD, FADD and caspase 8) and caspase 8 activity, thereby leading to apoptosis independent of RIPK1. In addition, inactivation or absence of cIAPs, TAK1, IKKα/β or TBK1 induces complex IIb formation (RIPK1, RIPK3, FADD and caspase 8) and leads to apoptosis dependent of RIPK1. When caspase 8 activity is inhibited, RIPK1 interacts with RIPK3 and forms the amyloid-like complex termed necrosome. Activated RIPK3 further recruits and phosphorylates the executioner MLKL. Phosphorylated MLKL translocates to the plasma membrane to rupture it and induce necroptosis, which is negatively regulated by ESCRT-III or Flotillin-mediated exocytosis or endocytosis, respectively.

2.4 Autophagy – a recycling factory for intracellular harmful materials

Autophagy (Greek for “self-eating”) regulates cellular homeostasis via ‘eating’ intracellular unfolded proteins or damaged organelles that is mediated by lysosomes upon some stresses, e.g., amino acid starvation, hypoxia, energy deprivation, ER stress, etc. This process is highly conserved in all eukaryotes. Although autophagy is generally known as a dynamic recycling system and pro-survival mechanism, autophagy might selectively degrade certain pro-survival proteins, ultimately resulting in cell death (termed autophagy-dependent cell death, a form of regulated cell death (RCD)). Hence, autophagy is crucial to keep the balance between cell death and survival (Galluzzi et al., 2018).

Autophagy was termed by Christian de Duve in 1963 from the observation that intracellular components can be delivered to and degraded in lysosomes, which contain numerous hydrolytic enzymes (Feng et al., 2014). Although autophagy was numerously reported at that time, owing to the limitation of experimental methods, the molecular mechanisms remained unclear until to the identification of the first autophagy-related gene *ATG1* in yeast by Yoshinori Ohsumi, who was awarded the Nobel Prize in Physiology or Medicine in 2016. To date, 42 *ATG* genes have been identified. The gene products are involved in different steps of autophagy, which plays crucial roles in neurodegenerative diseases, cancer, and inflammatory diseases (Mizushima, 2018). Currently, autophagy is classified into three subtypes: macroautophagy, microautophagy and chaperon-mediated autophagy (CMA). So far, microautophagy is not well characterized due to the limitation of observation techniques. However, it is thought that cytosolic materials are directly invaginated by lysosomal or late endosomal membranes (Bhutia et al., 2019; Sahu et al., 2011). In chaperone-mediated autophagy, cargo harboring a Lys-Phe-Glu-Arg-Gln (KFERQ)-like pentapeptide is selectively recognized by cytosolic heat shock-cognate chaperone of 70 kDa

(HSC70). Subsequently, the cargo is translocated into the lysosomal lumen with the combination of transmembrane protein Lamp-2A, serving as a receptor on the lysosomal membrane (Mizushima and Komatsu, 2011). Macroautophagy (hereafter referred to as autophagy) is the best investigated pathway in the three autophagic subtypes. Cargoes in the cytosol are engulfed by double-membraned vesicles, named autophagosomes, and finally degraded in lysosomes via the fusion of autophagosomes and lysosomes. The fusion process is mediated by soluble N-ethylmaleimide-sensitive-factor attachment receptor proteins (SNAREs), e.g., syntaxin17 (Itakura et al., 2012) or Ykt6 (Bas et al., 2018; Matsui et al., 2018) and generates the so called autolysosomes.

2.4.1 Autophagic regulation by upstream kinases

Autophagy can be initiated and induced by several stimuli, whereas amino acid starvation is the best studied so far. Upon the deprivation of nutrient or energy (due to the decrease of the cellular ATP/AMP ratio), the energy-sensing kinase AMP-activated protein kinase (AMPK) is activated by Liver Kinase B1 (LKB1, also known as STK11 (Serine/Threonine Kinase 11)) (Shackelford and Shaw, 2009; Shaw et al., 2004). AMPK is a heterotrimeric complex, containing α-catalytic subunits (AMPKα1/PRKAA1 or AMPKα2/PRKAA2), β-scaffold subunits (AMPKβ1/PRKAB1 or AMPKβ2/PRKAB2) and regulatory γ-subunits (AMPKγ1/PRKAG1, AMPKγ2/PRKAG2 or AMPKγ3/PRKAG3) (Shackelford and Shaw, 2009). However, LKB1 mainly phosphorylates AMPKα1 at Thr 183 or AMPKα2 at Thr 172 to regulate the activation loop upon energy stimulus. In addition to LKB1, both Ca^{2+}/calmodulin-dependent protein kinase kinase 2 (CaMKK2) and TAK1, can activate AMPK at Thr 183 or Thr 172, depending on the cytosolic Ca^{2+} level (Woods et al., 2005) or drug treatments (e.g., oligomycin, the antidiabetic drug metformin, 5-aminoimidazole-4-carboxamide riboside (AICAR)) (Xie et al., 2006), respectively.

In nutrient-rich conditions, the Ser/Thr kinase complex mTORC1, a central regulator of cell growth and rather sensitive to amino acids, growth factors, cellular energy and oxygen levels (Rabanal-Ruiz et al., 2017), is activated and inhibits autophagy by phosphorylating ATG13 at Ser 258 (mouse amino acid sequence) (Puente et al., 2016) and UNC-51-like kinase 1 (ULK1, the mammalian homolog of yeast Atg1) (at Ser 638 and Ser 758, human amino acid sequence) (Kim et al., 2011; Shang et al., 2011). These phosphorylation events inhibit ULK1 activity and the interaction between ULK1 and AMPK and hence prevent autophagy initiation (Kim et al., 2011). In contrast, upon nutrient deprivation, activated AMPK directly inhibits mTORC1 via phosphorylating the regulatory associated protein of MTOR complex 1

(Raptor) (Gwinn et al., 2008) or indirectly by phosphorylating the tuberous sclerosis complex subunit 2 (TSC2) (Inoki et al., 2003b). The later one promotes the transformation of Rheb-GTP (activator for mTORC1 kinase) to Rheb-GDP (inactivator for mTORC1 kinase) (Inoki et al., 2003a) and thereby inhibits mTORC1 activity. The inhibition of mTORC1, subsequently, leads to the dissociation of mTORC1 from ULK1 complex and the dephosphorylation of mTORC1-mediated phospho-sites in ULK1, hence leading to ULK1 activation (Alers et al., 2012). In parallel, activated AMPK can directly interact with and phosphorylate ULK1 at Ser 317, Ser 556, and Ser 638 (human amino acid sequence) to initiate autophagy (Alers et al., 2012). In addition, AMPK can also activate the pro-autophagy phosphatidylinositol 3-kinase catalytic subunit type 3 (PIK3C3, also known as VPS34) complex to induce autophagy by the phosphorylation of Beclin1 (Kim et al., 2013). After ULK1 is activated, it can further phosphorylate ATG13 and FIP200, which in turn promotes ULK1 activity and reinforces ULK1 complex formation (ULK1, ATG13, FIP200 and ATG101) (Jung et al., 2009; Mizushima, 2010). In addition, activated ULK1 also promotes the autophagic flux via phosphorylating several downstream effectors, e.g., Beclin1 (Russell et al., 2013), ATG14 (Park et al., 2016), ATG9 (Zhou et al., 2017), etc.

2.4.2 Autophagy nucleation

Upon nutrient deprivation, the ULK1 complex is translocated from the cytosol to subdomains of the ER to nucleate autophagosome formation. Currently, it is generally accepted that the early autophagic complex nucleates at the subdomains of ER, but exact location remains still controversial, e.g., the contact sites of ER-mitochondria (Hamasaki et al., 2013), autophagy-specific ER exit sites (Graef et al., 2013; Suzuki et al., 2013), ATG9-marked ER tubulovesicular regions (Karanasios et al., 2016), ER-Golgi intermediate compartment (Ge et al., 2013), isolation membrane-associated tubular/vesicular structures (Uemura et al., 2014) and phosphatidylinositol synthase (PIS)-enriched ER subdomains (Nishimura et al., 2017). In addition, the process of ULK1 translocation to the ER also requires additional proteins. For example, the Rab GTPase Rab1 and its effector C9orf72 regulate trafficking of ULK1 complex to the phagophores (Webster et al., 2016).

Following the recruitment of the ULK1 complex, another catalytic initiator complex is recruited to these subdomains of ER, i.e. the class III phosphoinositide 3-kinase (PtdIns3K, also known as PI3K). The core components of this lipid kinase complex are the catalytic subunit phosphatidylinositol 3-kinase catalytic subunit type 3 (PIK3C3, also known as VPS34), the accessory proteins Beclin1 and phosphoinositide 3-

kinase regulatory subunit 4 (PIK3R4, also known as VPS15 or p150). Depending on diverse regulatory mechanisms, the core complex can bind to ATG14 or UV radiation resistance associated gene (UVRAG), resulting in the formation of PtdIns3K (PI3K) complex I or II, respectively. Complex I is required for producing phosphatidylinositol 3-phosphate (PtdIns3P, also known as PI3P) at these subdomains and thereby positively regulates autophagosome nucleation and formation (Itakura et al., 2008). In contrast, complex II is mainly involved in endocytic sorting (Itakura et al., 2008), autophagosome and endosome maturation (Kim et al., 2015), and tubule scission of lysosomes (Munson et al., 2015). The PtdIns3K complex I can be recruited to the subdomains of ER by direct binding of Beclin1 (Huang et al., 2012) and ATG14 (Matsunaga et al., 2010) or via indirect recruitment by the interaction between ATG13 of the ULK1 complex and ATG14 (Park et al., 2016). At the subdomains, the PtdIns3K kinase is activated by ULK1-mediated phosphorylation of Beclin1 and ATG14 to promote the production of a pool of PI3P and drive omegasome formation (Egan et al., 2015; Park et al., 2016; Russell et al., 2013). Meanwhile, PI3P effectors are recruited to the emerging omegasome, e.g., double FYVE domain-containing protein 1 (DFCP1), which binds to PI3P by its two FYVE domains. Of note, DFCP1 is dispensable for autophagy induction, but it is specific marker for monitoring omegasomes and phagophores (Axe et al., 2008). Currently, in addition to ULK1 and PtdIns3K complexes, many reports have also shown the roles of ATG9 in autophagosome nucleation at ER subdomains (Karanasios et al., 2016; Kishi-Itakura et al., 2014; Nishimura et al., 2017).

2.4.3 Isolation membrane formation, elongation and closure

Subsequently, WD-repeat domain phosphoinositide-interacting proteins (WIPIs) are recruited to the omegasomes and facilitate the formation of phagophores. The WIPI protein family comprises four members (WIPI1-4), in which WIPI1 and WIPI2b were firstly identified to be recruited to omegasomes. Similar to DFCP1, WIPI1 can be used as a marker for omegasomes and phagophores (Mercer et al., 2018; Yoshii and Mizushima, 2017). In turn, WIPI2b can directly recruit ATG5–ATG12-ATG16L1 via the binding to ATG16L1 to facilitate LC3 lipidation and isolation membrane formation (Dooley et al., 2014). WIPI3 and WIPI4 are also thought to promote autophagosome formation (Bakula et al., 2017).

In mammals, a group of ATG8 family proteins was identified based on their amino acid sequence homology to yeast Atg8. This protein family consists of two subgroups: the LC3 subfamily (LC3A [variant 1 and variant 2], LC3B and LC3B2, and LC3C) (Bai et al., 2012), and the GABARAP/GATE-16 subfamily

(GABARAP, GABARAPL1, GABARAPL2 (also known as GATE-16) and GABARAPL3) (Weidberg et al., 2010). Both LC3 and GABARAP/GATE-16 proteins are indispensable for autophagosome formation, but it is thought that they act at distinct steps. LC3 mediates the elongation of the isolation membranes (phagophores) whereas GABARAP/GATE-16 functions at late steps of autophagosome formation and presumably at the closure of autophagosomes (Weidberg et al., 2010). To date, LC3B is the most extensively studied member and is used as a well-established marker for autophagosomes. Yeast Atg8 and its mammalian homologs (hereafter referred to as LC3) are ubiquitin-like proteins that are predominantly synthesized as precursors, unlipidated forms in the cytosol (known as LC3-I). The elongation of isolation membranes requires the covalent binding of the LC3 C-terminus to the amino group of phosphatidylethanolamine (PE), a major membrane phospholipid (Ichimura et al., 2000) and component of autophagosomes (Mizushima et al., 2011). The LC3–PE conjugation process requires another ubiquitin-like conjugation system: ATG12–ATG5. First of all, ubiquitin-like ATG12 harbors an exposed glycine at its C-terminus and is activated by the E1-like enzyme ATG7. Subsequently, ATG12 is transferred to the E2-like enzyme ATG10, and eventually conjugated to ATG5. The ATG12–ATG5 complex harbors E3-like enzyme activity. The ATG12–ATG5 complex also recruits ATG16L1 via the direct interaction between ATG5 and ATG16L1 and finally generates a multimeric protein complex through homodimerization of ATG16L1. Eventually, the complex is recruited to the isolation membranes by a direct binding between ATG16L1 and WIPI2 (Dooley et al., 2014).

For LC3-PE conjugation, pro-LC3 is C-terminally cleaved by the cysteine protease ATG4 to expose the glycine residue. Subsequently, the cleaved LC3-I is activated by the E1-like enzyme ATG7 and transferred to the E2-like enzyme ATG3. Finally, the LC3-I–ATG3 conjugate is also recruited to the isolation membranes by a direct interaction between ATG3 and ATG12, where LC3-I is covalently linked to PE in the membrane (known as LC3-II) via the E3-like catalytic function of ATG12–ATG5 (Mercer et al., 2018; Metlagel et al., 2013). LC3–PE (LC3-II) is located at the inner and outer membranes of the phagophores. Autophagy receptors can bind to LC3-II via an LC3-interacting region (LIR) motif. The LIR motif is constituted by the amino acid sequence W/Y/F-x-x-L/I/V and allows the recruitment of the autophagy receptors from the cytosol to autophagosomes. Autophagy receptors are also required for selective forms of autophagy and include sequestosome-1-like receptors (SLRs) (SQSTM1/p62, NBR1, NDP52, TAX1BP1, OPTN), mitophagy receptors (FUNDC1, BNIP3, Atg32, NIX), or other specialized receptors (Cbl, Stbd1) (Birgisdottir et al., 2013). So far, p62 is the best studied one and is also used as a marker for autophagosomes. The elongation of the isolation membranes and autophagosome maturation require

numerous lipids that is thought to be delivered from ATG9 vesicles since these constantly shuttle between multiple organelles like Golgi and endosomes and isolation membranes (Orsi et al., 2012).

2.4.4 The fusion of autophagosomes and lysosomes

After maturation, autophagosomes fuse with lysosomes to degrade the cargo delivered by autophagosomes. The fusion process between autophagosomes and lysosomes requires the activation of SNAREs. The fusion is mediated by the interaction between syntaxin 17 (STX17) and synaptosomal-associated protein 29 (SNAP29), which are recruited to the complete autophagosomes, and vesicle-associated membrane protein 8 (VAMP8), which is present on lysosomes (Itakura et al., 2012). Recently, some reports also show that Ykt 6 as a novel autophagosomal SNARE protein facilitates the fusion of autophagosomes and lysosomes, which is independent of syntaxin 17 (Matsui et al., 2018; Takats et al., 2018).

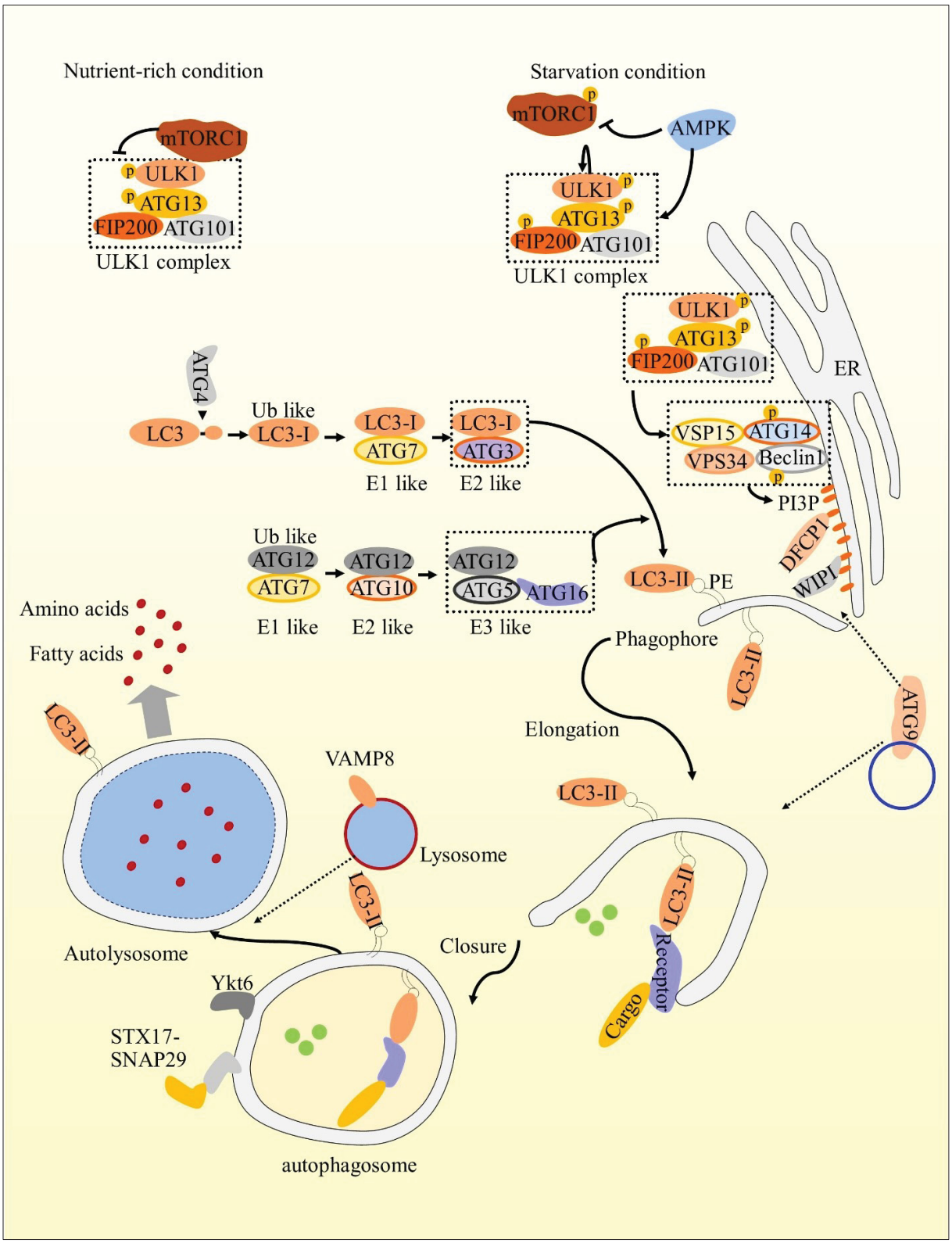

Figure 4. The autophagy pathway. In nutrient-rich conditions, mTORC1 interacts with the autophagy-initiating ULK1 complex and inhibits autophagy via restricting ULK1 complex activity. Upon energy deprivation, AMPK is activated and phosphorylates mTORC1, which in turn disassociates from the ULK1 complex and releases ULK1 activity. Moreover, activated AMPK can also directly phosphorylate the ULK1 complex and promote its activity, thus inducing autophagy. Activated ULK1 complex is recruited

to subdomains of ER to initiate autophagy. Subsequently, class III PtdIns3K lipid kinase complex is recruited to the sites, where it is activated by ULK1 and produces a pool of PI3P to form omegasomes. Omegasomes represent the sites of autophagic membrane initiation. PI3P further recruits the effectors DFCP1 and WIPIs to initiate membrane formation. LC3–PE bound on the membrane and lipid from ATG9 vesicles are required for the formation and the elongation of the isolation membranes. LC3–PE is located at the outer and inner membrane of the autophagosome. Autophagy receptors recognized by LC3 located at the inner autophagosomal membrane via their LIR motifs can selectively transfer cargos to autophagosomes. Eventually, autophagosomes fuse with lysosomes mediated by STX17 and SNAP29 on autophagosomal membranes and VAMP8 on the lysosomal membrane. Alternatively, this process can be mediated by Ykt6 independent of STX17. The cargo is degraded to amino acid and fatty acid in autolysosomes, which ultimately are transported back to the cytosol through lysosomal permeases and recycled for anabolic and catabolic processes.

2.5 Apoptosis and autophagy

Autophagy and apoptosis represent two distinct signaling pathways, in which autophagy mainly regulates cellular homeostasis and facilitates cell survival, whereas apoptosis predominantly promotes caspase-mediated cell death. However, these two pathways can cross-regulate each other under certain conditions. First of all, autophagy slows down apoptotic cell death e.g. by removing damaged mitochondria. In intrinsic apoptosis-mediated cell death, mitochondrial outer membrane permeabilization (MOMP) results in the release of pro-apoptotic proteins from mitochondria, which causes the reduction of the inner mitochondrial potential. As consequence, this can cause the accumulation of the kinase PTEN-induced putative kinase protein 1 (PINK1) on mitochondria and further recruits the E3 ubiquitin ligase parkin from the cytosol to the damaged mitochondria. Parkin then ubiquitylates several mitochondrial proteins. Finally, the ubiquitinated mitochondria are recognized by the ubiquitin-binding autophagy receptor p62 and removed by lysosomes (Marino et al., 2014; Youle and Narendra, 2011). Additionally, autophagy can also regulate apoptotic cell death by selectively degrading apoptosis-related proteins (Marino et al., 2014; Rubinstein and Kimchi, 2012). However, under some conditions, apoptosis can be activated by autophagy. For example, in cells treated by SKI-I (a pan-sphingosine kinase inhibitor) and bortezomib (a proteasome inhibitor), caspase 8 forms a complex with FADD and ATG5, which colocalizes with autophagosomes. Of note, the activity of caspase 8 is dependent on autophagosome formation, but not the degradative process (Young et al., 2012).

On the other side, apoptosis can also regulate autophagy. A series of caspases are highly activated during apoptosis to cleave multiple substrates, including several ATG proteins, e.g., ATG3 (Oral et al., 2012), ATG4D (Betin and Lane, 2009), and Beclin1 (Luo and Rubinsztein, 2010; Wirawan et al., 2010). The cleavage of these ATG proteins disturbs the autophagy process. Moreover, some truncated domains from the cleaved ATG proteins can in turn enhance apoptosis through translocating to mitochondria. Similar to caspase-mediated cleavage, ATG5 can also be cleaved by calpain, an apoptosis-related

protease. The truncated ATG5 translocates from the cytosol to mitochondria where it binds to the anti-apoptotic protein Bcl-xL and causes the release of cytochrome *c* and hence induces apoptosis (Yousefi et al., 2006).

2.6 Necroptosis and autophagy

Similar to the interconnection of apoptosis and autophagy, necroptosis and autophagy are also two contrary cell fate pathways. Necroptosis-mediated cell death can trigger severe inflammation via the release of damage-associated molecular patterns (DAMPs) since necroptosis does not generate apoptotic body-like compartments, which contain the DAMPs. Accordingly, the process is strictly regulated by the complex of RIPK1, RIPK3 and MLKL. So far, some reports have shown the association between necroptosis and autophagy, but the precise role of autophagy in cell death and necroptosis in autophagy is still poorly understood, especially how exactly autophagy and necroptosis modulate each other on the molecular level. One study shows that mouse prostate cells lacking Map3k7 (also known as TAK1) are sensitive to TRAIL-mediated necroptotic cell death. In this process the necrosome (RIPK1, RIPK3 and MLKL) is recruited to autophagosomes by the interaction between p62 and RIPK1. Therefore, autophagy can control cell death by serving as a scaffold (Goodall et al., 2016). Another report demonstrates that pro-necroptotic protein RIPK3 serves as a negative regulator of selective autophagy via disturbing p62-LC3 complex formation (Matsuzawa et al., 2015). In contrast, the results from another group indicate that RIPK3 positively regulates autophagy since depletion of RIP3 inhibits autophagic flux and leads to the accumulation of autophagosomes and amphisomes (Harris et al., 2015). Additionally, RIPK1 shows its negative regulatory function on basal autophagy via regulating transcription factor TFEB, which controls the expression of autophagy-related and lysosomal genes (Yonekawa et al., 2015). Taken together, it is crucial to explore the underlying mechanisms of the interconnection of necroptosis and autophagy. This knowledge will not only widen our understanding of the signaling pathways, but might also contribute to establish potential therapeutic targets in the future. The central aim of my thesis was the characterization of the cross-regulation between autophagy and necroptosis signaling pathways. From my work, two manuscripts were prepared which have been submitted for publication. The manuscript texts are included in this dissertation as a supplement. Additionally, I contributed to three additional manuscripts that have been published.

3. Manuscripts

Two manuscripts are from the thesis:

Wenxian Wu[*], Xiaojing Wang[*], Niklas Berleth, Jana Deitersen, Nora Wallot-Hieke, Philip Böhler, David Schlütermann, Fabian Stuhldreier, Jan Cox, Katharina Schmitz, Sabine Seggewiß, Christoph Peter, Anja Stefanski, Kai Stühler, Astrid Tschapek, Axel Gödecke & Björn Stork. *The autophagy-initiating kinase ULK1 controls RIPK1-mediated cell death*. **Submitted to CELL REPORTS**. [*] equal first author. The author of this dissertation conceived and designed the project, carried out the majority of these experiments, independently wrote the raw manuscript. Total contribution: about 70%.

Wenxian Wu, Xiaojing Wang, Niklas Berleth, Jana Deitersen, David Schlütermann, Fabian Stuhldreier, Nora Wallot-Hieke, Maria José Mendiburo, Christoph Peter & Björn Stork. *Pro-necroptotic RIPK3 controls AMPK activity to regulate autophagy*. **Submitted to AUTOPHAGY.** The author of this dissertation conceived and designed the project, carried out the majority of these experiments, independently wrote the raw manuscript. Total contribution: about 80%.

Additional publications:

Wallot-Hieke N, Verma N, Schlütermann D, Berleth N, Deitersen J, Böhler P, Stuhldreier F, **Wu W**, Seggewiß S, Peter C, Gohlke H, Mizushima N and Stork B. (2018) *Systematic Analysis of ATG13 Domain Requirements for Autophagy Induction*. Autophagy 14(5): 743-763.

Schlütermann D, Skowron MA, Berleth N, Böhler P, Deitersen J, Stuhldreier F, Wallot-Hieke N, **Wu W**, Peter C, Hoffmann MJ, Niegisch G and Stork B. (2018) *Targeting Urothelial Carcinoma Cells by Combining Cisplatin with a Specific Inhibitor of the Autophagy-Inducing Class III PtdIns3K Complex*. Urol Oncol 36(4): 160.e1-160.e13

Böhler P, Stuhldreier F, Anand R, Kondadi AK, Schlütermann D, Berleth N, Deitersen J, Wallot-Hieke N, **Wu W**, Frank M, Niemann H, Wesbuer E, Barbian A, Luyten T, Parys JB, Weidtkamp-Peters S, Borchardt A, Reichert AS, Peña-Blanco A, García-Sáez AJ, Itskanov S, van der Bliek AM, Proksch P, Wesselborg S and Stork B. (2018) *The Mycotoxin Phomoxanthone A Disturbs the Form and Function of the Inner Mitochondrial Membrane*. Cell Death Dis 9(3): 286.

4. Discussion

Apoptosis is a form of programmed cell death accompanied by high caspase activation, ultimately resulting in the cleavage of multiple cellular proteins. Necroptosis, another form of regulated cell death, is strictly controlled by caspase 8 and mediated by RIPK1, RIPK3 and MLKL. In most conditions, autophagy serves as pro-survival mechanism by degrading harmful intracellular materials. However, autophagy can sometimes promote cell death via selectively degrading pro-survival proteins and act as a form of regulated cell death.

So far, apoptosis and necroptosis are both well characterized signaling pathways, which cross-regulate each other via controlling the activity of caspase 8. Specifically, necroptosis can occur if caspase 8-mediated apoptotic cell death is inhibited by pharmacological compounds (e.g. Q-VD-OPh or z-VAD-FMK) under certain conditions. Meanwhile, pro-necroptotic RIPK3 can also function as a platform for the induction of apoptosis, independent of its kinase activity (Mandal et al., 2014; Newton et al., 2014). The crosstalk between apoptosis and autophagy is also well studied and is regulated by the balance of caspases, ATG proteins and Bcl-2. Nevertheless, the cross-regulation between necroptosis and autophagy is still poorly understood duo to the limited amount of studies so far. In this context, my thesis focused on the study of the cross-regulation of necroptosis and autophagy, with special regard to the RIPK1-RIPK3 and AMPK-ULK1 kinase complexes that represent the central signaling nodes of necroptosis and autophagy, respectively.

RIPK1 is a master regulator of apoptotic and necroptotic cell death. During these processes, its kinase activity is essential for the induction of necroptosis and most often required for the induction of apoptosis. Thereby, RIPK1 kinase activity has to be tightly controlled via posttranslational modifications including ubiquitination and phosphorylation. Ubiquitin chains on RIPK1 not only stabilize TNF receptor signaling complex I and inhibit RIPK1 activity, but also serve as a platform to recruit other kinases to further inhibit RIPK1 activity via direct phosphorylation. For example, linear-linked ubiquitin chains in complex I recruit IKK kinase complex (IKKα, IKKβ, and NEMO) via the interaction between NEMO and ubiquitin chains, where IKK kinase directly phosphorylates RIPK1 in the kinase domain (Ser 25, Ser 166) and in the intermediate domain (Ser 296, Ser 331, Ser 416) to inhibit RIPK1 activity and hence complex II formation (Dondelinger et al., 2015). In addition, TAK/TAB kinase complex (TAK1/TAB2/TAB3) can also be recruited to complex I via K63-linked ubiquitin chains, where TAK1 kinase directly phosphorylates RIPK1 at Ser 320 to block its activity (Geng et al., 2017). But this report is challenged by the studies from three other groups who showed that MK2/p38, the downstream kinase of TAK/TAB directly mediates the phosphorylation of RIPK1 at Ser 320 and Ser 335 (Dondelinger et al., 2017; Jaco et al., 2017; Menon et al.,

2017). Although the two phospho-acceptor sites Ser 320 and Ser 335 were also identified by mass spectrometry using recombinant ULK1 in this thesis, exchange of both serines for alanines did not change the detected signal of ULK1-dependent phosphorylation *in vitro*. However, the mutation of Ser 357 to alanine clearly reduced ULK1-mediated phosphorylation and additionally enhanced the formation of complex II and hence TNF-mediated cell death. Furthermore, a specific RIPK1 phospho-Ser 357 antibody was generated and the ULK1-dependent phosphorylation at Ser 357 was further confirmed *in vivo*. Recently, two groups reported that TBK1 is also recruited to complex I to phosphorylate RIPK1 and to restrict its activity (Lafont et al., 2018; Xu et al., 2018). To date, several kinase complexes contribute to the regulation of RIPK1 activity in complex I (TAK1, IKK, TBK1) or in the cytosol (MK2/p38, ULK1), but it appears that they function as inhibitory kinases independently of each other, since mutant cells harboring single deletion of these kinases are still sensitive to TNFα treatment.

One central question of this study was where ULK1 phosphorylates RIPK1, in the membrane-associated complex I or in the cytosol. The results indicate that the phosphorylation events predominantly occur in the cytosol, even though ULK1 can be recruited to the complex I. This might be explained by two models: 1) since there are various ubiquitin ligases and kinases in complex I, it is possible ULK1 can be ubiquitinated and/or phosphorylated and is thereby kept in an inactive state; 2) the poly-ubiquitin chains on RIPK1 prevent the interaction with ULK1 and hence block the phosphorylation within complex I. Although ULK1 cannot phosphorylate RIPK1 in complex I, it seems that the recruitment of ULK1 to complex I inhibits the translocation of activated RIPK1 from complex I to the cytosol. One explanation might be that ULK1 binds to the Ub chains of complex I and prevents the cleavage of Ub chains by de-ubiquitinases, thereby stabilizing complex I.

Although most reports have shown that the ULK1 complex (ULK1, ATG13, FIP200 and ATG101) mainly functions at early stages of the autophagic machinery, it appears that there exist stress-induced autophagy pathways that are either independent of ULK1 or independent of ULK1 association with the remaining complex components (Alers et al., 2011; Hieke et al., 2015; Wallot-Hieke et al., 2018). Furthermore, ULK1 also participates in distinct cellular signaling pathways apart of autophagy. For example, a recent finding shows that ULK1/2 localize to stress granules and phosphorylate valosin-containing protein (VCP), thereby increasing VCP's activity and ability to disassemble stress granules (Wang et al., 2019). Additionally, ULK-mediated phosphorylation of SEC16A can modulate the assembly of ER exit sites and ER-to-Golgi trafficking of specific cargo to regulate cellular homeostasis (Joo et al., 2016). Next, ULK1 can also serve as a key mediator of type I IFNR-generated signals that control gene transcription and induction of antineoplastic responses (Saleiro et al., 2015). Moreover, ULK1 directly

phosphorylates STING (stimulator of interferon genes) to prevent sustained innate immune signaling triggered by cyclic dinucleotides (Konno et al., 2013). Additionally, ULK1-dependent phosphorylation of Syntenin-1 (a PDZ domain-containing adaptor that controls trafficking of transmembrane proteins) regulates the interaction between Syntenin-1 and ubiquitin chains (Rajesh et al., 2011). According to the data obtained in this study, one additional autophagy-independent function of ULK1 was identified and characterized, i.e. the regulation of necroptosis via controlling RIPK1 activity and complex II formation.

The second central finding of this thesis is the observation that necroptosis can also regulate autophagy. One group showed that pro-necroptotic protein RIPK3 positively regulates autophagy flux since deficiency of RIPK3 blocks autophagic flux and results in the accumulation of autophagosomes and amphisomes (Harris et al., 2015). Another group reported that RIPK3 rather serves as a negative regulator of selective autophagy by binding to p62/SQSTM1 and thus regulating the interaction of the p62/SQSTM1-LC3 complex (Matsuzawa et al., 2015). So far, the precise molecular mechanism about the interconnection of autophagy and necroptosis is not clear. Here, a new regulatory function of RIPK3 in autophagy was identified upon TNFα/Q-VD-OPh (QVD) treatment in L929 cells. RIPK3 regulates autophagic flux upon TNFα/QVD treatment since deletion of RIPK3 inhibits LC3-II accumulation in L929 cells. More interestingly, during this process early pro-autophagic signals are not blocked, they are even activated (e.g. pro-autophagic markers like phosphorylation of ULK1 at Ser 555, Beclin1 at Ser 91 and AMPK at Thr 172/Thr 183). These phosphorylation events are directly mediated via the RIPK3-AMPK axis, i.e., RIPK3 phosphorylates AMPK at Thr 172/Thr 183 to induce its activity. Reversely, active AMPK can then affect autophagy flux via phosphorylating downstream kinases such as ULK1 and PI3K complexes. One open question is why RIPK3 has different regulatory functions on autophagy: on one side, RIPK3 inhibits LC3-II degradation in lysosome upon TNFα/QVD stimulation; on the other side, RIPK3 activates pro-autophagic proteins to induce autophagy. In order to profoundly explain the controversial results, the regulatory functions of RIPK3 in early and late autophagy have to be separated. As most reports show, the high phosphorylation status of autophagic proteins like ULK1, Beclin1 or AMPK indicates a potential autophagic activating effect (Egan et al., 2011; Kim et al., 2013). Although TNFα-induced necroptosis results in the activation of early autophagic signals, it is possible that necroptosis simultaneously inhibits the growth of autophagosomes, resulting in the accumulation of incomplete and immature autophagosomes. Of note, depletion of WIPI4 results in high LC3-II levels and the accumulation of enlarged and unclosed autophagosomes, suggesting that WIPI4 can regulate the growth and hence affect the size of autophagosomes (Bakula et al., 2017; Lu et al., 2011). A similar phenotype can be observed for the deletion of ATG2A and ATG2B, leading to the increase of LC3-II levels and the

formation of enlarged LC3 dots (Velikkakath et al., 2012). Accordingly, it has to be determined how necroptosis mediates LC3-II accumulation in the final step of autophagy upon TNFα/QVD treatment. It seems that the treatment of TNFα/QVD has no effect on lysosomal functions in L929 cells since the lysosomal cathepsins CTSB and CTSL remain functional, which is not the case upon treatment with bafilomycin A1 as positive control. There exist three models how the observed phenomenon can be explained: 1) Necroptosis induced by TNFα might mediate the degradation of SNARE proteins like syntaxin17 or Ykt 6 to disturb the fusion between autophagosomes and lysosomes; 2) Necroptosis induced by TNFα might inhibit the fusion of autophagosomes and lysosomes via disturbing the complex formation of syntaxin17/SNAP-29/VAMP8 which is essential for the process; 3) TNFα-induced necroptosis might disturb autophagosome growth via regulating the expression of intracellular WIPIs, ATG2A or ATG2B.

Another point to be discussed here is the regulation of AMPK activity. As AMPK is the central energy sensor of a cell, it is sensitive to the energy status, reactive oxygen species (ROS) levels or even pharmacological treatments. As described in the introduction, LKB1, CaMKK2, and TAK1 can phosphorylate AMPK. In this thesis, RIPK3 was identified as a novel AMPK activator. Nevertheless, a contribution of RIPK3-independent activation of AMPK during necroptosis cannot be excluded since a previous study has shown that necroptosis can result in decreased intracellular ATP levels, indicating that LKB1 probably also contributes to AMPK activation during necroptosis. In summary, within this thesis two new cross-regulatory pathways in the autophagy and necroptosis signaling network were identified, i.e., the RIPK1-ULK1 and RIPK3-AMPK axes. These data might pave the way for further studies focusing on the crosstalk between autophagy and necroptosis.

5. References

Alers, S., Loffler, A.S., Paasch, F., Dieterle, A.M., Keppeler, H., Lauber, K., Campbell, D.G., Fehrenbacher, B., Schaller, M., Wesselborg, S., et al. (2011). Atg13 and FIP200 act independently of Ulk1 and Ulk2 in autophagy induction. Autophagy 7, 1423-1433.

Alers, S., Loffler, A.S., Wesselborg, S., and Stork, B. (2012). Role of AMPK-mTOR-Ulk1/2 in the regulation of autophagy: cross talk, shortcuts, and feedbacks. Molecular and cellular biology 32, 2-11.

Alexopoulou, L., Holt, A.C., Medzhitov, R., and Flavell, R.A. (2001). Recognition of double-stranded RNA and activation of NF-kappaB by Toll-like receptor 3. Nature 413, 732-738.

Annibaldi, A., and Meier, P. (2018). Checkpoints in TNF-Induced Cell Death: Implications in Inflammation and Cancer. Trends in molecular medicine 24, 49-65.

Annibaldi, A., Wicky John, S., Vanden Berghe, T., Swatek, K.N., Ruan, J., Liccardi, G., Bianchi, K., Elliott, P.R., Choi, S.M., Van Coillie, S., et al. (2018). Ubiquitin-Mediated Regulation of RIPK1 Kinase Activity Independent of IKK and MK2. Molecular cell 69, 566-580 e565.

Axe, E.L., Walker, S.A., Manifava, M., Chandra, P., Roderick, H.L., Habermann, A., Griffiths, G., and Ktistakis, N.T. (2008). Autophagosome formation from membrane compartments enriched in phosphatidylinositol 3-phosphate and dynamically connected to the endoplasmic reticulum. The Journal of cell biology 182, 685-701.

Bai, H., Inoue, J., Kawano, T., and Inazawa, J. (2012). A transcriptional variant of the LC3A gene is involved in autophagy and frequently inactivated in human cancers. Oncogene 31, 4397-4408.

Bakula, D., Muller, A.J., Zuleger, T., Takacs, Z., Franz-Wachtel, M., Thost, A.K., Brigger, D., Tschan, M.P., Frickey, T., Robenek, H., et al. (2017). WIPI3 and WIPI4 beta-propellers are scaffolds for LKB1-AMPK-TSC signalling circuits in the control of autophagy. Nature communications 8, 15637.

Barnhart, B.C., Lee, J.C., Alappat, E.C., and Peter, M.E. (2003). The death effector domain protein family. Oncogene 22, 8634-8644.

Bas, L., Papinski, D., Licheva, M., Torggler, R., Rohringer, S., Schuschnig, M., and Kraft, C. (2018). Reconstitution reveals Ykt6 as the autophagosomal SNARE in autophagosome-vacuole fusion. The Journal of cell biology 217, 3656-3669.

Berger, S.B., Kasparcova, V., Hoffman, S., Swift, B., Dare, L., Schaeffer, M., Capriotti, C., Cook, M., Finger, J., Hughes-Earle, A., et al. (2014). Cutting Edge: RIP1 kinase activity is dispensable for normal development but is a key regulator of inflammation in SHARPIN-deficient mice. Journal of immunology 192, 5476-5480.

Bertrand, M.J., Milutinovic, S., Dickson, K.M., Ho, W.C., Boudreault, A., Durkin, J., Gillard, J.W., Jaquith, J.B., Morris, S.J., and Barker, P.A. (2008). cIAP1 and cIAP2 facilitate cancer cell survival by functioning as E3 ligases that promote RIP1 ubiquitination. Molecular cell 30, 689-700.

Betin, V.M., and Lane, J.D. (2009). Caspase cleavage of Atg4D stimulates GABARAP-L1 processing and triggers mitochondrial targeting and apoptosis. Journal of cell science 122, 2554-2566.

Bhutia, S.K., Praharaj, P.P., Bhol, C.S., Panigrahi, D.P., Mahapatra, K.K., Patra, S., Saha, S., Das, D.N., Mukhopadhyay, S., Sinha, N., et al. (2019). Monitoring and Measuring Mammalian Autophagy. Methods in molecular biology 1854, 209-222.

Birgisdottir, A.B., Lamark, T., and Johansen, T. (2013). The LIR motif - crucial for selective autophagy. Journal of cell science 126, 3237-3247.

Chen, W., Zhou, Z., Li, L., Zhong, C.Q., Zheng, X., Wu, X., Zhang, Y., Ma, H., Huang, D., Li, W., et al. (2013). Diverse sequence determinants control human and mouse receptor interacting protein 3 (RIP3) and mixed lineage kinase domain-like (MLKL) interaction in necroptotic signaling. The Journal of biological chemistry 288, 16247-16261.

Cho, Y.S., Challa, S., Moquin, D., Genga, R., Ray, T.D., Guildford, M., and Chan, F.K. (2009). Phosphorylation-driven assembly of the RIP1-RIP3 complex regulates programmed necrosis and virus-induced inflammation. Cell 137, 1112-1123.

Conte, D., Holcik, M., Lefebvre, C.A., Lacasse, E., Picketts, D.J., Wright, K.E., and Korneluk, R.G. (2006). Inhibitor of apoptosis protein cIAP2 is essential for lipopolysaccharide-induced macrophage survival. Molecular and cellular biology 26, 699-708.

Conze, D.B., Albert, L., Ferrick, D.A., Goeddel, D.V., Yeh, W.C., Mak, T., and Ashwell, J.D. (2005). Posttranscriptional downregulation of c-IAP2 by the ubiquitin protein ligase c-IAP1 in vivo. Molecular and cellular biology 25, 3348-3356.

Czabotar, P.E., Lessene, G., Strasser, A., and Adams, J.M. (2014). Control of apoptosis by the BCL-2 protein family: implications for physiology and therapy. Nature reviews. Molecular cell biology 15, 49-63.

Degterev, A., Hitomi, J., Germscheid, M., Ch'en, I.L., Korkina, O., Teng, X., Abbott, D., Cuny, G.D., Yuan, C., Wagner, G., et al. (2008). Identification of RIP1 kinase as a specific cellular target of necrostatins. Nature chemical biology 4, 313-321.

Degterev, A., Huang, Z., Boyce, M., Li, Y., Jagtap, P., Mizushima, N., Cuny, G.D., Mitchison, T.J., Moskowitz, M.A., and Yuan, J. (2005). Chemical inhibitor of nonapoptotic cell death with therapeutic potential for ischemic brain injury. Nature chemical biology 1, 112-119.

Dillon, C.P., Oberst, A., Weinlich, R., Janke, L.J., Kang, T.B., Ben-Moshe, T., Mak, T.W., Wallach, D., and Green, D.R. (2012). Survival function of the FADD-CASPASE-8-cFLIP(L) complex. Cell reports 1, 401-407.

Dillon, C.P., Weinlich, R., Rodriguez, D.A., Cripps, J.G., Quarato, G., Gurung, P., Verbist, K.C., Brewer, T.L., Llambi, F., Gong, Y.N., et al. (2014). RIPK1 blocks early postnatal lethality mediated by caspase-8 and RIPK3. Cell 157, 1189-1202.

Dondelinger, Y., Declercq, W., Montessuit, S., Roelandt, R., Goncalves, A., Bruggeman, I., Hulpiau, P., Weber, K., Sehon, C.A., Marquis, R.W., et al. (2014). MLKL compromises plasma membrane integrity by binding to phosphatidylinositol phosphates. Cell reports 7, 971-981.

Dondelinger, Y., Delanghe, T., Rojas-Rivera, D., Priem, D., Delvaeye, T., Bruggeman, I., Van Herreweghe, F., Vandenabeele, P., and Bertrand, M.J.M. (2017). MK2 phosphorylation of RIPK1 regulates TNF-mediated cell death. Nature cell biology 19, 1237-1247.

Dondelinger, Y., Jouan-Lanhouet, S., Divert, T., Theatre, E., Bertin, J., Gough, P.J., Giansanti, P., Heck, A.J., Dejardin, E., Vandenabeele, P., et al. (2015). NF-kappaB-Independent Role of IKKalpha/IKKbeta in Preventing RIPK1 Kinase-Dependent Apoptotic and Necroptotic Cell Death during TNF Signaling. Molecular cell 60, 63-76.

Dooley, H.C., Razi, M., Polson, H.E., Girardin, S.E., Wilson, M.I., and Tooze, S.A. (2014). WIPI2 links LC3 conjugation with PI3P, autophagosome formation, and pathogen clearance by recruiting Atg12-5-16L1. Molecular cell 55, 238-252.

Draber, P., Kupka, S., Reichert, M., Draberova, H., Lafont, E., de Miguel, D., Spilgies, L., Surinova, S., Taraborrelli, L., Hartwig, T., et al. (2015). LUBAC-Recruited CYLD and A20 Regulate Gene Activation and Cell Death by Exerting Opposing Effects on Linear Ubiquitin in Signaling Complexes. Cell reports 13, 2258-2272.

Dynek, J.N., Goncharov, T., Dueber, E.C., Fedorova, A.V., Izrael-Tomasevic, A., Phu, L., Helgason, E., Fairbrother, W.J., Deshayes, K., Kirkpatrick, D.S., et al. (2010). c-IAP1 and UbcH5 promote K11-linked polyubiquitination of RIP1 in TNF signalling. The EMBO journal 29, 4198-4209.

Egan, D.F., Chun, M.G., Vamos, M., Zou, H., Rong, J., Miller, C.J., Lou, H.J., Raveendra-Panickar, D., Yang, C.C., Sheffler, D.J., et al. (2015). Small Molecule Inhibition of the Autophagy Kinase ULK1 and Identification of ULK1 Substrates. Molecular cell 59, 285-297.

Egan, D.F., Shackelford, D.B., Mihaylova, M.M., Gelino, S., Kohnz, R.A., Mair, W., Vasquez, D.S., Joshi, A., Gwinn, D.M., Taylor, R., et al. (2011). Phosphorylation of ULK1 (hATG1) by AMP-activated protein kinase connects energy sensing to mitophagy. Science 331, 456-461.

Elliott, P.R., Leske, D., Hrdinka, M., Bagola, K., Fiil, B.K., McLaughlin, S.H., Wagstaff, J., Volkmar, N., Christianson, J.C., Kessler, B.M., et al. (2016). SPATA2 Links CYLD to LUBAC, Activates CYLD, and Controls LUBAC Signaling. Molecular cell 63, 990-1005.

Fan, W., Guo, J., Gao, B., Zhang, W., Ling, L., Xu, T., Pan, C., Li, L., Chen, S., Wang, H., et al. (2019). Flotillin-mediated endocytosis and ALIX-syntenin-1-mediated exocytosis protect the cell membrane from damage caused by necroptosis. Science signaling 12.

Feng, S., Yang, Y., Mei, Y., Ma, L., Zhu, D.E., Hoti, N., Castanares, M., and Wu, M. (2007). Cleavage of RIP3 inactivates its caspase-independent apoptosis pathway by removal of kinase domain. Cellular signalling 19, 2056-2067.

Feng, Y., He, D., Yao, Z., and Klionsky, D.J. (2014). The machinery of macroautophagy. Cell research 24, 24-41.

Fujita, H., Rahighi, S., Akita, M., Kato, R., Sasaki, Y., Wakatsuki, S., and Iwai, K. (2014). Mechanism underlying IkappaB kinase activation mediated by the linear ubiquitin chain assembly complex. Molecular and cellular biology 34, 1322-1335.

Fujita, H., Tokunaga, A., Shimizu, S., Whiting, A.L., Aguilar-Alonso, F., Takagi, K., Walinda, E., Sasaki, Y., Shimokawa, T., Mizushima, T., et al. (2018). Cooperative Domain Formation by Homologous Motifs in HOIL-1L and SHARPIN Plays A Crucial Role in LUBAC Stabilization. Cell reports 23, 1192-1204.

Galluzzi, L., Bravo-San Pedro, J.M., Vitale, I., Aaronson, S.A., Abrams, J.M., Adam, D., Alnemri, E.S., Altucci, L., Andrews, D., Annicchiarico-Petruzzelli, M., et al. (2015). Essential versus accessory aspects of cell death: recommendations of the NCCD 2015. Cell death and differentiation 22, 58-73.

Galluzzi, L., Lopez-Soto, A., Kumar, S., and Kroemer, G. (2016). Caspases Connect Cell-Death Signaling to Organismal Homeostasis. Immunity 44, 221-231.

Galluzzi, L., Vitale, I., Aaronson, S.A., Abrams, J.M., Adam, D., Agostinis, P., Alnemri, E.S., Altucci, L., Amelio, I., Andrews, D.W., et al. (2018). Molecular mechanisms of cell death: recommendations of the Nomenclature Committee on Cell Death 2018. Cell death and differentiation 25, 486-541.

Galluzzi, L., Vitale, I., Abrams, J.M., Alnemri, E.S., Baehrecke, E.H., Blagosklonny, M.V., Dawson, T.M., Dawson, V.L., El-Deiry, W.S., Fulda, S., et al. (2012). Molecular definitions of cell death subroutines: recommendations of the Nomenclature Committee on Cell Death 2012. Cell death and differentiation 19, 107-120.

Ge, L., Melville, D., Zhang, M., and Schekman, R. (2013). The ER-Golgi intermediate compartment is a key membrane source for the LC3 lipidation step of autophagosome biogenesis. eLife 2, e00947.

Geng, J., Ito, Y., Shi, L., Amin, P., Chu, J., Ouchida, A.T., Mookhtiar, A.K., Zhao, H., Xu, D., Shan, B., et al. (2017). Regulation of RIPK1 activation by TAK1-mediated phosphorylation dictates apoptosis and necroptosis. Nature communications 8, 359.

Gong, Y.N., Guy, C., Olauson, H., Becker, J.U., Yang, M., Fitzgerald, P., Linkermann, A., and Green, D.R. (2017). ESCRT-III Acts Downstream of MLKL to Regulate Necroptotic Cell Death and Its Consequences. Cell 169, 286-300 e216.

Goodall, M.L., Fitzwalter, B.E., Zahedi, S., Wu, M., Rodriguez, D., Mulcahy-Levy, J.M., Green, D.R., Morgan, M., Cramer, S.D., and Thorburn, A. (2016). The Autophagy Machinery Controls Cell Death Switching between Apoptosis and Necroptosis. Developmental cell 37, 337-349.

Graef, M., Friedman, J.R., Graham, C., Babu, M., and Nunnari, J. (2013). ER exit sites are physical and functional core autophagosome biogenesis components. Molecular biology of the cell 24, 2918-2931.

Green, D.R., Ferguson, T., Zitvogel, L., and Kroemer, G. (2009). Immunogenic and tolerogenic cell death. Nature reviews. Immunology 9, 353-363.

Grootjans, S., Vanden Berghe, T., and Vandenabeele, P. (2017). Initiation and execution mechanisms of necroptosis: an overview. Cell death and differentiation 24, 1184-1195.

Gwinn, D.M., Shackelford, D.B., Egan, D.F., Mihaylova, M.M., Mery, A., Vasquez, D.S., Turk, B.E., and Shaw, R.J. (2008). AMPK phosphorylation of raptor mediates a metabolic checkpoint. Molecular cell 30, 214-226.

Haas, T.L., Emmerich, C.H., Gerlach, B., Schmukle, A.C., Cordier, S.M., Rieser, E., Feltham, R., Vince, J., Warnken, U., Wenger, T., et al. (2009). Recruitment of the linear ubiquitin chain assembly complex stabilizes the TNF-R1 signaling complex and is required for TNF-mediated gene induction. Molecular cell 36, 831-844.

Hamasaki, M., Furuta, N., Matsuda, A., Nezu, A., Yamamoto, A., Fujita, N., Oomori, H., Noda, T., Haraguchi, T., Hiraoka, Y., et al. (2013). Autophagosomes form at ER-mitochondria contact sites. Nature 495, 389-393.

Harris, K.G., Morosky, S.A., Drummond, C.G., Patel, M., Kim, C., Stolz, D.B., Bergelson, J.M., Cherry, S., and Coyne, C.B. (2015). RIP3 Regulates Autophagy and Promotes Coxsackievirus B3 Infection of Intestinal Epithelial Cells. Cell host & microbe 18, 221-232.

He, S., Liang, Y., Shao, F., and Wang, X. (2011). Toll-like receptors activate programmed necrosis in macrophages through a receptor-interacting kinase-3-mediated pathway. Proceedings of the National Academy of Sciences of the United States of America 108, 20054-20059.

He, S., Wang, L., Miao, L., Wang, T., Du, F., Zhao, L., and Wang, X. (2009). Receptor interacting protein kinase-3 determines cellular necrotic response to TNF-alpha. Cell 137, 1100-1111.

He, S., and Wang, X. (2018). RIP kinases as modulators of inflammation and immunity. Nature immunology 19, 912-922.

Heard, K.N., Bertrand, M.J., and Barker, P.A. (2015). cIAP2 supports viability of mice lacking cIAP1 and XIAP. The EMBO journal 34, 2393-2395.

Heger, K., Wickliffe, K.E., Ndoja, A., Zhang, J., Murthy, A., Dugger, D.L., Maltzman, A., de Sousa, E.M.F., Hung, J., Zeng, Y., et al. (2018). OTULIN limits cell death and inflammation by deubiquitinating LUBAC. Nature 559, 120-124.

Hieke, N., Loffler, A.S., Kaizuka, T., Berleth, N., Bohler, P., Driessen, S., Stuhldreier, F., Friesen, O., Assani, K., Schmitz, K., et al. (2015). Expression of a ULK1/2 binding-deficient ATG13 variant can partially restore autophagic activity in ATG13-deficient cells. Autophagy 11, 1471-1483.

Hildebrand, J.M., Tanzer, M.C., Lucet, I.S., Young, S.N., Spall, S.K., Sharma, P., Pierotti, C., Garnier, J.M., Dobson, R.C., Webb, A.I., et al. (2014). Activation of the pseudokinase MLKL unleashes the four-helix bundle domain to induce membrane localization and necroptotic cell death. Proceedings of the National Academy of Sciences of the United States of America 111, 15072-15077.

Hoshino, K., Takeuchi, O., Kawai, T., Sanjo, H., Ogawa, T., Takeda, Y., Takeda, K., and Akira, S. (1999). Cutting edge: Toll-like receptor 4 (TLR4)-deficient mice are hyporesponsive to lipopolysaccharide: evidence for TLR4 as the Lps gene product. Journal of immunology 162, 3749-3752.

Huang, W., Choi, W., Hu, W., Mi, N., Guo, Q., Ma, M., Liu, M., Tian, Y., Lu, P., Wang, F.L., et al. (2012). Crystal structure and biochemical analyses reveal Beclin 1 as a novel membrane binding protein. Cell research 22, 473-489.

Ichimura, Y., Kirisako, T., Takao, T., Satomi, Y., Shimonishi, Y., Ishihara, N., Mizushima, N., Tanida, I., Kominami, E., Ohsumi, M., et al. (2000). A ubiquitin-like system mediates protein lipidation. Nature 408, 488-492.

Ikeda, F., Deribe, Y.L., Skanland, S.S., Stieglitz, B., Grabbe, C., Franz-Wachtel, M., van Wijk, S.J., Goswami, P., Nagy, V., Terzic, J., et al. (2011). SHARPIN forms a linear ubiquitin ligase complex regulating NF-kappaB activity and apoptosis. Nature 471, 637-641.

Inoki, K., Li, Y., Xu, T., and Guan, K.L. (2003a). Rheb GTPase is a direct target of TSC2 GAP activity and regulates mTOR signaling. Genes & development 17, 1829-1834.

Inoki, K., Zhu, T., and Guan, K.L. (2003b). TSC2 mediates cellular energy response to control cell growth and survival. Cell 115, 577-590.

Itakura, E., Kishi-Itakura, C., and Mizushima, N. (2012). The hairpin-type tail-anchored SNARE syntaxin 17 targets to autophagosomes for fusion with endosomes/lysosomes. Cell 151, 1256-1269.

Itakura, E., Kishi, C., Inoue, K., and Mizushima, N. (2008). Beclin 1 forms two distinct phosphatidylinositol 3-kinase complexes with mammalian Atg14 and UVRAG. Molecular biology of the cell 19, 5360-5372.

Jaco, I., Annibaldi, A., Lalaoui, N., Wilson, R., Tenev, T., Laurien, L., Kim, C., Jamal, K., Wicky John, S., Liccardi, G., et al. (2017). MK2 Phosphorylates RIPK1 to Prevent TNF-Induced Cell Death. Molecular cell 66, 698-710 e695.

Joo, J.H., Wang, B., Frankel, E., Ge, L., Xu, L., Iyengar, R., Li-Harms, X., Wright, C., Shaw, T.I., Lindsten, T., et al. (2016). The Noncanonical Role of ULK/ATG1 in ER-to-Golgi Trafficking Is Essential for Cellular Homeostasis. Molecular cell 62, 491-506.

Jung, C.H., Jun, C.B., Ro, S.H., Kim, Y.M., Otto, N.M., Cao, J., Kundu, M., and Kim, D.H. (2009). ULK-Atg13-FIP200 complexes mediate mTOR signaling to the autophagy machinery. Molecular biology of the cell 20, 1992-2003.

Kaiser, W.J., Daley-Bauer, L.P., Thapa, R.J., Mandal, P., Berger, S.B., Huang, C., Sundararajan, A., Guo, H., Roback, L., Speck, S.H., et al. (2014). RIP1 suppresses innate immune necrotic as well as apoptotic cell death during mammalian parturition. Proceedings of the National Academy of Sciences of the United States of America 111, 7753-7758.

Kaiser, W.J., Sridharan, H., Huang, C., Mandal, P., Upton, J.W., Gough, P.J., Sehon, C.A., Marquis, R.W., Bertin, J., and Mocarski, E.S. (2013). Toll-like receptor 3-mediated necrosis via TRIF, RIP3, and MLKL. The Journal of biological chemistry 288, 31268-31279.

Kanayama, A., Seth, R.B., Sun, L., Ea, C.K., Hong, M., Shaito, A., Chiu, Y.H., Deng, L., and Chen, Z.J. (2004). TAB2 and TAB3 activate the NF-kappaB pathway through binding to polyubiquitin chains. Molecular cell 15, 535-548.

Karanasios, E., Walker, S.A., Okkenhaug, H., Manifava, M., Hummel, E., Zimmermann, H., Ahmed, Q., Domart, M.C., Collinson, L., and Ktistakis, N.T. (2016). Autophagy initiation by ULK complex assembly on ER tubulovesicular regions marked by ATG9 vesicles. Nature communications 7, 12420.

Kerr, J.F., Wyllie, A.H., and Currie, A.R. (1972). Apoptosis: a basic biological phenomenon with wide-ranging implications in tissue kinetics. British journal of cancer 26, 239-257.

Kim, J., Kim, Y.C., Fang, C., Russell, R.C., Kim, J.H., Fan, W., Liu, R., Zhong, Q., and Guan, K.L. (2013). Differential regulation of distinct Vps34 complexes by AMPK in nutrient stress and autophagy. Cell 152, 290-303.

Kim, J., Kundu, M., Viollet, B., and Guan, K.L. (2011). AMPK and mTOR regulate autophagy through direct phosphorylation of Ulk1. Nature cell biology 13, 132-141.

Kim, Y.M., Jung, C.H., Seo, M., Kim, E.K., Park, J.M., Bae, S.S., and Kim, D.H. (2015). mTORC1 phosphorylates UVRAG to negatively regulate autophagosome and endosome maturation. Molecular cell 57, 207-218.

Kishi-Itakura, C., Koyama-Honda, I., Itakura, E., and Mizushima, N. (2014). Ultrastructural analysis of autophagosome organization using mammalian autophagy-deficient cells. Journal of cell science 127, 4089-4102.

Kolb, J.P., Oguin, T.H., 3rd, Oberst, A., and Martinez, J. (2017). Programmed Cell Death and Inflammation: Winter Is Coming. Trends in immunology 38, 705-718.

Komander, D., and Barford, D. (2008). Structure of the A20 OTU domain and mechanistic insights into deubiquitination. The Biochemical journal 409, 77-85.

Konno, H., Konno, K., and Barber, G.N. (2013). Cyclic dinucleotides trigger ULK1 (ATG1) phosphorylation of STING to prevent sustained innate immune signaling. Cell 155, 688-698.

Kroemer, G., El-Deiry, W.S., Golstein, P., Peter, M.E., Vaux, D., Vandenabeele, P., Zhivotovsky, B., Blagosklonny, M.V., Malorni, W., Knight, R.A., et al. (2005). Classification of cell death:

recommendations of the Nomenclature Committee on Cell Death. Cell death and differentiation 12 Suppl 2, 1463-1467.

Kroemer, G., Galluzzi, L., Vandenabeele, P., Abrams, J., Alnemri, E.S., Baehrecke, E.H., Blagosklonny, M.V., El-Deiry, W.S., Golstein, P., Green, D.R., et al. (2009). Classification of cell death: recommendations of the Nomenclature Committee on Cell Death 2009. Cell death and differentiation 16, 3-11.

Kupka, S., De Miguel, D., Draber, P., Martino, L., Surinova, S., Rittinger, K., and Walczak, H. (2016). SPATA2-Mediated Binding of CYLD to HOIP Enables CYLD Recruitment to Signaling Complexes. Cell reports 16, 2271-2280.

Lafont, E., Draber, P., Rieser, E., Reichert, M., Kupka, S., de Miguel, D., Draberova, H., von Massenhausen, A., Bhamra, A., Henderson, S., et al. (2018). TBK1 and IKKepsilon prevent TNF-induced cell death by RIPK1 phosphorylation. Nature cell biology 20, 1389-1399.

Laster, S.M., Wood, J.G., and Gooding, L.R. (1988). Tumor necrosis factor can induce both apoptic and necrotic forms of cell lysis. Journal of immunology 141, 2629-2634.

Li, H., Zhu, H., Xu, C.J., and Yuan, J. (1998). Cleavage of BID by caspase 8 mediates the mitochondrial damage in the Fas pathway of apoptosis. Cell 94, 491-501.

Li, J., McQuade, T., Siemer, A.B., Napetschnig, J., Moriwaki, K., Hsiao, Y.S., Damko, E., Moquin, D., Walz, T., McDermott, A., et al. (2012). The RIP1/RIP3 necrosome forms a functional amyloid signaling complex required for programmed necrosis. Cell 150, 339-350.

Li, P., Nijhawan, D., Budihardjo, I., Srinivasula, S.M., Ahmad, M., Alnemri, E.S., and Wang, X. (1997). Cytochrome c and dATP-dependent formation of Apaf-1/caspase-9 complex initiates an apoptotic protease cascade. Cell 91, 479-489.

Lu, Q., Yang, P., Huang, X., Hu, W., Guo, B., Wu, F., Lin, L., Kovacs, A.L., Yu, L., and Zhang, H. (2011). The WD40 repeat PtdIns(3)P-binding protein EPG-6 regulates progression of omegasomes to autophagosomes. Developmental cell 21, 343-357.

Luo, S., and Rubinsztein, D.C. (2010). Apoptosis blocks Beclin 1-dependent autophagosome synthesis: an effect rescued by Bcl-xL. Cell death and differentiation 17, 268-277.

Maelfait, J., Liverpool, L., Bridgeman, A., Ragan, K.B., Upton, J.W., and Rehwinkel, J. (2017). Sensing of viral and endogenous RNA by ZBP1/DAI induces necroptosis. The EMBO journal 36, 2529-2543.

Mahoney, D.J., Cheung, H.H., Mrad, R.L., Plenchette, S., Simard, C., Enwere, E., Arora, V., Mak, T.W., Lacasse, E.C., Waring, J., et al. (2008). Both cIAP1 and cIAP2 regulate TNFalpha-mediated NF-kappaB activation. Proceedings of the National Academy of Sciences of the United States of America 105, 11778-11783.

Mandal, P., Berger, S.B., Pillay, S., Moriwaki, K., Huang, C., Guo, H., Lich, J.D., Finger, J., Kasparcova, V., Votta, B., et al. (2014). RIP3 induces apoptosis independent of pronecrotic kinase activity. Molecular cell 56, 481-495.

Marino, G., Niso-Santano, M., Baehrecke, E.H., and Kroemer, G. (2014). Self-consumption: the interplay of autophagy and apoptosis. Nature reviews. Molecular cell biology 15, 81-94.

Matsui, T., Jiang, P., Nakano, S., Sakamaki, Y., Yamamoto, H., and Mizushima, N. (2018). Autophagosomal YKT6 is required for fusion with lysosomes independently of syntaxin 17. The Journal of cell biology 217, 2633-2645.

Matsunaga, K., Morita, E., Saitoh, T., Akira, S., Ktistakis, N.T., Izumi, T., Noda, T., and Yoshimori, T. (2010). Autophagy requires endoplasmic reticulum targeting of the PI3-kinase complex via Atg14L. The Journal of cell biology 190, 511-521.

Matsuzawa, Y., Oshima, S., Nibe, Y., Kobayashi, M., Maeyashiki, C., Nemoto, Y., Nagaishi, T., Okamoto, R., Tsuchiya, K., Nakamura, T., et al. (2015). RIPK3 regulates p62-LC3 complex formation via the caspase-8-dependent cleavage of p62. Biochemical and biophysical research communications 456, 298-304.

McIlwain, D.R., Berger, T., and Mak, T.W. (2013). Caspase functions in cell death and disease. Cold Spring Harbor perspectives in biology 5, a008656.

McIlwain, D.R., Berger, T., and Mak, T.W. (2015). Caspase functions in cell death and disease. Cold Spring Harbor perspectives in biology 7.

Menon, M.B., Gropengiesser, J., Fischer, J., Novikova, L., Deuretzbacher, A., Lafera, J., Schimmeck, H., Czymmeck, N., Ronkina, N., Kotlyarov, A., et al. (2017). p38(MAPK)/MK2-dependent phosphorylation controls cytotoxic RIPK1 signalling in inflammation and infection. Nature cell biology 19, 1248-1259.

Mercer, T.J., Gubas, A., and Tooze, S.A. (2018). A molecular perspective of mammalian autophagosome biogenesis. The Journal of biological chemistry 293, 5386-5395.

Metlagel, Z., Otomo, C., Takaesu, G., and Otomo, T. (2013). Structural basis of ATG3 recognition by the autophagic ubiquitin-like protein ATG12. Proceedings of the National Academy of Sciences of the United States of America 110, 18844-18849.

Micheau, O., and Tschopp, J. (2003). Induction of TNF receptor I-mediated apoptosis via two sequential signaling complexes. Cell 114, 181-190.

Mizushima, N. (2010). The role of the Atg1/ULK1 complex in autophagy regulation. Current opinion in cell biology 22, 132-139.

Mizushima, N. (2018). A brief history of autophagy from cell biology to physiology and disease. Nature cell biology 20, 521-527.

Mizushima, N., and Komatsu, M. (2011). Autophagy: renovation of cells and tissues. Cell 147, 728-741.

Mizushima, N., Yoshimori, T., and Ohsumi, Y. (2011). The role of Atg proteins in autophagosome formation. Annual review of cell and developmental biology 27, 107-132.

Moulin, M., Anderton, H., Voss, A.K., Thomas, T., Wong, W.W., Bankovacki, A., Feltham, R., Chau, D., Cook, W.D., Silke, J., et al. (2012). IAPs limit activation of RIP kinases by TNF receptor 1 during development. The EMBO journal 31, 1679-1691.

Munson, M.J., Allen, G.F., Toth, R., Campbell, D.G., Lucocq, J.M., and Ganley, I.G. (2015). mTOR activates the VPS34-UVRAG complex to regulate autolysosomal tubulation and cell survival. The EMBO journal 34, 2272-2290.

Murphy, J.M., Czabotar, P.E., Hildebrand, J.M., Lucet, I.S., Zhang, J.G., Alvarez-Diaz, S., Lewis, R., Lalaoui, N., Metcalf, D., Webb, A.I., et al. (2013). The pseudokinase MLKL mediates necroptosis via a molecular switch mechanism. Immunity 39, 443-453.

Murphy, J.M., Lucet, I.S., Hildebrand, J.M., Tanzer, M.C., Young, S.N., Sharma, P., Lessene, G., Alexander, W.S., Babon, J.J., Silke, J., et al. (2014). Insights into the evolution of divergent nucleotide-binding mechanisms among pseudokinases revealed by crystal structures of human and mouse MLKL. The Biochemical journal 457, 369-377.

Nagata, S. (1997). Apoptosis by death factor. Cell 88, 355-365.

Nagata, S. (2018). Apoptosis and Clearance of Apoptotic Cells. Annual review of immunology 36, 489-517.

Newton, K., Dugger, D.L., Wickliffe, K.E., Kapoor, N., de Almagro, M.C., Vucic, D., Komuves, L., Ferrando, R.E., French, D.M., Webster, J., et al. (2014). Activity of protein kinase RIPK3 determines whether cells die by necroptosis or apoptosis. Science 343, 1357-1360.

Nishimura, T., Tamura, N., Kono, N., Shimanaka, Y., Arai, H., Yamamoto, H., and Mizushima, N. (2017). Autophagosome formation is initiated at phosphatidylinositol synthase-enriched ER subdomains. The EMBO journal 36, 1719-1735.

Oberst, A., Dillon, C.P., Weinlich, R., McCormick, L.L., Fitzgerald, P., Pop, C., Hakem, R., Salvesen, G.S., and Green, D.R. (2011). Catalytic activity of the caspase-8-FLIP(L) complex inhibits RIPK3-dependent necrosis. Nature 471, 363-367.

Ofengeim, D., and Yuan, J. (2013). Regulation of RIP1 kinase signalling at the crossroads of inflammation and cell death. Nature reviews. Molecular cell biology 14, 727-736.

Oral, O., Oz-Arslan, D., Itah, Z., Naghavi, A., Deveci, R., Karacali, S., and Gozuacik, D. (2012). Cleavage of Atg3 protein by caspase-8 regulates autophagy during receptor-activated cell death. Apoptosis : an international journal on programmed cell death 17, 810-820.

Ori, D., Kato, H., Sanjo, H., Tartey, S., Mino, T., Akira, S., and Takeuchi, O. (2013). Essential roles of K63-linked polyubiquitin-binding proteins TAB2 and TAB3 in B cell activation via MAPKs. Journal of immunology 190, 4037-4045.

Orsi, A., Razi, M., Dooley, H.C., Robinson, D., Weston, A.E., Collinson, L.M., and Tooze, S.A. (2012). Dynamic and transient interactions of Atg9 with autophagosomes, but not membrane integration, are required for autophagy. Molecular biology of the cell 23, 1860-1873.

Park, J.M., Jung, C.H., Seo, M., Otto, N.M., Grunwald, D., Kim, K.H., Moriarity, B., Kim, Y.M., Starker, C., Nho, R.S., et al. (2016). The ULK1 complex mediates MTORC1 signaling to the autophagy initiation machinery via binding and phosphorylating ATG14. Autophagy 12, 547-564.

Pasparakis, M., and Vandenabeele, P. (2015). Necroptosis and its role in inflammation. Nature 517, 311-320.

Peltzer, N., Darding, M., Montinaro, A., Draber, P., Draberova, H., Kupka, S., Rieser, E., Fisher, A., Hutchinson, C., Taraborrelli, L., et al. (2018). LUBAC is essential for embryogenesis by preventing cell death and enabling haematopoiesis. Nature 557, 112-117.

Peltzer, N., Darding, M., and Walczak, H. (2016). Holding RIPK1 on the Ubiquitin Leash in TNFR1 Signaling. Trends in cell biology 26, 445-461.

Peltzer, N., Rieser, E., Taraborrelli, L., Draber, P., Darding, M., Pernaute, B., Shimizu, Y., Sarr, A., Draberova, H., Montinaro, A., et al. (2014). HOIP deficiency causes embryonic lethality by aberrant TNFR1-mediated endothelial cell death. Cell reports 9, 153-165.

Peltzer, N., and Walczak, H. (2019). Cell Death and Inflammation - A Vital but Dangerous Liaison. Trends in immunology 40, 387-402.

Pop, C., Oberst, A., Drag, M., Van Raam, B.J., Riedl, S.J., Green, D.R., and Salvesen, G.S. (2011). FLIP(L) induces caspase 8 activity in the absence of interdomain caspase 8 cleavage and alters substrate specificity. The Biochemical journal 433, 447-457.

Puente, C., Hendrickson, R.C., and Jiang, X. (2016). Nutrient-regulated Phosphorylation of ATG13 Inhibits Starvation-induced Autophagy. The Journal of biological chemistry 291, 6026-6035.

Quarato, G., Guy, C.S., Grace, C.R., Llambi, F., Nourse, A., Rodriguez, D.A., Wakefield, R., Frase, S., Moldoveanu, T., and Green, D.R. (2016). Sequential Engagement of Distinct MLKL Phosphatidylinositol-Binding Sites Executes Necroptosis. Molecular cell 61, 589-601.

Rabanal-Ruiz, Y., Otten, E.G., and Korolchuk, V.I. (2017). mTORC1 as the main gateway to autophagy. Essays in biochemistry 61, 565-584.

Rahighi, S., Ikeda, F., Kawasaki, M., Akutsu, M., Suzuki, N., Kato, R., Kensche, T., Uejima, T., Bloor, S., Komander, D., et al. (2009). Specific recognition of linear ubiquitin chains by NEMO is important for NF-kappaB activation. Cell 136, 1098-1109.

Rajesh, S., Bago, R., Odintsova, E., Muratov, G., Baldwin, G., Sridhar, P., Rajesh, S., Overduin, M., and Berditchevski, F. (2011). Binding to syntenin-1 protein defines a new mode of ubiquitin-based interactions regulated by phosphorylation. The Journal of biological chemistry 286, 39606-39614.

Reed, J.C., Doctor, K.S., and Godzik, A. (2004). The domains of apoptosis: a genomics perspective. Science's STKE : signal transduction knowledge environment 2004, re9.

Rickard, J.A., Anderton, H., Etemadi, N., Nachbur, U., Darding, M., Peltzer, N., Lalaoui, N., Lawlor, K.E., Vanyai, H., Hall, C., et al. (2014a). TNFR1-dependent cell death drives inflammation in Sharpin-deficient mice. eLife 3.

Rickard, J.A., O'Donnell, J.A., Evans, J.M., Lalaoui, N., Poh, A.R., Rogers, T., Vince, J.E., Lawlor, K.E., Ninnis, R.L., Anderton, H., et al. (2014b). RIPK1 regulates RIPK3-MLKL-driven systemic inflammation and emergency hematopoiesis. Cell 157, 1175-1188.

Riley, J.S., Malik, A., Holohan, C., and Longley, D.B. (2015). DED or alive: assembly and regulation of the death effector domain complexes. Cell death & disease 6, e1866.

Rodgers, M.A., Bowman, J.W., Fujita, H., Orazio, N., Shi, M., Liang, Q., Amatya, R., Kelly, T.J., Iwai, K., Ting, J., et al. (2014). The linear ubiquitin assembly complex (LUBAC) is essential for NLRP3 inflammasome activation. The Journal of experimental medicine 211, 1333-1347.

Rothe, M., Pan, M.G., Henzel, W.J., Ayres, T.M., and Goeddel, D.V. (1995). The TNFR2-TRAF signaling complex contains two novel proteins related to baculoviral inhibitor of apoptosis proteins. Cell 83, 1243-1252.

Rubinstein, A.D., and Kimchi, A. (2012). Life in the balance - a mechanistic view of the crosstalk between autophagy and apoptosis. Journal of cell science 125, 5259-5268.

Russell, R.C., Tian, Y., Yuan, H., Park, H.W., Chang, Y.Y., Kim, J., Kim, H., Neufeld, T.P., Dillin, A., and Guan, K.L. (2013). ULK1 induces autophagy by phosphorylating Beclin-1 and activating VPS34 lipid kinase. Nature cell biology 15, 741-750.

Sahu, R., Kaushik, S., Clement, C.C., Cannizzo, E.S., Scharf, B., Follenzi, A., Potolicchio, I., Nieves, E., Cuervo, A.M., and Santambrogio, L. (2011). Microautophagy of cytosolic proteins by late endosomes. Developmental cell 20, 131-139.

Saleiro, D., Mehrotra, S., Kroczynska, B., Beauchamp, E.M., Lisowski, P., Majchrzak-Kita, B., Bhagat, T.D., Stein, B.L., McMahon, B., Altman, J.K., et al. (2015). Central role of ULK1 in type I interferon signaling. Cell reports 11, 605-617.

Schlicher, L., Wissler, M., Preiss, F., Brauns-Schubert, P., Jakob, C., Dumit, V., Borner, C., Dengjel, J., and Maurer, U. (2016). SPATA2 promotes CYLD activity and regulates TNF-induced NF-kappaB signaling and cell death. EMBO reports 17, 1485-1497.

Schulze-Osthoff, K., Ferrari, D., Los, M., Wesselborg, S., and Peter, M.E. (1998). Apoptosis signaling by death receptors. European journal of biochemistry 254, 439-459.

Schweichel, J.U., and Merker, H.J. (1973). The morphology of various types of cell death in prenatal tissues. Teratology 7, 253-266.

Shackelford, D.B., and Shaw, R.J. (2009). The LKB1-AMPK pathway: metabolism and growth control in tumour suppression. Nature reviews. Cancer 9, 563-575.

Shan, B., Pan, H., Najafov, A., and Yuan, J. (2018). Necroptosis in development and diseases. Genes & development 32, 327-340.

Shang, L., Chen, S., Du, F., Li, S., Zhao, L., and Wang, X. (2011). Nutrient starvation elicits an acute autophagic response mediated by Ulk1 dephosphorylation and its subsequent dissociation from AMPK. Proceedings of the National Academy of Sciences of the United States of America 108, 4788-4793.

Shaw, R.J., Kosmatka, M., Bardeesy, N., Hurley, R.L., Witters, L.A., DePinho, R.A., and Cantley, L.C. (2004). The tumor suppressor LKB1 kinase directly activates AMP-activated kinase and regulates apoptosis in response to energy stress. Proceedings of the National Academy of Sciences of the United States of America 101, 3329-3335.

Sun, L., Wang, H., Wang, Z., He, S., Chen, S., Liao, D., Wang, L., Yan, J., Liu, W., Lei, X., et al. (2012). Mixed lineage kinase domain-like protein mediates necrosis signaling downstream of RIP3 kinase. Cell 148, 213-227.

Suzuki, K., Akioka, M., Kondo-Kakuta, C., Yamamoto, H., and Ohsumi, Y. (2013). Fine mapping of autophagy-related proteins during autophagosome formation in Saccharomyces cerevisiae. Journal of cell science 126, 2534-2544.

Tait, S.W., and Green, D.R. (2010). Mitochondria and cell death: outer membrane permeabilization and beyond. Nature reviews. Molecular cell biology 11, 621-632.

Takaoka, A., Wang, Z., Choi, M.K., Yanai, H., Negishi, H., Ban, T., Lu, Y., Miyagishi, M., Kodama, T., Honda, K., et al. (2007). DAI (DLM-1/ZBP1) is a cytosolic DNA sensor and an activator of innate immune response. Nature 448, 501-505.

Takats, S., Glatz, G., Szenci, G., Boda, A., Horvath, G.V., Hegedus, K., Kovacs, A.L., and Juhasz, G. (2018). Non-canonical role of the SNARE protein Ykt6 in autophagosome-lysosome fusion. PLoS genetics 14, e1007359.

Tang, D., Kang, R., Berghe, T.V., Vandenabeele, P., and Kroemer, G. (2019). The molecular machinery of regulated cell death. Cell research.

Taylor, R.C., Cullen, S.P., and Martin, S.J. (2008). Apoptosis: controlled demolition at the cellular level. Nature reviews. Molecular cell biology 9, 231-241.

Tibbetts, M.D., Zheng, L., and Lenardo, M.J. (2003). The death effector domain protein family: regulators of cellular homeostasis. Nature immunology 4, 404-409.

Tokunaga, F., Nishimasu, H., Ishitani, R., Goto, E., Noguchi, T., Mio, K., Kamei, K., Ma, A., Iwai, K., and Nureki, O. (2012). Specific recognition of linear polyubiquitin by A20 zinc finger 7 is involved in NF-kappaB regulation. The EMBO journal 31, 3856-3870.

Tokunaga, F., Sakata, S., Saeki, Y., Satomi, Y., Kirisako, T., Kamei, K., Nakagawa, T., Kato, M., Murata, S., Yamaoka, S., et al. (2009). Involvement of linear polyubiquitylation of NEMO in NF-kappaB activation. Nature cell biology 11, 123-132.

Uemura, T., Yamamoto, M., Kametaka, A., Sou, Y.S., Yabashi, A., Yamada, A., Annoh, H., Kametaka, S., Komatsu, M., and Waguri, S. (2014). A cluster of thin tubular structures mediates transformation of the endoplasmic reticulum to autophagic isolation membrane. Molecular and cellular biology 34, 1695-1706.

Upton, J.W., Kaiser, W.J., and Mocarski, E.S. (2012). DAI/ZBP1/DLM-1 complexes with RIP3 to mediate virus-induced programmed necrosis that is targeted by murine cytomegalovirus vIRA. Cell host & microbe 11, 290-297.

Varfolomeev, E., Goncharov, T., Fedorova, A.V., Dynek, J.N., Zobel, K., Deshayes, K., Fairbrother, W.J., and Vucic, D. (2008). c-IAP1 and c-IAP2 are critical mediators of tumor necrosis factor alpha (TNFalpha)-induced NF-kappaB activation. The Journal of biological chemistry 283, 24295-24299.

Velikkakath, A.K., Nishimura, T., Oita, E., Ishihara, N., and Mizushima, N. (2012). Mammalian Atg2 proteins are essential for autophagosome formation and important for regulation of size and distribution of lipid droplets. Molecular biology of the cell 23, 896-909.

Vincenz, C. (2001). Death receptors and apoptosis. Deadly signaling and evasive tactics. Cardiology clinics 19, 31-43.

Wagner, S.A., Satpathy, S., Beli, P., and Choudhary, C. (2016). SPATA2 links CYLD to the TNF-alpha receptor signaling complex and modulates the receptor signaling outcomes. The EMBO journal 35, 1868-1884.

Walczak, H. (2013). Death receptor-ligand systems in cancer, cell death, and inflammation. Cold Spring Harbor perspectives in biology 5, a008698.

Wallot-Hieke, N., Verma, N., Schlutermann, D., Berleth, N., Deitersen, J., Bohler, P., Stuhldreier, F., Wu, W., Seggewiss, S., Peter, C., et al. (2018). Systematic analysis of ATG13 domain requirements for autophagy induction. Autophagy 14, 743-763.

Wang, B., Maxwell, B.A., Joo, J.H., Gwon, Y., Messing, J., Mishra, A., Shaw, T.I., Ward, A.L., Quan, H., Sakurada, S.M., et al. (2019). ULK1 and ULK2 Regulate Stress Granule Disassembly Through Phosphorylation and Activation of VCP/p97. Molecular cell.

Wang, C., Deng, L., Hong, M., Akkaraju, G.R., Inoue, J., and Chen, Z.J. (2001). TAK1 is a ubiquitin-dependent kinase of MKK and IKK. Nature 412, 346-351.

Wang, H., Sun, L., Su, L., Rizo, J., Liu, L., Wang, L.F., Wang, F.S., and Wang, X. (2014). Mixed lineage kinase domain-like protein MLKL causes necrotic membrane disruption upon phosphorylation by RIP3. Molecular cell 54, 133-146.

Wang, L., Du, F., and Wang, X. (2008). TNF-alpha induces two distinct caspase-8 activation pathways. Cell 133, 693-703.

Warren, C.F.A., Wong-Brown, M.W., and Bowden, N.A. (2019). BCL-2 family isoforms in apoptosis and cancer. Cell death & disease 10, 177.

Webster, C.P., Smith, E.F., Bauer, C.S., Moller, A., Hautbergue, G.M., Ferraiuolo, L., Myszczynska, M.A., Higginbottom, A., Walsh, M.J., Whitworth, A.J., et al. (2016). The C9orf72 protein interacts with Rab1a and the ULK1 complex to regulate initiation of autophagy. The EMBO journal 35, 1656-1676.

Weidberg, H., Shvets, E., Shpilka, T., Shimron, F., Shinder, V., and Elazar, Z. (2010). LC3 and GATE-16/GABARAP subfamilies are both essential yet act differently in autophagosome biogenesis. The EMBO journal 29, 1792-1802.

Wertz, I.E., O'Rourke, K.M., Zhou, H., Eby, M., Aravind, L., Seshagiri, S., Wu, P., Wiesmann, C., Baker, R., Boone, D.L., et al. (2004). De-ubiquitination and ubiquitin ligase domains of A20 downregulate NF-kappaB signalling. Nature 430, 694-699.

Westphal, D., Dewson, G., Czabotar, P.E., and Kluck, R.M. (2011). Molecular biology of Bax and Bak activation and action. Biochimica et biophysica acta 1813, 521-531.

Wirawan, E., Vande Walle, L., Kersse, K., Cornelis, S., Claerhout, S., Vanoverberghe, I., Roelandt, R., De Rycke, R., Verspurten, J., Declercq, W., et al. (2010). Caspase-mediated cleavage of Beclin-1 inactivates Beclin-1-induced autophagy and enhances apoptosis by promoting the release of proapoptotic factors from mitochondria. Cell death & disease 1, e18.

Witt, A., and Vucic, D. (2017). Diverse ubiquitin linkages regulate RIP kinases-mediated inflammatory and cell death signaling. Cell death and differentiation 24, 1160-1171.

Woods, A., Dickerson, K., Heath, R., Hong, S.P., Momcilovic, M., Johnstone, S.R., Carlson, M., and Carling, D. (2005). Ca2+/calmodulin-dependent protein kinase kinase-beta acts upstream of AMP-activated protein kinase in mammalian cells. Cell metabolism 2, 21-33.

Xie, M., Zhang, D., Dyck, J.R., Li, Y., Zhang, H., Morishima, M., Mann, D.L., Taffet, G.E., Baldini, A., Khoury, D.S., et al. (2006). A pivotal role for endogenous TGF-beta-activated kinase-1 in the LKB1/AMP-activated protein kinase energy-sensor pathway. Proceedings of the National Academy of Sciences of the United States of America 103, 17378-17383.

Xie, T., Peng, W., Yan, C., Wu, J., Gong, X., and Shi, Y. (2013). Structural insights into RIP3-mediated necroptotic signaling. Cell reports 5, 70-78.

Xu, D., Jin, T., Zhu, H., Chen, H., Ofengeim, D., Zou, C., Mifflin, L., Pan, L., Amin, P., Li, W., et al. (2018). TBK1 Suppresses RIPK1-Driven Apoptosis and Inflammation during Development and in Aging. Cell 174, 1477-1491 e1419.

Yang, Q.H., and Du, C. (2004). Smac/DIABLO selectively reduces the levels of c-IAP1 and c-IAP2 but not that of XIAP and livin in HeLa cells. The Journal of biological chemistry 279, 16963-16970.

Yang, Y., Fang, S., Jensen, J.P., Weissman, A.M., and Ashwell, J.D. (2000). Ubiquitin protein ligase activity of IAPs and their degradation in proteasomes in response to apoptotic stimuli. Science 288, 874-877.

Yatim, N., Jusforgues-Saklani, H., Orozco, S., Schulz, O., Barreira da Silva, R., Reis e Sousa, C., Green, D.R., Oberst, A., and Albert, M.L. (2015). RIPK1 and NF-kappaB signaling in dying cells determines cross-priming of CD8(+) T cells. Science 350, 328-334.

Yonekawa, T., Gamez, G., Kim, J., Tan, A.C., Thorburn, J., Gump, J., Thorburn, A., and Morgan, M.J. (2015). RIP1 negatively regulates basal autophagic flux through TFEB to control sensitivity to apoptosis. EMBO reports 16, 700-708.

Yoshii, S.R., and Mizushima, N. (2017). Monitoring and Measuring Autophagy. International journal of molecular sciences 18.

Youle, R.J., and Narendra, D.P. (2011). Mechanisms of mitophagy. Nature reviews. Molecular cell biology 12, 9-14.

Young, M.M., Takahashi, Y., Khan, O., Park, S., Hori, T., Yun, J., Sharma, A.K., Amin, S., Hu, C.D., Zhang, J., et al. (2012). Autophagosomal membrane serves as platform for intracellular death-inducing

signaling complex (iDISC)-mediated caspase-8 activation and apoptosis. The Journal of biological chemistry 287, 12455-12468.

Yousefi, S., Perozzo, R., Schmid, I., Ziemiecki, A., Schaffner, T., Scapozza, L., Brunner, T., and Simon, H.U. (2006). Calpain-mediated cleavage of Atg5 switches autophagy to apoptosis. Nature cell biology 8, 1124-1132.

Yuan, S., Yu, X., Topf, M., Ludtke, S.J., Wang, X., and Akey, C.W. (2010). Structure of an apoptosome-procaspase-9 CARD complex. Structure 18, 571-583.

Zhang, D.W., Shao, J., Lin, J., Zhang, N., Lu, B.J., Lin, S.C., Dong, M.Q., and Han, J. (2009). RIP3, an energy metabolism regulator that switches TNF-induced cell death from apoptosis to necrosis. Science 325, 332-336.

Zhang, T., Zhang, Y., Cui, M., Jin, L., Wang, Y., Lv, F., Liu, Y., Zheng, W., Shang, H., Zhang, J., et al. (2016). CaMKII is a RIP3 substrate mediating ischemia- and oxidative stress-induced myocardial necroptosis. Nature medicine 22, 175-182.

Zhou, C., Ma, K., Gao, R., Mu, C., Chen, L., Liu, Q., Luo, Q., Feng, D., Zhu, Y., and Chen, Q. (2017). Regulation of mATG9 trafficking by Src- and ULK1-mediated phosphorylation in basal and starvation-induced autophagy. Cell research 27, 184-201.

Declaration

I, Wenxian Wu hereby declare under oath that I fulfill the compilation of my dissertation independently and without any inappropriate assistance from the external part according to the principle of assurance of Good Scientific Practice at Heinrich Heine University Düsseldorf.

Date/place

Wenxian Wu

Manuscript I

The autophagy-initiating kinase ULK1 controls RIPK1-mediated cell death

AUTHORS/AFFILIATIONS

Wenxian Wu[1,], Xiaojing Wang[1], Niklas Berleth[1], Jana Deitersen[1], Nora Wallot-Hieke[1], Philip Böhler[1], David Schlütermann[1], Fabian Stuhldreier[1], Jan Cox[1], Katharina Schmitz[1], Sabine Seggewiß[1], Christoph Peter[1], Gary Kasof[2], Anja Stefanski[3], Kai Stühler[3], Astrid Tschapek[4], Axel Gödecke[4], Björn Stork[1,*]

[1]*Institute of Molecular Medicine I, Medical Faculty, Heinrich Heine University Düsseldorf, 40225 Düsseldorf, Germany*

[2]*Cell Signaling Technology, Danvers, MA 01923, USA*[3]*Molecular Proteomics Laboratory, BMFZ, Heinrich-Heine-University, 40225 Düsseldorf, Germany*

[4]*Institute of Cardiovascular Physiology, Medical Faculty, Heinrich Heine University Düsseldorf, 40225 Düsseldorf, Germany*

These authors contributed equally: Wenxian Wu, Xiaojing Wang

CONTACT

*Corresponding author:

Björn Stork, Universitätsstr. 1, Building 23.12, 40225 Düsseldorf, Germany,

Tel.: +49 (0)211 81 11954, Fax: +49 (0)211 81 14103, E-mail: bjoern.stork@uni-duesseldorf.de

RUNNING TITLE: ULK1 regulates RIPK1

KEYWORDS: ULK1, RIPK1, RIPK3, Autophagy, Necroptosis

ABBREVIATIONS: 3-MA, 3-methyladenine; ATG, autophagy-related; DD, death domain; GFP, green fluorescent protein; EBSS, Earle's Balanced Salt Solution; FADD, Fas-associated protein with death domain; ID, intermediary domain; IKK, inhibitor of nuclear factor κ-B kinase; MEF, murine embryonic

fibroblast; MK2, MAPK-activated protein kinase 2; MLKL, mixed-lineage kinase domain-like protein; RHIM, RIPK homotypic interaction motif; RIPK1/3, receptor-interacting kinase 1/3; TAK1, transforming growth factor β-activated kinase 1; TNFα, tumor necrosis factor α; TNFR1, TNF receptor 1; ULK1, UNC-51 like autophagy activating kinase 1

SUMMARY

Autophagy, apoptosis and necroptosis are stress responses governing the ultimate fate of a cell. However, the crosstalk between these cellular stress responses is not entirely understood. Especially, it is not clear whether the autophagy-initiating kinase ULK1 and the apoptosis/necroptosis-regulating kinase RIPK1 are involved in this potential crosstalk. Here, we identify RIPK1 as a novel substrate of ULK1. ULK1-dependent phosphorylation of RIPK1 reduces complex IIb/necrosome assembly and TNFα-induced cell death, whereas deprivation of ULK1 significantly enhances TNFα-induced cell death. We observe that ULK1 phosphorylates multiple sites of RIPK1, but it appears that especially phosphorylation of S357 within the intermediary domain of RIPK1 mediates this cell death-inhibiting effect. Collectively, we propose that ULK1 is a novel regulator of RIPK1-mediated cell death.

INTRODUCTION

Tumor necrosis factor α (TNFα) is a proinflammatory cytokine that regulates both transcription of inflammatory and prosurvival genes and cell death pathways. The receptor-interacting kinase 1 (RIPK1) is a central mediator of TNFα-induced signaling cascades. RIPK1 is composed of an N-terminal kinase domain, an intermediary domain (ID) containing a RIPK homotypic interaction motif (RHIM), and a C-terminal death domain (DD). Upon TNFα stimulation, RIPK1 is recruited to the TNF receptor 1 (TNFR1) via its DD, ultimately leading to the formation of a TNFR1 signaling complex termed complex I. RIPK1 becomes ubiquitinated in its ID within complex I, and cell death is prevented. Upon dissociation of RIPK1 from complex I, different cytosolic RIPK1-containing complexes have been described (complex IIa, complex IIb, or necrosomes) (reviewed in (Annibaldi and Meier, 2018; Grootjans et al., 2017)). These complexes support either apoptosis (complex IIa, complex IIb) or necroptosis (necrosomes), which is the prototype of programmed necrosis. TNFα-induced apoptosis requires non-ubiquitinated RIPK1 and active caspase-8 within complex IIa or IIb (Brenner et al., 2015). Necroptosis represents an inflammatory form of cell death triggered by several stimuli, including death receptor ligands, interferons, lipopolysaccharide or dsRNA (Grootjans et al., 2017). TNFα-induced necroptosis is the best characterized necroptotic pathway. The execution of necroptosis is mainly mediated by receptor-interacting kinase 3 (RIPK3) and mixed lineage kinase domain-like (MLKL) (reviewed in (Annibaldi and Meier, 2018; Grootjans et al., 2017)). The RHIM domains of RIPK1 and RIPK3 are indispensable for the formation of amyloid microfilaments called necrosomes. Necroptosis and the formation of necrosomes can be inhibited by caspase-8-dependent cleavage of RIPK1 or RIPK3 (Feng et al., 2007; Lin et al., 1999; O'Donnell et al., 2011). Accordingly, necroptosis can be enhanced by caspase inhibitors such as Q-VD-OPh or z-VAD-FMK (Cho et al., 2009; He et al., 2009; Trichonas et al., 2010; Zhang et al., 2009). Most importantly, the kinase activities of both RIPK1 and RIPK3 are required for assembling and activating RIPK1-RIPK3 necrosomes, since specific kinase inhibitors (necrostatin 1 or the GSK inhibitors of RIPK3) or kinase-dead variants of RIPK1/3 block necroptosis (Degterev et al., 2005; Mandal et al., 2014). Recently it became evident that RIPK1 has a scaffolding function independent of its kinase activity and that RIPK1 can, under certain conditions, suppress RIPK3 and thus block RIPK3-dependent necroptosis (Dannappel et al., 2014; Dillon et al., 2014; Kaiser et al., 2014; Kearney et al., 2014; Orozco et al., 2014; Rickard et al.,

2014). Upon oligomerization of RIPK3 within the necrosome, RIPK3 autophosphorylates and becomes activated. Subsequently, MLKL is recruited to the necrosome and becomes phosphorylated by activated RIPK3. Phosphorylated MLKL is translocated to the plasma membrane, ultimately leading to the disruption of the plasma membrane (Sun et al., 2012). In the last decade, necroptosis has been demonstrated to be involved in host defense against viruses, inflammation, tissue injury, and cancers (Aaes et al., 2016; Artal-Sanz and Tavernarakis, 2005; Cho et al., 2009; Christofferson and Yuan, 2010; Kaiser et al., 2011; Trichonas et al., 2010; Wang et al., 2014).

Macroautophagy (hereafter referred to as autophagy) is another cellular stress response contributing to cellular homeostasis. During autophagy, cytoplasmic components including long-lived or damaged proteins and organelles are sequestered by a double-membraned vesicle termed autophagosome. Subsequently, autophagosomes fuse with lysosomes and the engulfed material becomes degraded (Levine and Kroemer, 2008; Mizushima and Komatsu, 2011; Wesselborg and Stork, 2015; Yang and Klionsky, 2010). The ULK1 complex is central for the initiation of autophagic processes. The core complex is composed of the Ser/Thr kinase unc-51 like kinase 1 (ULK1) and the associated proteins autophagy-related (ATG) protein 13 (ATG13), focal adhesion kinase family interacting protein of 200 kDa (FIP200), and ATG101. To date, several autophagy-relevant substrates of ULK1 have been identified, including the associated components of the ULK1 complex, several subunits of the class III phosphatidylinositol 3-kinase PIK3C3/Beclin 1 complex, and others (Egan et al., 2015; Joo et al., 2011; Jung et al., 2009; Lim et al., 2015; Papinski et al., 2014; Park et al., 2016; Russell et al., 2013; Wu et al., 2014; Zhou et al., 2017). Next to autophagy-relevant proteins, additional ULK1 substrates with no or at least no apparent function in autophagy have been described, such as Syntenin-1, mitogen-activated protein kinase (MAPK) p38α, stimulator of interferon genes (STING), and SEC16 homolog A (SEC16A) (Joo et al., 2016; Konno et al., 2013; Rajesh et al., 2011; Saleiro et al., 2015). These substrates and additional ULK1-interacting proteins already indicate that ULK1 – next to its essential role for the induction of autophagy – participates in additional cellular signaling pathways.

Autophagy, apoptosis and necroptosis regulate cell death and survival to support cellular homeostasis. However, the relationship between these processes downstream of the TNFR1 remains enigmatic so far. Although some recent reports suggest a crosstalk between the effector proteins of these cellular

stress responses (Goodall et al., 2016; Harris et al., 2015; Matsuzawa et al., 2015; Yonekawa et al., 2015), the underlying mechanisms are poorly understood. Especially, it is unknown whether the autophagy-initiating kinase ULK1 and/or the cell death-regulating kinase RIPK1 are involved in this crosstalk. In this study, we aimed at investigating the influence of autophagy on TNFα-induced cell death in general and the influence of ULK1 on RIPK1 in particular. We observe that autophagy-modulating treatments affect TNFα-induced cell death in murine L929 fibroblasts, i.e. inhibition of autophagy promotes cell death whereas induction of autophagy by starvation strongly blocks TNFα-induced cell death. Further, we find that ULK1 is an important regulator of cell death induced by TNFα. Ablation of ULK1 expression significantly enhances TNFα-induced complex IIb/necrosome formation and cell death. Furthermore, we identified RIPK1 as substrate of ULK1. ULK1-dependent phosphorylation of RIPK1 reduces TNFα-induced cell death. This effect largely depends on ULK1-dependent phosphorylation of RIPK1 within the intermediary domain at S357, leading to destabilized complexes IIb/necrosomes. In summary, we identified a regulatory mechanism between the autophagy-initiating kinase ULK1 and the cell death-regulating kinase RIPK1.

RESULTS

Autophagy in general and ULK1 in particular inhibit TNFα-induced cell death in the murine fibroblasts

In order to investigate the influence of autophagy on TNFα-induced cell death, we induced or inhibited autophagy, respectively, and analyzed TNFα-induced cell death in the murine fibroblast cell line L929. In this cell line, TNFα treatment predominantly induces cell death by necroptosis (Zhang et al., 2009). We found that inhibiting early autophagy with the PtdIns3K inhibitor 3-methyladenine (3-MA) enhanced cell death induced by TNFα (Figure S1A and S1B). In contrast, induction of autophagy by amino acid starvation (EBSS) reduced cell death induced by TNFα compared to TNFα treatment alone (Figure S1A and S1B). These data indicate that autophagy generally affects TNFα-induced cell death. As the ULK1 complex is central for the initiation of autophagic processes, we next aimed at investigating the specific function of ULK1 during TNFα-induced cell death. For that, we silenced ULK1 by siRNA. We found that knockdown of ULK1 significantly increased TNFα-induced cell death for different incubation times or TNFα concentrations compared to control siRNA (Figures 1A-1D). Since we observed increased necroptosis upon ULK1 knockdown, we analyzed MLKL phosphorylation under these conditions. We found that ULK1 silencing in L929 cells resulted in an increased phosphorylation of MLKL at S345, indicating a higher RIPK3 activity compared to scramble siRNA-transfected cells (Figure 1E). In order to confirm our results in a further cellular model system, we analyzed the effect of ULK1 silencing on cell death induction in murine embryonic fibroblasts (MEFs). For that, we employed the standard treatment for apoptosis/necroptosis induction, i.e. TNFα (T) in combination with a SMAC mimetic (S) (here Birinapant), either without or with the pan caspase inhibitor z-VAD (Z), from now on TS or TSZ, respectively (He et al., 2009; Jaco et al., 2017). Also in MEFs, cell death was significantly increased in cells with down-regulated ULK1 (Figure 1F). To ultimately confirm that the kinase activity of ULK1 is important for the regulation of TNFα-induced cell death, we made use of *ulk1 ulk2* double-knockout (DKO) MEFs reconstituted with either wild-type ULK1 or a kinase-dead variant. TNFα-induced cell death was increased in DKO MEFs and in MEFs expressing the kinase-dead variant of ULK1, whereas cell death was reduced in cells expressing wild-type ULK1 (Figure 1G). Collectively, these data indicate that ULK1 exerts an inhibitory effect on TNFα-induced cell death, and that this effect depends on the kinase activity of ULK1.

ULK1 inhibition results in increased complex IIb/necrosome formation

In order to further investigate the effect of ULK1 on the TNFα-induced cell death signaling pathway, we analyzed complex IIb/necrosome assembly under control or ULK1-inhibiting conditions, respectively. ULK1 was inhibited using the compound MRT68921 (Petherick et al., 2015). Complex IIb/necrosome was purified using anti-FADD antibodies. We analyzed RIPK1 autophosphorylation at S166, which correlates with the formation of cytotoxic RIPK1 complexes (Degterev et al., 2008; Dondelinger et al., 2017; Jaco et al., 2017; Menon et al., 2017; Newton et al., 2016), and necroptosis-related RIPK1 ubiquitination, which has been shown to maintain RIPK1 kinase activity in the necrosome (de Almagro et al., 2017). We observed slightly increased and earlier RIPK1 association with FADD and RIPK1 autophosphorylation at S166 upon TNFα/QVD (TQ) in L929 cells treated with MRT68921 (Figure 2A). Furthermore, we observed increased RIPK1 ubiquitination in complex IIb/necrosome, and increased generation of the p43 fragment of caspase-8 in MRT68921-treated cells (please note that caspase inhibition using z-VAD or QVD does not block the generation of the p43 fragment, ref. (Biton and Ashkenazi, 2011; Guo et al., 2016)). Similar results were obtained using MEFs treated with TSZ (Figure 2B) or TZ (Figure S2) in the presence of MRT68921. Furthermore, these results were confirmed using the alternative ULK1 inhibitor SBI-0206965 (Egan et al., 2015) (Figure 2C). In order to exclude non-specific effects of the ULK1 inhibitors, we also investigated complex IIb/necrosome assembly in the *ulk1 ulk2* DKO MEFs described above. RIPK1 association with FADD and RIPK1 autophosphorylation at S166 were increased in ULK1/2-deficient MEFs and in MEFs expressing the kinase-dead variant of ULK1 compared to cells expressing wild-type ULK1 (Figure 2D), confirming the results obtained with the ULK1 inhibitors. Next, we analyzed the interaction between RIPK1 and RIPK3 in L929 and MEFs. We observed enhanced association of these two proteins in cells treated with the ULK1 inhibitor MRT68921 (Figures 2E and 2F). Taken together, it appears that ULK1 inhibition or deficiency result in an increased association of autophosphorylated and ubiquitinated RIPK1 with complex IIb/necrosome.

ULK1 interacts with RIPK1

According to our data, ULK1 directly affects TNFα-induced cell death and complex IIb/necrosome

formation in L929 cells and MEFs. We next tested if ULK1 can interact with RIPK1. First, we transiently transfected cDNA encoding FLAG-RIPK1 into HEK293 cells inducibly expressing GFP or GFP-ULK1, respectively. Following induction of GFP or GFP-ULK1 expression and anti-GFP purification, we detected co-purification of FLAG-RIPK1 from GFP-ULK1-expressing cells, but not from cells expressing GPF alone (Figure S3A). In a similar approach, we co-purified GFP-ULK1 from MYC-RIPK1-expressing cells following an anti-MYC immunopurification (Figure S3B). In the next step, we aimed at investigating the interaction between endogenously expressed ULK1 and RIPK1. Purification of ULK1 clearly led to the co-purification of RIPK1, and it appears that this interaction is increased upon TNFα/QVD treatment (Figure S3C). Similarly, an increased interaction upon TNFα treatment was observed when endogenous RIPK1 was purified from GFP-ULK1-expressing cells (Figure S3D). Next to immunopurifications, we performed affinity purifications using GST fusion proteins containing full length and truncated versions of RIPK1. FLAG-ULK1 was co-purified with full length GST-RIPK1 (Figure S3E) and the truncated versions of RIPK1 containing amino acids 250-475 or 476-671, respectively, associated with GFP-ULK1 (Figure S3F). In order to analyze the interaction between ULK1 and RIPK1 by an alternative approach, we performed a proximity ligation assay that allows detection of a protein-protein interaction using antibody-mediated recognition combined with exponential signal amplification by PCR. We employed *ripk1* KO MEFs transfected with either empty vector or cDNA encoding FLAG-tagged human RIPK1. The RIPK1-expressing cells displayed strong signals with significant difference to control cells (Figure S3G). Of note, we also found that poly-ubiquitination of RIPK1 apparently affects the interaction between RIPK1 and ULK1 since abolishment of RIPK1 poly-ubiquitination (RIPK1 K377R mutant, ref. (Ea et al., 2006)) resulted in a stronger interaction with ULK1 (Figure S3H). Collectively, these data indicate that ULK1 can associate with RIPK1.

ULK1 directly phosphorylates RIPK1 within the intermediary domain at S357

Since we observed that ULK1 interacts with RIPK1, we next tested if ULK1 can phosphorylate RIPK1. In a first approach, we expressed FLAG-RIPK1 in GFP-ULK1-expressing cells and observed a post-translational modification of RIPK1 that was sensitive towards treatment with alkaline phosphatase (Figure S4A). We next analyzed serine phosphorylation of kinase-dead MYC-RIPK1 purified from cells expressing GFP-ULK1, a kinase-inactivated version of GFP-ULK1, or GFP alone by

immunoblotting. Kinase-dead RIPK1 was employed in order to exclude signals derived from autophosphorylation. Serine phosphorylation of RIPK1 was reduced in cells expressing GFP alone or the kinase-dead version of ULK1 (Figure S4B). For an *in vitro* kinase assay with recombinant ULK1, we employed the truncated GST-RIPK1 fusion proteins described above as substrates. Notably, we only detected phosphorylation of GST-RIPK1(250-475), but not of GST-hRIPK1(1-249) or GST-hRIPK1(476-671) (Figure 3A). The human RIPK1 peptide 250-475 contains 33 serine/threonine residues. Using mass spectrometry, we identified phospho-acceptor sites of GST-RIPK1(250-475) at S262, S291, S296, S320, S333, S335, T337, S345, S346, S357, and S389 (Table S1). Of these, S357 gained our major interest, since it nicely fits the previously reported ULK1 consensus phosphorylation motif. It has been suggested that ULK1 prefers hydrophobic residues at the -3, +1, and +2 positions (Egan et al., 2015). Furthermore, this residue is conserved across diverse species (Figure 3B). We exchanged S357 for alanine in the GST-RIPK1(250-475) fusion protein and observed a clearly reduced phosphorylation signal in the *in vitro* kinase assay (Figure S4C). Importantly, this reduction could not be achieved by exchanging any other of the identified residues for alanine (Figure S4C). Next, we aimed at confirming the central role of S357 as ULK1-dependent phospho-acceptor site and thus generated a phospho-specific RIPK1 S357 antibody. We repeated the *in vitro* kinase assay using GST alone, GST-RIPK1(250-475) or GST-RIPK1(250-475) S357A as substrates. The phospho signal completely disappeared for the S357A variant (Figure 3C). Subsequently, we wanted to investigate S357 phosphorylation in our cellular model systems. First, we confirmed the specificity of the phospho-specific antibody in *ripk1* KO MEFs transfected with either empty vector or cDNA encoding wild-type RIPK1 (Figure S4D). Next, we expressed either wild-type RIPK1 or the S357A variant in GFP-ULK1-expressing HEK293 cells and analyzed the corresponding lysates by immunoblotting for RIPK1 phospho-S357. We observed that cellular phosphorylation was reduced for the S357A variant (Figure 3D). Furthermore, S357 phosphorylation of wild-type RIPK1 was sensitive towards alkaline phosphatase treatment (Figure 3E) or treatment with the ULK1 inhibitor MRT68921 (Figure 3F). Finally, we repeated the analysis shown in Figure S4B using the phospho-specific antibody and found that phosphorylation of kinase-dead RIPK1 at S357 was reduced in cells expressing GFP alone or the kinase-dead version of ULK1, but was clearly detectable in cells expressing wild-type GFP-ULK1 (Figure 3G). Collectively, our results suggest that S357 within the intermediary domain (ID) of RIPK1 represents the major ULK1-dependent phospho-acceptor site. We also used the phospho-specific

antibody in order to investigate whether complex I-associated or cytosolic RIPK1 becomes phosphorylated by ULK1. For that, we treated *ulk1/2* DKO MEFs transfected with either empty vector or cDNA encoding FLAG-ULK1 with mTNFα. Then, complex I was immunopurified by anti-TNFR1-antibodies. RIPK1 association with complex I was slightly increased in ULK1 expressing MEFs, although RIPK1 activity was similar in both cell lines (Figure 4). Of note, RIPK1 phosphorylation at S357 was almost not detectable in complex I, although ULK1 was co-purified. We also analyzed post-TNFR1 IP lysates depleted of complex I. In this fraction, RIPK1 phosphorylation at S357 was clearly detectable and RIPK1 activity was reduced by ULK1 expression (Figure 4). Taken together, it appears that ULK1 supports the association of RIPK1 with complex I and negatively regulates the activity of cytosolic RIPK1.

ULK1-dependent phosphorylation of RIPK1 at S357 inhibits TNFα-induced cell death

So far, our data demonstrate that the autophagy-initiating kinase ULK1 inhibits TNFα-induced cell death pathways. Furthermore, we observed the interaction between ULK1 and RIPK1 and the ULK1-dependent phosphorylation of RIPK1 at S357 within the ID. Next, we wanted to analyze whether this phosphorylation mediates the inhibitory effect of ULK1 on TNFα-induced cell death. For that, we reconstituted *ripk1* KO MEFs with cDNAs encoding either wild-type RIPK1 or the S357A variant, respectively. First, we investigated both RIPK1 and MLKL phosphorylation upon treatment with TSZ. In cells expressing the phosphorylation-incompetent S357A variant of RIPK1, both RIPK1 autophosphorylation at S166 and MLKL phosphorylation at S345 were clearly increased, indicating an augmented induction of necroptosis (Figure 5A). Second, we analyzed cell death induction by propidium iodide. Also in this readout, TS- or TSZ-induced cell death was enhanced in cells expressing the RIPK1 S357A variant (Figure 5B). Of note, siRNA-mediated knockdown of ULK1 sensitized only RIPK1 wild-type-expressing cells to TSZ-induced cell death, but not cells expressing the S357A variant (Figure 5B), indicating that ULK1 indeed targets this site in RIPK1 in order to regulate TNFα-induced cell death. Finally, we investigated complex IIb/necrosome formation upon TSZ treatment in these two cell lines. In RIPK1 S357A-expressing cells, the complex IIb/necrosome was clearly stabilized, as deduced from increased RIPK1 S166 phosphorylation, increased generation of the p43 caspase-8 fragment, and increased association of RIPK3 (Figure 5C). Collectively, our data suggest that

autophagy and specifically ULK1 play a vital role in regulating TNFα-induced cell death. ULK1 associates with and phosphorylates RIPK1. ULK1-dependent phosphorylation of S357 within the ID of RIPK1 is sufficient to reduce TNFα-induced cell death (Figure S5). In turn, complex IIb/necrosome formation and TNFα-induced cell death are intensified in cells expressing a RIPK1 variant which cannot be phosphorylated by ULK1.

DISCUSSION

Autophagy, apoptosis and necroptosis influence cellular homeostasis. To date, it is not known if and how the effector proteins of autophagy and TNFα-induced signaling pathways cross-regulate each other, although recent reports have suggested the existence of this crosstalk (Goodall et al., 2016; Harris et al., 2015; Yonekawa et al., 2015). In this study, we have identified and characterized the crosstalk between autophagy and TNFα-induced cell death pathways. More specifically, we revealed that the autophagy-inducing kinase ULK1 controls the cell death-regulating kinase RIPK1. Initially, we observed that siRNA-mediated reduction of ULK1 expression or the pharmacological inhibition of autophagy in general or ULK1 in particular enhance TNFα-induced cell death. In turn, promoting autophagy by EBSS suppresses TNFα-induced cell death. These data clearly support the generally cyto-protective function of autophagy. Furthermore, we found that ULK1 directly interacts with and phosphorylates RIPK1. ULK1-dependent phosphorylation of RIPK1 at S357 is sufficient to mediate the inhibitory effect of ULK1 on TNFα-induced cell death.

Initially, we observed that EBSS-mediated induction of autophagy reduces TNFα-induced cell death. EBSS treatment represents a rather harsh method of starvation-induced autophagy, and we do not postulate that the observed effect of EBSS on TNFα-induced cell death is solely mediated via ULK1. In contrast, we believe that there exist multiple layers of crosstalk between autophagy and necroptosis, similar to the crosstalk between autophagy and apoptosis. Along these lines, 3-MA targets the class III phosphatidylinositol 3-kinase PIK3C3/Beclin 1 complex, which is downstream of ULK1. Although ULK1 should not be affected by 3-MA treatment, we observed an increase in TNFα-induced cell death, indicating that there are different autophagy-dependent pathways to regulate necroptosis. This has also been confirmed by observations of other groups. Matsuzawa-Ishimoto et al. reported that ATG16L1—which is a component of the autophagy-regulating ubiquitin-like conjugation systems and also downstream of ULK1—prevents necroptosis in the intestinal epithelium (Matsuzawa-Ishimoto et al., 2017). Additionally, Lu et al. reported that phosphoglycerate mutase family member 5 (PGAM5) regulates mitophagic protection against necroptosis (Lu et al., 2016). Nevertheless, we demonstrate that the inhibition, knockdown or complete loss of ULK1 increase TNFα-induced cell death, clearly supporting a necroptosis-regulatory function of this autophagy-activating kinase.

RIPK1 is a central regulator of the cell fate decision, and RIPK1 signaling can mediate survival, apoptosis, and necroptosis. These functions are controlled by diverse post-translational modifications, including ubiquitination, phosphorylation, or caspase-mediated cleavage (reviewed in (Annibaldi and Meier, 2018; Grootjans et al., 2017)). Within the TNFα receptor-associated complex I, RIPK1 becomes ubiquitinated, autophosphorylates and is thus activated. In 2008, Degterev et al. reported that necrostatin-1 inhibits RIPK1 kinase activity (Degterev et al., 2008). Using RIPK1 kinase assays, the authors observed that S14/15, S20, S161 and S166 represent autophosphorylation sites, whereas other residues of RIPK1 (S6, S25, S303, S320, S330/331 and S333) were phosphorylated even without kinase reaction (Degterev et al., 2008). Of note, all autophosphorylated serine residues are located in the N-terminal kinase domain. Next to this autophosphorylation, in recent years other kinases have been reported to phosphorylate RIPK1 in order to establish a "RIPK1 phospho-barcode" responsible for the divergent RIPK1 signaling outcomes. Ubiquitination of RIPK1 and other components of complex I leads to the recruitment of further kinase complexes, such as TAK1-TAB2-TAB3 or IKKα-IKKβ-NEMO, respectively (Annibaldi and Meier, 2018; Ori et al., 2013; Rahighi et al., 2009). IKKα-IKKβ directly phosphorylate RIPK1 within complex I and thus prevent the formation of complex II and ultimately the induction of RIPK1-dependent cell death (Dondelinger et al., 2015). The IKKα-IKKβ-dependent phospho-sites of RIPK1 are located in the kinase domain (S25, S166) and in the ID (S296, S331, S416) (Dondelinger et al., 2015). Recently, three works reported the phosphorylation of cytosolic RIPK1 by MK2, which acts downstream of the TAK1-TAB2-TAB3 complex (Annibaldi and Meier, 2018; Dondelinger et al., 2017; Jaco et al., 2017; Menon et al., 2017). Similar to the IKKα-IKKβ-mediated phosphorylation of RIPK1, the MK2-dependent phosphorylation prevents formation of complex II and cell death induction. The three groups reported phosphorylation of RIPK1 at S320 and S335 (Annibaldi and Meier, 2018; Dondelinger et al., 2017; Jaco et al., 2017; Menon et al., 2017). Finally, two other groups suggested the phosphorylation of S320 by IKK or TAK1 (Annibaldi and Meier, 2018; Geng et al., 2017; Mohideen et al., 2017). Although we have also identified S320 and S335 in our mass spectrometric analyses, exchange of these serines for alanines did not alter the intensity of the ULK1-dependent phosphorylation pattern. However, mutation of S357 to alanine clearly reduced ULK1-mediated phosphorylation. To our knowledge, phosphorylation of RIPK1 at S357 has not been reported so far. Similar to the IKKα-IKKβ- or MK2-mediated phosphorylation of RIPK1, ULK1-dependent phosphorylation inhibits the pro-death signaling pathways of RIPK1. Both

IKKα-IKKβ and MK2 have been proposed to suppress RIPK1 autoactivation as detected by autophosphorylation of S166 (Annibaldi and Meier, 2018; Dondelinger et al., 2017; Dondelinger et al., 2015; Jaco et al., 2017; Menon et al., 2017). Along these lines, our data similarly suggest that abrogation of the ULK1-dependent phosphorylation of RIPK1, as achieved by expression of the S357A variant, increases RIPK1 kinase activity, since we also observe an increased autophosphorylation of this RIPK1 variant at S166 compared to wild-type RIPK1. Furthermore, we observed increased association of RIPK3 and the p43 fragment of caspase-8 with RIPK1 S357A, indicating an increased stability of complex IIb/necrosome in these cells. For IKKα-IKKβ and MK2 it has been suggested that these upstream kinases do not depend on each other but rather operate additively. Accordingly, we think that the phosphorylations of RIPK1 by IKKα-IKKβ, MK2 or ULK1 complement each other in order to suppress cell death. It has been suggested that different subcellular pools of RIPK1 are targeted by IKKα-IKKβ and MK2, i.e. complex I-associated RIPK1 vs. cytosolic RIPK1 (Annibaldi and Meier, 2018; Dondelinger et al., 2017; Jaco et al., 2017; Menon et al., 2017). Whereas IKKα-IKKβ targets complex I-associated RIPK1, MK2 phosphorylates both complex I-associated and cytosolic RIPK1, although MK2 itself is apparently not recruited to the TNFR1-associated complex (Jaco et al., 2017). With regard to ULK1, it appears that cytosolic RIPK1 is preferentially phosphorylated. Furthermore, especially the cytosolic activity of RIPK1 is reduced in ULK1-expressing cells. In contrast, TNFR1-associated RIPK1 does not reveal a detectable phosphorylation of S357, although RIPK1 appears to be stabilized in this complex I. We think that ULK1 associates with both complex I-bound and cytosolic RIPK1, and that ULK1-dependent phosphorylation might be hampered by RIPK1 ubiquitination. Additionally, RIPK1 that is not phosphorylated at S357 is stabilized in complex I. In contrast, cytosolic RIPK1 becomes phosphorylated by ULK1, resulting in a reduced RIPK1 activity. Future studies will have to reveal whether the inactivation of all upstream regulatory kinases is required for “complete” induction of the pro-death RIPK1 activity or whether indeed different subcellular pools of RIPK1 are targeted by these kinases. Generally, it is conceivable that the autophagy-inducing and thus *bona fide* cyto-protective kinase ULK1 contributes to the control of RIPK1-mediated cell death.

In summary, we describe a novel cross-regulation between the executioner kinases of autophagy and TNFα-induced cell death pathways. Presumably, there exist several additional levels of crosstalk between these two cellular stress responses and the understanding of this molecular crosstalk will be

important for the optimization of current and future therapeutic approaches.

EXPERIMENTAL PROCEDURES

Antibodies and reagents

Anti-Actin (Sigma-Aldrich; A5316), anti-FLAG (Sigma; F3165), anti-GFP (D5.1) (Cell Signaling Technology; 2956), anti-GST (SIGMA; G7781), anti-MLKL (Sigma; SAB1302339), anti-MLKL phospho-S345 [EPR9515(2)] (Abcam; ab196436), anti-MYC (9B11) (Cell Signaling Technology; 2276), anti-Phosphoserine antibody (Abcam; ab9332), anti-RIPK1 (BD Biosciences; 610459), anti-RIPK1 (Cell Signaling Technology; 3493S), anti-RIPK1 phospho-S166 (Cell Signaling Technology; 31122 for mouse and 65746 for human), anti-RIPK1 phospho-S357 (developed in collaboration with Cell Signaling Technology; 1:500 for immunoblotting), anti-FADD (Santa Cruz; sc-6036 for IPs shown in Figures 2A, 2B, 2C and 2D), anti-FADD (Merck Millipore; 05-486 for IP shown in Figure S2A), anti-caspase-8 (mouse) monoclonal antibody (1G12) (Enzo Life Sciences; ALX-804-447-C100), anti-cleaved caspase-8 (Asp387) (D5B2) XP® Rabbit mAb (Cell Signaling Technology; 8592s), anti-TNFR1 antibody (BD Pharmingen; 559915), and anti-ULK1 (clone D8H5) (Cell Signaling Technology; 8054). IRDye 800- or IRDye 680-conjugated secondary antibodies were purchased from LI-COR Biosciences (926-32210/11, 926-68070/71, 926-68024 and 926-32214). 3-Methyladenine (Sigma; M9281), FLAG-mTNFα (Enzo Life Sciences; ALX-522-009-C050), TNF Recombinant Mouse Protein (Thermo Scientific; PMC3014), active GST-hULK1 (1-649) (Sigma; SRP5096), Q-VD-OPh (Selleck Chemicals; S7311 and MP BIOMEDICALS; 03OPH109), z-VAD-FMK (Selleck Chemicals; S7023), SBI-0206965 (Xcess Biosciences; M60268), MRT68921 HCl (Selleck Chemicals; S7949), Birinapant [SMAC-mimetic] (Selleck Chemicals; S7015), Alkaline Phosphatase (Thermo Fisher; EF0654), Protein G Sepharose 4 Fast Flow (GE Healthcare Life Sciences; 17061801), Protein A/G PLUS-Agarose (Santa Cruz; sc-2003), Lipofectamine RNAiMAX Transfection Reagent (Thermo Fisher; 13778150), Lipofectamine® 2000 Transfection Reagent (Thermo Fisher; 11668027; used in L929 cells), Fugene 6 (Promega; E2692; used in PlatE or HEK293 cells).

Constructs and siRNAs

MYC-hRIPK1 was kindly provided by Prof. Sudan He (Cyrus Tang Hematology Center, Soochow University, China). AMPKβ2 cDNA was cloned from HEK293 cDNA. Then, AMPKβ2 cDNA was

subcloned into pGEX-6P-1 (GE Healthcare). pMSCVblast/GFP-ULK1 was previously described (Hieke et al., 2015). cDNA of full length hRIPK1 or truncated hRIPK1(1-249), hRIPK1(250-475), hRIPK1(476-671) harboring Xho I and Not I restriction enzyme sites were amplified from MYC-hRIPK1. PCR fragments were inserted into pGEX-5X-3 vector to generate cDNAs encoding GST-hRIPK1 variants. cDNA of full length hRIPK1 harboring Xho I and Not I restriction enzyme sites amplified from MYC-hRIPK1 was inserted into pCI-neo-3xFLAG-RIPK3 vector (kindly provided by Prof. Sudan He (Cyrus Tang Hematology Center, Soochow University, China)) digested with Xho I and Not I restriction enzymes to generate pCI-neo-3xFLAG-RIPK1. cDNA of full length 3xFLAG-hRIPK1 harboring Bgl II and Not I restriction enzyme sites amplified from pCI-neo-3xFLAG-RIPK1 was inserted into pMSCVpuro vector to generate pMSCVpuro-3xFLAG-RIPK1. cDNA of full length hRIPK1 single or multi point mutants (S320A, S333A, S335A, T337A, S345A, S346A, S357A, K377R) harboring Xho I and Not I restriction enzyme sites amplified from MYC-hRIPK1 by overlap PCR was inserted into pMSCVpuro-3xFLAG-RIPK1 digested with Xho I and Not I restriction enzymes to generate pMSCVpuro-3xFLAG-RIPK1 mutants. cDNAs of GST-hRIPK1(250-475) single or multi point mutants (S320A, S333A, S335A, T337A, S345A, S346A, S357A) harboring Xho I and Not I restriction enzyme sites and amplified from corresponding pMSCVpuro-3xFLAG-RIPK1 vectors were inserted into pGEX-5X-3 vector digested with Xho I and Not I restriction enzymes to generate cDNAs encoding GST-hRIPK1 mutants. Alternatively, cDNAs of GST-hRIPK1(250-475) single or multi point mutants (S262A, S291A, S296A, S389A) were generated from GST-hRIPK1(250-475) WT via one-step PCR (one pair of fully complementary primers). Sequences of all oligonucleotides used for amplification or mutagenesis PCRs are listed in Table S2. Mouse ULK1 (ON-TARGETplus siRNA SMARTpool, L-040155-00-0010) and control siRNAs (ON-TARGETplus non-targeting pool, D-001810-10-20) were obtained from Dharmacon.

Cell lines

Ripk1 KO MEFs were kindly provided by Michelle Kelliher (University of Massachusetts Medical School, USA). *Ripk3* KO MEFs were kindly provided by Jiahuai Han (School of Life Sciences, Xiamen University, China). *Ulk1/2* DKO MEFs were kindly provided by Tullia Lindsten (Memorial Sloan Kettering Cancer Center, New York, USA). Flp-In™ TREx™ 293 inducibly expressing GFP-VECTOR, GFP-ULK1 or GFP-ULK1 kinase dead (KD) were described previously (Löffler et al., 2011). For the generation of

L929 cells stably expressing GFP-ULK1, or MEFs stably expressing FLAG-hRIPK1, the vectors pMSCVblast/GFP-ULK1 or pMSCVpuro/FLAG-hRIPK1 were transfected into PlatE cells (kindly provided by Toshio Kitamura, Institute of Medical Science, University of Tokyo, Japan) using FuGENE® 6 (Promega; E2692). After 48h, retroviral supernatant was collected and used for the infection of L929 cells or MEFs in combination with 10 µg/ml polybrene. After 12 h, cells were selected in medium containing puromycin (2.5 µg/ml for MEFs; 50 µg/ml for L929 cells) or blasticidine (35 µg/ml for MEFs and L929 cells). MEFs and Flp-In™ T-REx™ 293 cell lines were cultured in high D-glucose DMEM (Thermo Fisher; 41965-039) supplemented with 10% FCS (GE Healthcare; A15-101, or Thermo Fisher; 10270-106), 100 U/ml penicillin and 100 µg/ml streptomycin at 37°C and 5% CO_2. For the induction of GFP, GFP-ULK1 or GFP-ULK1 kinase dead (KD), Flp-In™ T-REx™ 293 were cultured in full medium including 0.1 µg/ml doxycycline (Clontech; 631311) overnight.

Protein expression and purification

pGEX-5X-3- or pGEX-6P-1-based vectors containing cDNAs of interest were transformed into *E. coli* BL 21. Target protein expression was induced by 0.1-1 mM IPTG for 3-5 h at 30°C. Bacteria were harvested and resuspended in bacterial lysis buffer (300 mM NaCl, 50 mM Tris-HCl (pH 8.0), 5 mM EDTA, 0.01% Igepal, 100 ng/ml lysozyme, 1x protease inhibitor cocktail). After sonification and centrifugation at 10,000 g for 20 min, the supernatant was incubated with glutathione Sepharose 4B beads (GE Healthcare; 17-0756-01) overnight. After washing 3 times with lysis buffer, soluble proteins were obtained by incubation of the beads with elution buffer (50 mM Tris-HCl (pH 8.0), 20 mM glutathione reduced) for 10 min at room temperature (3-5 times). Purified proteins were stored at -20 or -80°C.

In vitro kinase assay

For *in vitro* kinase assays, 1-2 µg substrate were incubated with 0.25-0.5 µg activated kinase in kinase buffer (50 mM Tris-Cl pH 7.5, 0.1 mM EGTA, 1 mM DTT, 7.5 mM $Mg(CH_3COO)_2$, 2 µM ATP (non-radioactive) with or without 10 µCi [γ-^{32}P]-ATP) for 45 min at 30°C. The kinase reaction was stopped after adding the loading buffer and boiling for 5 min at 95°C. After Coomassie staining or

immunoblotting, autoradiography was performed or phosphorylation was detected using anti-phosphoserine antibody. ATP (non-radioactive) (Cell Signaling Technology; #9804), $Mg(CH_3COO)_2$ (AppliChem; #A6999), [γ-^{32}P]-ATP (Hartmann Analytics; #SRP 301). Activated ULK1 (1-649) (SIGMA; SRP5096).

Protein dephosphorylation assay

Two duplicate samples were separated by the same SDS-PAGE and then transferred to the same PVDF membrane. Following blocking with 5% BSA in TBS-T for 1 h at room temperature, the PVDF membrane was washed with TBS-T twice (5 min each). The membrane was cut into two halves with one sample on each membrane. The two membranes were placed into two tubes with or without 10 U alkaline phosphatase (2 ml reaction volume) and incubated for 1 h at 37°C with shaking (350 rpm). After washing twice with TBS-T (5 min each), the membranes were incubated with the corresponding primary antibodies at 4°C overnight.

Immunoblotting and Immunopurification

For immunoblotting, cells were lysed in 1% NP-40 lysis buffer (50 mM Tris-Cl pH 7.5, 150 mM NaCl , 1 mM EDTA, 1% NP-40, 10% glycerin, 1 mM Na_3VO_4, 50 mM NaF and protease inhibitor cocktail [Sigma-Aldrich; P2714]). An equal amount of protein (30-50 µg) were separated by SDS-PAGE, and then transferred to PVDF membrane (Millipore; IPFL00010). Target proteins were detected by the indicated primary antibodies, followed by the corresponding IRDye®800- or IRDye®680-conjugated secondary antibodies (LI-COR Biosciences). Signals were detected with an Odyssey Infrared Imaging system (LI-COR Biosciences). For immunopurification, cells were lysed in the same lysis buffer for 30 min on ice. After 10,000 g centrifugation for 10 min, the supernatants were incubated with indicated beads [GFP-Trap®_A (ChromoTek; gta-20 or ANTI-FLAG® M2 Affinity Gel (Sigma; A2220) or ANTI-c-Myc Agarose Affinity Gel (Sigma; A7470)] overnight. Thereafter, the beads were washed five times with lysis buffer, and boiled in sample buffer for 5 min at 95°C. Purified proteins were analyzed by immunoblotting.

For complex I IP, cells were stimulated with 100 ng/ml mTNFα as indicated. Cells were lysed in 0.5% NP-40 IP lysis buffer (20 mM Tris-HCl, [pH 7.4], 150 mM NaCl, 0.5% Nonidet P40, 10% glycerol, 1× complete protease inhibitor Cocktail (Sigma; P2714), 1× PhosSTOP (Roche; 04906837001) and 10 µM PR619) and rotated for 20 minutes at 4°C. After centrifugation at 17,000 g for 10 min, the supernatant was precleared using Protein G Sepharose beads for 30 min at 4°C. After that, the precleared supernatant was incubated with FLAG beads (Sigma; A2220) overnight. Beads were washed 4 times using IP buffer and eluted with 2× SDS-Loading buffer for 10 minutes at 95°C. For complex II IP, MEFs and L929 cells were stimulated as indicated in the figure legends and cells were lysed in 1% Triton X-100 IP lysis buffer (30 mM Tris-HCl [pH 7.4], 120 mM NaCl, 2 mM EDTA, 2 mM KCl, 1% Triton X-100, complete protease-inhibitor cocktail) on ice for 20 minutes and centrifuged at 17,000 g for 10 min. Supernatant was precleared using Protein G Sepharose beads for 30 min at 4°C. 25 µl protein G beads were blocked for 1 h with lysis buffer containing 1% BSA and bound with 1.5 µg FADD antibody (Santa Cruz; sc-6036) for 2 h and incubated with lysates for 4 h at 4°C or lysates were incubated with 3 µg FADD antibody (Merck Millipore; 05-486) for 6-8 h and then incubated with 25 µl protein G beads blocked for 1 h with lysis buffer containing 1% BSA overnight. Beads were washed 4 times using IP buffer and were boiled with 2× SDS-Loading buffer for 10 min at 95°C.

GST-Pulldown

GST fusion proteins were purified from *E. coli* BL21 with glutathione Sepharose 4B beads (GE Healthcare; 17-0756-01). For GST pulldown, 2 µg of GST fusion protein were incubated with 1 mg of Flp-In™ T-REx™ 293 cell lysate in 1% NP-40 lysis buffer at 4°C overnight and then washed five times with lysis buffer. The beads were boiled with sample buffer at 95°C for 5 min and purified proteins were analyzed by Coomassie and immunoblotting.

Cell death and cell viability assay

Total cells treated with indicated stimuli were trypsinized and collected, then incubated in propidium iodide (PI) (5 µg/ml) solution at 4°C for 1 h. PI-positive cells were measured by flow cytometer (LSRFortessa, BD Biosciences). For cell viability assay, ATP level is measured by CellTiter-Glo® kit (Promega; G7570) according to the manufacturer's instructions.

Mass spectrometry

Acetone precipitation of protein samples was performed for 4 h at -20°C. After incubation, the proteins were resuspended in 40 mM ammonium bicarbonate and digested with trypsin (Promega, trypsin:protein ratio 1:100) over night at 37°C. Digests were quenched by acidification with trifluoracetic acid (TFA) and concentrated in vacuum. Subsequently, mass spectrometry based analysis of peptides was carried out.

Peptide separation and analysis was performed on an UltiMate3000 LC system coupled online to an Orbitrap XL mass spectrometer (both Thermo Fisher Scientific). Peptides were concentrated using in-house packed 100 µm ID reversed-phase (RP) precolumn (ReproSil-Pur C18-AQ 3 µm resin, Dr. Maisch GmbH) with 0.1% (v/v) TFA and then separated on a 75 µm ID x 18 cm RP column (in-house packed, ReproSil-Pur C18-AQ 3 µm resin, Dr. Maisch GmbH) using a binary gradient (solvent A: 0.1% formic acid, solvent B: 0.1% (v/v) formic acid in 84% (v/v) acetonitrile) delivered at 230 nl/min: 40% solvent B in 65 min and 98% solvent B in 15 min.

Peptides were directly eluted to nano-electrospray ion source equipped with distal coated SilicaTip Emitter (New Objective). The electrospray voltage was set at 1.5 V and the capillary temperature was maintained at 200°C. At first a full scan (m/z 350-2000, automatic gain control target value of $1e^6$, resolution r = 60,000 at m/z 400) was performed in the orbitrap analyzer. Up to the ten most intense multiple charged ions in each full scan MS/MS spectra were acquired in the linear ion trap with the following parameters: normalized collision energy 35%, dynamic exclusion 30 s, automatic gain control 5,000 ions. Multistage activation was enabled using neutral loss masses of phosphoric acid at 98, 49 and 32.6 m/z.

Raw data were processed with MaxQuant v. 1.5.3.30. (ref. (Cox and Mann, 2008)) MS/MS spectra were searched against protein sequences of generated fusion proteins and human ULK1 (Swiss-Prot 2016_08) with default search parameters unless otherwise stated. Phosphorylation of serine, threonine and tyrosine, oxidation of methionine and acetylation of protein N-termini were set as variable modifications. The resultant peptide list was filtered for phosphorylated peptides with a score greater than 40 and a posterior error probability score (PEP) less than 0.01. Only phosphorylation sites with a localization probability score over 0.75 were considered.

Alternatively, samples were separated by a 4-12% polyacrylamide gel. After Coomassie brilliant blue

staining, the protein containing bands were excised and processed as described elsewhere (Poschmann et al., 2014). Briefly, bands were destained, washed, reduced with dithiothreitol, alkylated with iodoacetamide and digested with trypsin (Serva) in 50 mM NH_4HCO_3 overnight at 37°C. Peptides were extracted with 0.1% trifluoroacetic acid and subjected to liquid chromatography. For peptide separation over a 55 minute LC-gradient with 300 ml/min an Ultimate 3000 Rapid Separation liquid chromatography system (Thermo Scientific) equipped with an Acclaim PepMap 100 C18 column (75 µm inner diameter, 25 cm length, 2 mm particle size from Thermo Scientific) was used. MS analysis was carried out on a Q-Exactive plus mass spectrometer (Thermo Scientific) operating in positive mode and equipped with a nano electrospray ionization source. Capillary temperature was set to 250°C and source voltage to 1.4 kV. Survey scans were carried out over a mass range from 200-2,000 m/z at a resolution of 70,000 (at 200 m/z). The target value for the automatic gain control was 3,000,000 and the maximum fill time 50 ms. The 20 most intense peptide ions (excluding singly charged ions) were selected for fragmentation. Peptide fragments were analyzed using a maximal fill time of 50 ms and automatic gain control target value of 100,000 and a resolution of 17,500 (at 200 m/z). Already fragmented ions were excluded for fragmentation for 10 seconds. Acquired spectra were searched using Mascot 2.4 within Proteome Discoverer version 1.4.1.14 against the SwissProt homo sapiens proteome dataset (release 2016_06, 20200 sequences). Carbamidomethyl at cysteines was set as fixed modification and phosphorylation at serine, threonine and tyrosine and methionine oxidation were considered as variable modifications as well as tryptic cleavage specificity (cleavage behind K and R) with a maximum of two missed cleavage sites. Predefined values were used for other parameters including a false discovery rate of 1% on peptide level, a main search precursor mass tolerance of 10 ppm and mass tolerance of 10 mmu for fragment spectra.

Statistical analysis

For CellTiter-Glo® assays, shown data represent mean of at least triplicates ± SD. Cell viability of untreated control cells was set to 100%. For PI uptake, shown data represent mean of at least three independent experiments ± SD. Absolute values are shown. For the quantification of immunoblots, the density of each protein band was divided by the average of the density of all bands from the same protein on the membrane. Subsequently, fold changes were calculated by dividing each

normalized ratio (protein to loading control) by the average of the ratios of the control lane (as indicated in the corresponding figure legend). For figures 1A-F and 5A, statistical analyses were performed using repeated measures two-way ANOVA (corrected by Sidak's multiple comparisons test). For figure 1G, statistical analysis was performed using repeated measures two-way ANOVA (corrected by Tukey's multiple comparisons test). For figure 5B, statistical analysis was performed using repeated measures two-way ANOVA (corrected by Sidak's multiple comparisons test or by Tukey's multiple comparisons test). For figure S3G, statistical analysis was performed using an unpaired t test with Welch's correction. Compared treatments or cell lines are indicated in the bar diagrams or the corresponding legends. *P* values < 0.05 were considered statistically significant. All statistical data were calculated with GraphPad Prism (version 7.01).

ACKNOWLEDGMENTS

We thank Michelle Kelliher (University of Massachusetts Medical School, USA) for providing *ripk1* KO MEFs and Sudan He (Cyrus Tang Hematology Center, Soochow University, China) for providing pcDNA3.1-MYC-hRIPK1. We thank Jiahuai Han for providing *ripk3* KO MEFs. We thank Tullia Lindsten for providing *ulk1/2* DKO MEFs. We thank Onur Eren and Manolis Pasparakis for providing anti-FADD antibody (Santa Cruz; sc-6036), protocols and helpful discussions. We also thank Daichao Xu for helpful discussion. This work was supported by the Deutsche Forschungsgemeinschaft STO 864/4-1, STO 864/5-1 and GRK 2158 (to BS), the Research Committee of the Medical Faculty of the Heinrich Heine University Düsseldorf (22/2015 to BS), and the Düsseldorf School of Oncology (to BS; funded by the Comprehensive Cancer Center Düsseldorf/Deutsche Krebshilfe and the Medical Faculty of the Heinrich-Heine-University Düsseldorf).

CONFLICT OF INTEREST STATEMENT

Gary Kasof is employed by Cell Signaling Technology.

AUTHOR CONTRIBUTION STATEMENT

WW designed the experiments, performed cell viability assays, and *in vitro* kinase assays. XW cloned constructs encoding RIPK1 variants, purified GST-RIPK1 proteins and performed proximity ligation assay. WW and XW performed immunoblot analyses. NB, JC and CP supported *in vitro* kinase assays. JD, NWH, PB, DS, FS, KSc and SS gave technical support. GK generated RIPK1 phospho-S357 antibody. AS, KSt, AT and AG performed mass spectrometric analyses. WW, GK, AS, KSt, AT, AG and BS analyzed and interpreted the data and wrote the manuscript. BS supervised the project. All authors discussed the results and commented on the manuscript.

FIGURE LEGENDS

Figure 1:

ULK1 inhibits TNFα-induced cell death in L929 cells. (**A**) and (**B**) L929 cells were transfected with scramble or ULK1 siRNAs. 48 h post transfection, cells were treated with 10 ng/ml TNFα for indicated times. Then cell viability was measured by the quantification of ATP levels using CellTiter-Glo® kit and cell death was determined by the flow cytometric measurement of propidium iodide (PI) uptake. Data represent mean of four (cell viability) or three independent experiments (PI uptake) ± SD. (**C**) and (**D**) L929 cells were transfected with scramble or ULK1 siRNAs. 48 h post transfection, cells were treated with indicated concentrations of TNFα for 6 h. Subsequently, cell viability was measured by the quantification of ATP levels using CellTiter-Glo® kit and cell death was determined by the flow cytometric measurement of propidium iodide (PI) uptake. Data represent mean of triplicates ± SD. (**E**) L929 cells were transfected with scramble or ULK1 siRNAs. 48 h post transfection, cells were exposed to 10 ng/ml TNFα for indicated times. Then, cells were lysed and cleared cellular lysates were subjected to SDS-PAGE and immunoblotting for ULK1, phospho-MLKL (S345), MLKL, and Actin. The quantifications of the ratios of phospho-MLKL/Actin and MLKL/Actin are shown in the bar diagrams. **(F)** Murine embryonic fibroblasts (MEFs) were transfected with scramble or ULK1 siRNAs. 48 h post transfection, cells were exposed to 30 ng/ml TNFα and 100 nM SMAC-mimetic with or without 20 µM z-VAD for 4 h (TS or TSZ). Cell death was determined by the flow cytometric measurement of propidium iodide (PI) uptake. Data represent mean of six independent experiments ± SD. **(G)** *ulk1/2* DKO MEFs transfected with either empty vector (VC) or cDNAs encoding wild-type (WT) or kinase-dead (KD) ULK1 were exposed to 30 ng/ml TNFα and 100 nM SMAC-mimetic with or without 20 µM z-VAD for 6 h (TS or TSZ). Cell death was determined by the flow cytometric measurement of propidium iodide (PI) uptake. Data represent mean of three independent experiments ± SD. (**A-G**) For CellTiter-Glo® assays (**A** and **C**), cell viability of untreated control cells was set to 100%. For PI uptake, absolute values are shown (**B**, **D, F** and **G**). For the quantification of the immunoblot (**E**), the density of each protein band was divided by the average of the density of all bands from the same protein on the membrane. Then, fold changes were calculated by dividing each normalized ratio (protein to loading control) by the average of the ratios of the control lane (0 h TNFα for each cell line). Statistical

analyses were performed using repeated measures two-way ANOVA (corrected by Sidak's multiple comparisons test for **A**-**F** and corrected by Tukey's multiple comparisons test for **G**), comparing scramble siRNA- to the corresponding siULK1-transfected cells (**A-F**) or comparing vector or ULK1 KD to ULK1 WT upon TS or TSZ treatments (**G**). **P* < 0.05, ***P* < 0.01, ****P* < 0.001, *****P* < 0.0001

Figure 2:

ULK1 restricts the formation of complex IIb/necrosome. (**A**) L929 cells were pretreated with DMSO or 5 μM MRT68921 (ULK1 inhibitor) for 1 h, followed by treatment with 10 ng/ml TNFα and 30 μM QVD (TQ) for indicated times. Cells were lysed and TNFα-induced complex-IIb/necrosome was purified using anti-FADD antibodies. Purified proteins were subjected to SDS-PAGE and immunoblotting for FADD, RIPK1, phospho-RIPK1 (S166), caspase-8, and cleaved caspase-8. (**B**) MEFs were pretreated with DMSO or 5 μM MRT68921 for 1 h, followed by treatment with 30 ng/ml TNFα, 20 μM z-VAD and 100 nM SMAC-mimetic for 1 h (TSZ). Cells were lysed and TNFα-induced complex-IIb/necrosome was purified using anti-FADD antibodies. Purified proteins were subjected to SDS-PAGE and immunoblotting for FADD, RIPK1, phospho-RIPK1 (S166), caspase-8, and cleaved caspase-8. (**C**) MEFs were pretreated with DMSO or 10 μM SBI-0206965 (ULK1 inhibitor) for 1 h, followed by treatment with 30 ng/ml TNFα and 20 μM z-VAD with 100 nM SMAC-mimetic 1 h (TSZ). Cells were lysed and TNFα-induced complex-IIb/necrosome was purified using anti-FADD antibodies. Purified proteins were subjected to SDS-PAGE and immunoblotting for FADD, RIPK1, phospho-RIPK1 (S166), caspase-8, and cleaved caspase-8. (**D**) *ulk1/2* DKO MEFs transfected with either empty vector (VC) or cDNAs encoding wild-type (WT) or kinase-dead (KD) ULK1 were exposed to 30 ng/ml TNFα and 20 μM z-VAD for 4 h (TZ). Cells were lysed and TNFα-induced complex-IIb/necrosome was purified using anti-FADD antibodies. Purified proteins were subjected to SDS-PAGE and immunoblotting for FADD, RIPK1, phospho-RIPK1 (S166), caspase-8, and cleaved caspase-8. The input was additionally subjected to immunoblotting for ULK1. (**E**) L929 cells were pretreated with DMSO or 5 μM MRT68921 for 1 h, followed by treatment with 10 ng/ml TNFα and 30 μM QVD (TQ) for indicated times. Cells were lysed and cleared cellular lysates were subjected to immunopurification with anti-RIPK1 antibodies. Purified proteins were subjected to SDS-PAGE and analyzed by immunoblotting for RIPK1, phospho-RIPK1 (S166), MLKL, phospho-MLKL (S345), and RIPK3. (**F**) *ripk3*

KO MEFs stably expressing FLAG-mRIPK3 were pretreated with DMSO or 5 μM MRT68921 for 1 h, followed by treatment with 30 ng/ml TNFα, 20 μM z-VAD and 100 nM SMAC-mimetic (TSZ) for indicated times. Cells were lysed and TNFα-induced complex-IIb/necrosome was purified using anti-FLAG beads. Purified proteins were subjected to SDS-PAGE and analyzed by immunoblotting for RIPK1, phospho-RIPK1 (S166), MLKL, phospho-MLKL (S345), and RIPK3.

Figure 3:

ULK1 directly phosphorylates RIPK1 at Serine 357. (**A**) For *in vitro* kinase assay, purified GST, GST-hAMPKβ2, GST-hRIPK1(1-249), GST-hRIPK1(250-475) or GST-hRIPK1(476-671) were incubated with activated ULK1 and [γ-^{32}P]-ATP. The reactions were subjected to SDS-PAGE. After Coomassie staining and drying of the gels, autoradiography was performed. (**B**) Partial alignment of amino acid sequences of RIPK1 from six different species. The evolutionarily conserved S357 is highlighted in orange. The putative ULK1 consensus phosphorylation motif is defined by aromatic or aliphatic amino acids at positions −3, +1 and +2 from the phospho-acceptor site (highlighted in grey) (Egan et al., 2015). (**C**) GST or indicated GST-RIPK1 proteins were purified and were incubated with activated ULK1 and cold ATP. The reactions were subjected to SDS-PAGE and analyzed by immunoblotting for phospho-RIPK1 (S357), ULK1 and GST. (**D**) HEK293 cells inducibly expressing GFP-ULK1 were transfected with cDNA encoding FLAG-RIPK1 WT or FLAG-RIPK1 S357A for 24 h. Then, cells were exposed to 10 μM Necrostatin-1 for 1 h. Cells were lysed and cleared cellular lysates were subjected to SDS-PAGE and analyzed by immunoblotting for phospho RIPK1 (S357), FLAG, GFP and Actin. (**E**) HEK293 cells inducibly expressing GFP-ULK1 were transfected with cDNA encoding FLAG-RIPK1 WT or FLAG-RIPK1 S357A for 24 h. Then, cells were lysed and cleared cellular lysates were subjected to SDS-PAGE. After transfer of proteins to a PVDF membrane, the membrane was incubated with or without alkaline phosphatase and analyzed by immunoblotting for phospho-RIPK1 (S357), FLAG, GFP and Actin. (**F**) HEK293 cells inducibly expressing GFP, GFP-ULK1 wild-type (WT) or GFP-ULK1 kinase dead (KD) were transfected with cDNA encoding kinase-dead MYC-RIPK1 for 24 h. Then, cells were lysed and cleared cellular lysates were subjected to SDS-PAGE and analyzed by immunoblotting for phospho-RIPK1 (S357), MYC, Actin and GFP. (**G**) HEK293 cells inducibly expressing GFP-ULK1 were transfected with cDNA encoding FLAG-RIPK1 WT or FLAG-RIPK1 S357A for 24 h. Then, cells were

exposed to 5 μM MRT68921 or DMSO for 1 h. Cells were lysed and cleared cellular lysates were subjected to SDS-PAGE and analyzed by immunoblotting for phospho-RIPK1 (S357), FLAG, GFP and Actin.

Figure 4:

ULK1 regulates the distribution of RIPK1 between complex I and complex II. *ulk1/2* DKO MEFs transfected with empty vector or cDNA encoding FLAG-ULK1 were treated with 100 ng/ml mTNFα for indicated times. Cells were lysed and complex I was purified using anti-TNFR1 antibodies. Post-FLAG IP lysates depleted of complex I were subjected to RIPK1 immunopurification with anti-RIPK1 antibodies. Purified proteins were subjected SDS-PAGE and analyzed by immunoblotting for ULK1, RIPK1, phospho-RIPK1 (S166), phospho-RIPK1 (S357), and TNFR1.

Figure 5:

ULK1-dependent phosphorylation of RIPK1 inhibits TNFα-induced cell death. (**A**) *ripk1* KO MEFs stably expressing FLAG-RIPK1 WT and FLAG-RIPK1 S357A were treated with 30 ng/ml TNFα/100 nM SMAC-mimetic/20 μM z-VAD (TSZ) for indicated times. Cells were lysed and cleared cellular lysates were subjected to SDS-PAGE and immunoblotting for phospho-RIPK1 (S166), FLAG, phospho-MLKL (S345), MLKL and Actin. The quantifications of the ratios of phospho-MLKL/Actin and MLKL/Actin are shown in the bar diagrams and are from three independent experiments. (**B**) *ripk1* KO MEFs over-expressing mRIPK3 reconstituted with pMSCVpuro vector, pMSCVpuro-FLAG-RIPK1 WT or pMSCVpuro-FLAG-RIPK1 S357A were transfected with scramble or ULK1 siRNAs for 48 h. Cells were treated with 30 ng/ml TNFα and 100 nM SMAC-mimetic without (TS) or with 20 μM z-VAD (TSZ) for 2.5 h and cells were trypsinized and collected. Thereafter, pellets were incubated with 5 μg/ml propidium iodide (PI). PI-positive cells were quantified by flow cytometry. Data represent mean ± SD from five independent experiments. (**C**) *ripk1* KO MEFs over-expressing mRIPK3 were reconstituted with pMSCVpuro-FLAG-RIPK1 WT or pMSCVpuro-FLAG-RIPK1 S357A. Cells were treated with 30 ng/ml TNFα / 100 nM SMAC-mimetic / 20 μM z-VAD (TSZ) / for 30 min. Cells were lysed and complex IIb/necrosome was purified using anti-FADD. Purified proteins were subjected to SDS-PAGE

and immunoblotting for FADD, RIPK1, phospho-RIPK1 (S166), MLKL, phospho-MLKL (S345), caspase-8, cleaved caspase-8, RIPK3, and Actin. (**A** and **B**) For the quantification of the immunoblot (**A**), the density of each protein band was divided by the average of the density of all bands from the same protein on the membrane. Then, fold changes were calculated by dividing each normalized ratio (protein to loading control) by the average of the ratios of the control lane (for pMLKL/Actin: 2 h TSZ, *ripk1* KO + RIPK1 WT; for MLKL/Actin: 0 h TSZ, *ripk1* KO + RIPK1 WT). For PI uptake, absolute values are shown (**B**). Statistical analyses were performed using repeated measures two-way ANOVA (corrected by Sidak's multiple comparisons test for **A** [comparison of identical time points between two cell lines] and **B** [comparison of identical cell lines between two siRNAs), or corrected by Tukey's multiple comparisons test for **B** [comparison of two cell lines within identical siRNA]). ns = not significant, *P < 0.05, **P < 0.01, ****P < 0.0001

Figure S1:

Autophagy regulates TNFα-induced cell death. (**A**) and (**B**) Murine L929 cells were exposed to TNFα, TNFα/3-MA, TNFα/EBSS, 3-MA, or EBSS for indicated times (TNFα: 10 ng/ml; 3-MA: 5 mM). Subsequently, cell viability was measured by the quantification of ATP levels using CellTiter-Glo® kit and cell death was determined by the flow cytometric measurement of propidium iodide (PI) uptake. Individual data points of two experiments are shown. For CellTiter-Glo® assays (**A**), cell viability of untreated control cells was set to 100%. For PI uptake, absolute values are shown (**B**).

Figure S2:

ULK1 restricts the formation of complex IIb/necrosome. MEFs were pretreated with DMSO or 5 μM MRT68921 for 1 h, followed by treatment with 30 ng/ml TNFα and 20 μM z-VAD (TZ) for 4 h. Cells were lysed and TNFα-induced complex-IIb/necrosome was purified using anti-FADD antibodies. Purified proteins were subjected to SDS-PAGE and immunoblotting for FADD, RIPK1, phospho-RIPK1 (S166), caspase-8, and cleaved caspase-8.

Figure S3:

ULK1 interacts with RIPK1. (**A**) HEK293 cells inducibly expressing GFP or GFP-ULK1 were transfected with a vector encoding FLAG-RIPK1 for 24 h. Then, cells were lysed and cleared cellular lysates were subjected to immunopurification with GFP-Trap® agarose. Purified proteins were subjected to SDS-PAGE and analyzed by immunoblotting for FLAG or GFP. (**B**) HEK293 cells inducibly expressing GFP or GFP-ULK1 were transfected with a vector encoding MYC-RIPK1 for 24 h. Then, cells were lysed and cleared cellular lysates were subjected to immunopurification with anti-MYC beads. Purified proteins were subjected to SDS-PAGE and analyzed by immunoblotting for MYC and GFP. (**C**) L929 cells were treated with regular medium or TNFα/QVD for 3 h. Then cells were collected and lysed. Cleared cellular lysates were incubated with normal IgG or anti-ULK1 beads overnight. After washing three times, purified proteins were subjected to SDS-PAGE and analyzed by immunoblotting for ULK1 and RIPK1. (**D**) L929 cells stably expressing GFP-ULK1 were exposed to regular medium or TNFα for 6 h. Then, cells were lysed and cleared cellular lysates were subjected to immunopurification with GFP-Trap® agarose. Purified proteins were subjected to SDS-PAGE and analyzed by immunoblotting for GFP and RIPK1. (**E**) GST, GST-RIPK1 or GST-ATG13 bound to glutathione beads were incubated with cleared cellular lysates of HEK 293 cells inducibly expressing FLAG-ULK1 overnight. After washing the beads three times, purified proteins were subjected to SDS-PAGE and analyzed by immunoblotting for FLAG. Presence of GST proteins was confirmed by immunoblotting for RIPK1 and ATG13 using anti-RIPK1 and anti-ATG13 antibodies. (**F**) GST-RIPK1(1-249), GST-RIPK1(250-475) or GST-RIPK1(476-671) proteins were incubated with cleared cellular lysates of HEK293 cells inducibly expressing GFP-ULK1 in the presence of GFP-Trap® agarose overnight. After washing the beads three times, purified proteins were subjected to SDS-PAGE and analyzed by immunoblotting for GFP and GST. (**G**) RIPK1 KO MEFs transfected with either empty vector or cDNA encoding FLAG-hRIPK1 were seeded on coverslips. The next day, cells were directly fixed and used for proximity ligation assay (PLA) as described in the material and methods section (anti-ULK1 antibody: CST, 8054; anti-RIPK1 antibody: BD Biosciences; 610459). Nuclei were stained with DAPI. Signals and nuclei per image were counted and the signal:nuclei ratio was calculated. Data are represented as mean ± SD. A minimum of 107 cells was analyzed**.** Statistical analysis was performed using an unpaired t test with Welch's correction. (**H**) *ripk1* KO MEFs transfected with empty vector or with cDNA encoding wild-type RIPK1 or the

K377R variant were exposed to 30 ng/ml TNFα, 20 μM z-VAD and 100 nM SMAC-mimetic (TSZ) for 1 h. Then, cells were lysed and cleared cellular lysates were subjected to immunopurification with ULK1 antibodies. Purified proteins were subjected to SDS-PAGE and analyzed by immunoblotting for ULK1 and RIPK1.

Figure S4:

ULK1 directly phosphorylates RIPK1. (**A**) HEK293 cells inducibly expressing GFP-ULK1 were transfected with cDNA encoding FLAG-RIPK1 for 24h. Then, cells were lysed and cleared cellular lysates were subjected to immunopurification with anti-FLAG beads. Purified proteins were subjected to SDS-PAGE. After transfer of proteins to a PVDF membrane, the membrane was incubated with or without alkaline phosphatase and analyzed by immunoblotting for phospho-serine (pSer) and FLAG. (**B**) HEK293 cells inducibly expressing GFP, GFP-ULK1 or GFP-ULK1 kinase dead (KD) were transfected with a vector encoding kinase-dead MYC-RIPK1 for 24 h. Then, cells were lysed and cleared cellular lysates were subjected to immunopurification with anti-MYC agarose. Purified proteins were subjected to SDS-PAGE and analyzed by immunoblotting for phospho-serine (pSer), MYC and GFP. (**C**) Indicated GST-RIPK1 proteins were purified and were incubated with activated ULK1 and non-radioactive ATP. The reactions were subjected to SDS-PAGE and analyzed by immunoblotting for pSer and ULK1. In parallel, the different GST-RIPK1 proteins were quantified by Coomassie staining. (**D**) *ripk1* KO MEFs transfected with empty vector or cDNA encoding FLAG-RIPK1 were exposed to 30 ng/ml TNFα for indicated times. Then, cells were lysed and cleared cellular lysates were subjected to immunopurification with anti-FLAG M2 Affinity Gel. Purified proteins were subjected to SDS-PAGE and analyzed by immunoblotting for phospho-RIPK1 (S357) and RIPK1.

Figure S5:

ULK1 regulates RIPK1 function via the phosphorylation of S357. ULK1 associates with both complex I-bound and cytosolic RIPK1. Apparently, ULK1 preferentially phosphorylates cytosolic RIPK1 at S357. This phosphorylation impedes the formation of complex IIb/necrosome and thus inhibits cell

death. TNFR1-associated RIPK1 is not phosphorylated at S357, but stabilized in this complex.

REFERENCES

Aaes, T.L., Kaczmarek, A., Delvaeye, T., De Craene, B., De Koker, S., Heyndrickx, L., Delrue, I., Taminau, J., Wiernicki, B., De Groote, P*., et al.* (2016). Vaccination with Necroptotic Cancer Cells Induces Efficient Anti-tumor Immunity. Cell reports *15*, 274-287.

Annibaldi, A., and Meier, P. (2018). Checkpoints in TNF-Induced Cell Death: Implications in Inflammation and Cancer. Trends Mol Med *24*, 49-65.

Artal-Sanz, M., and Tavernarakis, N. (2005). Proteolytic mechanisms in necrotic cell death and neurodegeneration. FEBS letters *579*, 3287-3296.

Biton, S., and Ashkenazi, A. (2011). NEMO and RIP1 control cell fate in response to extensive DNA damage via TNF-alpha feedforward signaling. Cell *145*, 92-103.

Brenner, D., Blaser, H., and Mak, T.W. (2015). Regulation of tumour necrosis factor signalling: live or let die. Nat Rev Immunol *15*, 362-374.

Cho, Y.S., Challa, S., Moquin, D., Genga, R., Ray, T.D., Guildford, M., and Chan, F.K. (2009). Phosphorylation-driven assembly of the RIP1-RIP3 complex regulates programmed necrosis and virus-induced inflammation. Cell *137*, 1112-1123.

Christofferson, D.E., and Yuan, J. (2010). Necroptosis as an alternative form of programmed cell death. Current opinion in cell biology *22*, 263-268.

Cox, J., and Mann, M. (2008). MaxQuant enables high peptide identification rates, individualized p.p.b.-range mass accuracies and proteome-wide protein quantification. Nat Biotechnol *26*, 1367-1372.

Dannappel, M., Vlantis, K., Kumari, S., Polykratis, A., Kim, C., Wachsmuth, L., Eftychi, C., Lin, J., Corona, T., Hermance, N*., et al.* (2014). RIPK1 maintains epithelial homeostasis by inhibiting apoptosis and necroptosis. Nature *513*, 90-94.

de Almagro, M.C., Goncharov, T., Izrael-Tomasevic, A., Duttler, S., Kist, M., Varfolomeev, E., Wu, X., Lee, W.P., Murray, J., Webster, J.D*., et al.* (2017). Coordinated ubiquitination and phosphorylation of RIP1 regulates necroptotic cell death. Cell Death Differ *24*, 26-37.

Degterev, A., Hitomi, J., Germscheid, M., Ch'en, I.L., Korkina, O., Teng, X., Abbott, D., Cuny, G.D., Yuan, C., Wagner, G*., et al.* (2008). Identification of RIP1 kinase as a specific cellular target of necrostatins. Nature chemical biology *4*, 313-321.

Degterev, A., Huang, Z., Boyce, M., Li, Y., Jagtap, P., Mizushima, N., Cuny, G.D., Mitchison, T.J., Moskowitz, M.A., and Yuan, J. (2005). Chemical inhibitor of nonapoptotic cell death with therapeutic potential for ischemic brain injury. Nature chemical biology *1*, 112-119.

Dillon, C.P., Weinlich, R., Rodriguez, D.A., Cripps, J.G., Quarato, G., Gurung, P., Verbist, K.C., Brewer, T.L., Llambi, F., Gong, Y.N*., et al.* (2014). RIPK1 blocks early postnatal lethality mediated by caspase-8 and RIPK3. Cell *157*, 1189-1202.

Dondelinger, Y., Delanghe, T., Rojas-Rivera, D., Priem, D., Delvaeye, T., Bruggeman, I., Van Herreweghe, F., Vandenabeele, P., and Bertrand, M.J.M. (2017). MK2 phosphorylation of RIPK1 regulates TNF-mediated cell death. Nature cell biology *19*, 1237-1247.

Dondelinger, Y., Jouan-Lanhouet, S., Divert, T., Theatre, E., Bertin, J., Gough, P.J., Giansanti, P., Heck, A.J., Dejardin, E., Vandenabeele, P*., et al.* (2015). NF-kappaB-Independent Role of IKKalpha/IKKbeta in Preventing RIPK1 Kinase-Dependent Apoptotic and Necroptotic Cell Death during TNF Signaling. Molecular cell *60*, 63-76.

Ea, C.K., Deng, L., Xia, Z.P., Pineda, G., and Chen, Z.J. (2006). Activation of IKK by TNFalpha requires site-specific ubiquitination of RIP1 and polyubiquitin binding by NEMO. Molecular cell *22*, 245-257.

Egan, D.F., Chun, M.G., Vamos, M., Zou, H., Rong, J., Miller, C.J., Lou, H.J., Raveendra-Panickar, D., Yang, C.C., Sheffler, D.J*., et al.* (2015). Small Molecule Inhibition of the Autophagy Kinase ULK1 and Identification of ULK1 Substrates. Molecular cell *59*, 285-297.

Feng, S., Yang, Y., Mei, Y., Ma, L., Zhu, D.E., Hoti, N., Castanares, M., and Wu, M. (2007). Cleavage of RIP3 inactivates its caspase-independent apoptosis pathway by removal of kinase domain. Cellular signalling *19*, 2056-2067.

Geng, J., Ito, Y., Shi, L., Amin, P., Chu, J., Ouchida, A.T., Mookhtiar, A.K., Zhao, H., Xu, D., Shan, B*., et al.* (2017). Regulation of RIPK1 activation by TAK1-mediated phosphorylation dictates apoptosis and necroptosis. Nature communications *8*, 359.

Goodall, M.L., Fitzwalter, B.E., Zahedi, S., Wu, M., Rodriguez, D., Mulcahy-Levy, J.M., Green, D.R., Morgan, M., Cramer, S.D., and Thorburn, A. (2016). The Autophagy Machinery Controls Cell Death Switching between Apoptosis and Necroptosis. Developmental cell *37*, 337-349.

Grootjans, S., Vanden Berghe, T., and Vandenabeele, P. (2017). Initiation and execution mechanisms of necroptosis: an overview. Cell Death Differ *24*, 1184-1195.

Guo, X., Yin, H., Chen, Y., Li, L., Li, J., and Liu, Q. (2016). TAK1 regulates caspase 8 activation and necroptotic signaling via multiple cell death checkpoints. Cell death & disease *7*, e2381.

Harris, K.G., Morosky, S.A., Drummond, C.G., Patel, M., Kim, C., Stolz, D.B., Bergelson, J.M., Cherry, S., and Coyne, C.B. (2015). RIP3 Regulates Autophagy and Promotes Coxsackievirus B3 Infection of Intestinal Epithelial Cells. Cell host & microbe *18*, 221-232.

He, S., Wang, L., Miao, L., Wang, T., Du, F., Zhao, L., and Wang, X. (2009). Receptor interacting protein kinase-3 determines cellular necrotic response to TNF-alpha. Cell *137*, 1100-1111.

Hieke, N., Löffler, A.S., Kaizuka, T., Berleth, N., Böhler, P., Driessen, S., Stuhldreier, F., Friesen, O., Assani, K., Schmitz, K*., et al.* (2015). Expression of a ULK1/2 binding-deficient ATG13 variant can partially restore autophagic activity in ATG13-deficient cells. Autophagy *11*, 1471-1483.

Jaco, I., Annibaldi, A., Lalaoui, N., Wilson, R., Tenev, T., Laurien, L., Kim, C., Jamal, K., Wicky John, S., Liccardi, G*., et al.* (2017). MK2 Phosphorylates RIPK1 to Prevent TNF-Induced Cell Death. Molecular cell *66*, 698-710 e695.

Joo, J.H., Dorsey, F.C., Joshi, A., Hennessy-Walters, K.M., Rose, K.L., McCastlain, K., Zhang, J., Iyengar, R., Jung, C.H., Suen, D.F*., et al.* (2011). Hsp90-Cdc37 chaperone complex regulates Ulk1- and Atg13-mediated mitophagy. Molecular cell *43*, 572-585.

Joo, J.H., Wang, B., Frankel, E., Ge, L., Xu, L., Iyengar, R., Li-Harms, X., Wright, C., Shaw, T.I., Lindsten, T*., et al.* (2016). The Noncanonical Role of ULK/ATG1 in ER-to-Golgi Trafficking Is Essential for Cellular Homeostasis. Molecular cell *62*, 491-506.

Jung, C.H., Jun, C.B., Ro, S.H., Kim, Y.M., Otto, N.M., Cao, J., Kundu, M., and Kim, D.H. (2009). ULK-Atg13-FIP200 complexes mediate mTOR signaling to the autophagy machinery. Molecular biology of the cell *20*, 1992-2003.

Kaiser, W.J., Daley-Bauer, L.P., Thapa, R.J., Mandal, P., Berger, S.B., Huang, C., Sundararajan, A., Guo, H., Roback, L., Speck, S.H*., et al.* (2014). RIP1 suppresses innate immune necrotic as well as apoptotic cell death during mammalian parturition. Proceedings of the National Academy of Sciences of the United States of America *111*, 7753-7758.

Kaiser, W.J., Upton, J.W., Long, A.B., Livingston-Rosanoff, D., Daley-Bauer, L.P., Hakem, R., Caspary, T., and Mocarski, E.S. (2011). RIP3 mediates the embryonic lethality of caspase-8-deficient mice. Nature *471*, 368-372.

Kearney, C.J., Cullen, S.P., Clancy, D., and Martin, S.J. (2014). RIPK1 can function as an inhibitor rather than an

initiator of RIPK3-dependent necroptosis. The FEBS journal *281*, 4921-4934.

Konno, H., Konno, K., and Barber, G.N. (2013). Cyclic dinucleotides trigger ULK1 (ATG1) phosphorylation of STING to prevent sustained innate immune signaling. Cell *155*, 688-698.

Levine, B., and Kroemer, G. (2008). Autophagy in the pathogenesis of disease. Cell *132*, 27-42.

Lim, J., Lachenmayer, M.L., Wu, S., Liu, W., Kundu, M., Wang, R., Komatsu, M., Oh, Y.J., Zhao, Y., and Yue, Z. (2015). Proteotoxic stress induces phosphorylation of p62/SQSTM1 by ULK1 to regulate selective autophagic clearance of protein aggregates. PLoS genetics *11*, e1004987.

Lin, Y., Devin, A., Rodriguez, Y., and Liu, Z.G. (1999). Cleavage of the death domain kinase RIP by caspase-8 prompts TNF-induced apoptosis. Genes & development *13*, 2514-2526.

Löffler, A.S., Alers, S., Dieterle, A.M., Keppeler, H., Franz-Wachtel, M., Kundu, M., Campbell, D.G., Wesselborg, S., Alessi, D.R., and Stork, B. (2011). Ulk1-mediated phosphorylation of AMPK constitutes a negative regulatory feedback loop. Autophagy *7*, 696-706.

Lu, W., Sun, J., Yoon, J.S., Zhang, Y., Zheng, L., Murphy, E., Mattson, M.P., and Lenardo, M.J. (2016). Mitochondrial Protein PGAM5 Regulates Mitophagic Protection against Cell Necroptosis. PLoS One *11*, e0147792.

Mandal, P., Berger, S.B., Pillay, S., Moriwaki, K., Huang, C., Guo, H., Lich, J.D., Finger, J., Kasparcova, V., Votta, B.*, et al.* (2014). RIP3 induces apoptosis independent of pronecrotic kinase activity. Molecular cell *56*, 481-495.

Matsuzawa-Ishimoto, Y., Shono, Y., Gomez, L.E., Hubbard-Lucey, V.M., Cammer, M., Neil, J., Dewan, M.Z., Lieberman, S.R., Lazrak, A., Marinis, J.M.*, et al.* (2017). Autophagy protein ATG16L1 prevents necroptosis in the intestinal epithelium. J Exp Med *214*, 3687-3705.

Matsuzawa, Y., Oshima, S., Nibe, Y., Kobayashi, M., Maeyashiki, C., Nemoto, Y., Nagaishi, T., Okamoto, R., Tsuchiya, K., Nakamura, T.*, et al.* (2015). RIPK3 regulates p62-LC3 complex formation via the caspase-8-dependent cleavage of p62. Biochemical and biophysical research communications *456*, 298-304.

Menon, M.B., Gropengiesser, J., Fischer, J., Novikova, L., Deuretzbacher, A., Lafera, J., Schimmeck, H., Czymmeck, N., Ronkina, N., Kotlyarov, A.*, et al.* (2017). p38(MAPK)/MK2-dependent phosphorylation controls cytotoxic RIPK1 signalling in inflammation and infection. Nature cell biology *19*, 1248-1259.

Mizushima, N., and Komatsu, M. (2011). Autophagy: renovation of cells and tissues. Cell *147*, 728-741.

Mohideen, F., Paulo, J.A., Ordureau, A., Gygi, S.P., and Harper, J.W. (2017). Quantitative Phospho-proteomic Analysis of TNFalpha/NFkappaB Signaling Reveals a Role for RIPK1 Phosphorylation in Suppressing Necrotic Cell Death. Mol Cell Proteomics *16*, 1200-1216.

Newton, K., Wickliffe, K.E., Maltzman, A., Dugger, D.L., Strasser, A., Pham, V.C., Lill, J.R., Roose-Girma, M., Warming, S., Solon, M.*, et al.* (2016). RIPK1 inhibits ZBP1-driven necroptosis during development. Nature *540*, 129-133.

O'Donnell, M.A., Perez-Jimenez, E., Oberst, A., Ng, A., Massoumi, R., Xavier, R., Green, D.R., and Ting, A.T. (2011). Caspase 8 inhibits programmed necrosis by processing CYLD. Nature cell biology *13*, 1437-1442.

Ori, D., Kato, H., Sanjo, H., Tartey, S., Mino, T., Akira, S., and Takeuchi, O. (2013). Essential roles of K63-linked polyubiquitin-binding proteins TAB2 and TAB3 in B cell activation via MAPKs. J Immunol *190*, 4037-4045.

Orozco, S., Yatim, N., Werner, M.R., Tran, H., Gunja, S.Y., Tait, S.W., Albert, M.L., Green, D.R., and Oberst, A. (2014). RIPK1 both positively and negatively regulates RIPK3 oligomerization and necroptosis. Cell Death Differ *21*, 1511-1521.

Papinski, D., Schuschnig, M., Reiter, W., Wilhelm, L., Barnes, C.A., Maiolica, A., Hansmann, I., Pfaffenwimmer, T., Kijanska, M., Stoffel, I.*, et al.* (2014). Early steps in autophagy depend on direct phosphorylation of Atg9 by

the Atg1 kinase. Molecular cell *53*, 471-483.

Park, J.M., Jung, C.H., Seo, M., Otto, N.M., Grunwald, D., Kim, K.H., Moriarity, B., Kim, Y.M., Starker, C., Nho, R.S.*, et al.* (2016). The ULK1 complex mediates MTORC1 signaling to the autophagy initiation machinery via binding and phosphorylating ATG14. Autophagy *12*, 547-564.

Petherick, K.J., Conway, O.J., Mpamhanga, C., Osborne, S.A., Kamal, A., Saxty, B., and Ganley, I.G. (2015). Pharmacological inhibition of ULK1 kinase blocks mammalian target of rapamycin (mTOR)-dependent autophagy. The Journal of biological chemistry *290*, 11376-11383.

Poschmann, G., Seyfarth, K., Besong Agbo, D., Klafki, H.W., Rozman, J., Wurst, W., Wiltfang, J., Meyer, H.E., Klingenspor, M., and Stuhler, K. (2014). High-fat diet induced isoform changes of the Parkinson's disease protein DJ-1. J Proteome Res *13*, 2339-2351.

Rahighi, S., Ikeda, F., Kawasaki, M., Akutsu, M., Suzuki, N., Kato, R., Kensche, T., Uejima, T., Bloor, S., Komander, D.*, et al.* (2009). Specific recognition of linear ubiquitin chains by NEMO is important for NF-kappaB activation. Cell *136*, 1098-1109.

Rajesh, S., Bago, R., Odintsova, E., Muratov, G., Baldwin, G., Sridhar, P., Rajesh, S., Overduin, M., and Berditchevski, F. (2011). Binding to syntenin-1 protein defines a new mode of ubiquitin-based interactions regulated by phosphorylation. The Journal of biological chemistry *286*, 39606-39614.

Rickard, J.A., O'Donnell, J.A., Evans, J.M., Lalaoui, N., Poh, A.R., Rogers, T., Vince, J.E., Lawlor, K.E., Ninnis, R.L., Anderton, H.*, et al.* (2014). RIPK1 regulates RIPK3-MLKL-driven systemic inflammation and emergency hematopoiesis. Cell *157*, 1175-1188.

Russell, R.C., Tian, Y., Yuan, H., Park, H.W., Chang, Y.Y., Kim, J., Kim, H., Neufeld, T.P., Dillin, A., and Guan, K.L. (2013). ULK1 induces autophagy by phosphorylating Beclin-1 and activating VPS34 lipid kinase. Nature cell biology *15*, 741-750.

Saleiro, D., Mehrotra, S., Kroczynska, B., Beauchamp, E.M., Lisowski, P., Majchrzak-Kita, B., Bhagat, T.D., Stein, B.L., McMahon, B., Altman, J.K.*, et al.* (2015). Central role of ULK1 in type I interferon signaling. Cell reports *11*, 605-617.

Sun, L., Wang, H., Wang, Z., He, S., Chen, S., Liao, D., Wang, L., Yan, J., Liu, W., Lei, X.*, et al.* (2012). Mixed lineage kinase domain-like protein mediates necrosis signaling downstream of RIP3 kinase. Cell *148*, 213-227.

Trichonas, G., Murakami, Y., Thanos, A., Morizane, Y., Kayama, M., Debouck, C.M., Hisatomi, T., Miller, J.W., and Vavvas, D.G. (2010). Receptor interacting protein kinases mediate retinal detachment-induced photoreceptor necrosis and compensate for inhibition of apoptosis. Proceedings of the National Academy of Sciences of the United States of America *107*, 21695-21700.

Wang, X., Li, Y., Liu, S., Yu, X., Li, L., Shi, C., He, W., Li, J., Xu, L., Hu, Z.*, et al.* (2014). Direct activation of RIP3/MLKL-dependent necrosis by herpes simplex virus 1 (HSV-1) protein ICP6 triggers host antiviral defense. Proceedings of the National Academy of Sciences of the United States of America *111*, 15438-15443.

Wesselborg, S., and Stork, B. (2015). Autophagy signal transduction by ATG proteins: from hierarchies to networks. Cellular and molecular life sciences : CMLS *72*, 4721-4757.

Wu, W., Tian, W., Hu, Z., Chen, G., Huang, L., Li, W., Zhang, X., Xue, P., Zhou, C., Liu, L.*, et al.* (2014). ULK1 translocates to mitochondria and phosphorylates FUNDC1 to regulate mitophagy. EMBO reports *15*, 566-575.

Yang, Z., and Klionsky, D.J. (2010). Eaten alive: a history of macroautophagy. Nature cell biology *12*, 814-822.

Yonekawa, T., Gamez, G., Kim, J., Tan, A.C., Thorburn, J., Gump, J., Thorburn, A., and Morgan, M.J. (2015). RIP1 negatively regulates basal autophagic flux through TFEB to control sensitivity to apoptosis. EMBO reports *16*, 700-708.

Zhang, D.W., Shao, J., Lin, J., Zhang, N., Lu, B.J., Lin, S.C., Dong, M.Q., and Han, J. (2009). RIP3, an energy metabolism regulator that switches TNF-induced cell death from apoptosis to necrosis. Science *325*, 332-336.

Zhou, C., Ma, K., Gao, R., Mu, C., Chen, L., Liu, Q., Luo, Q., Feng, D., Zhu, Y., and Chen, Q. (2017). Regulation of mATG9 trafficking by Src- and ULK1-mediated phosphorylation in basal and starvation-induced autophagy. Cell research *27*, 184-201.

Figure 1

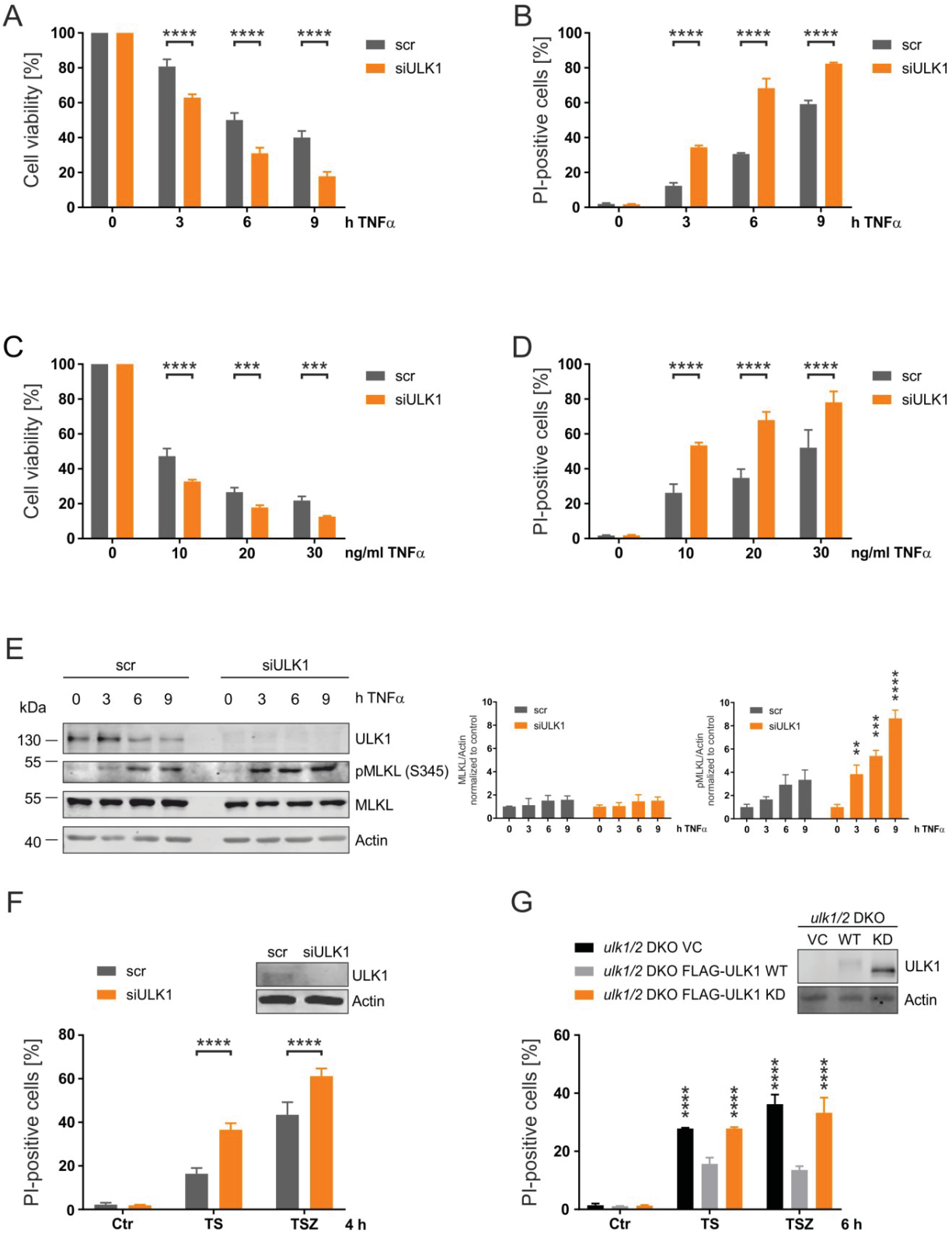
A
Cell viability [%]
scr
siULK1
h TNFα
B
PI-positive cells [%]
C
ng/ml TNFα
D
E
kDa
ULK1
pMLKL (S345)
MLKL
Actin
MLKL/Actin normalized to control
pMLKL/Actin normalized to control
F
Ctr
TS
TSZ
4 h
G
ulk1/2 DKO VC
ulk1/2 DKO FLAG-ULK1 WT
ulk1/2 DKO FLAG-ULK1 KD
ulk1/2 DKO
VC
WT
KD
6 h

Figure 2

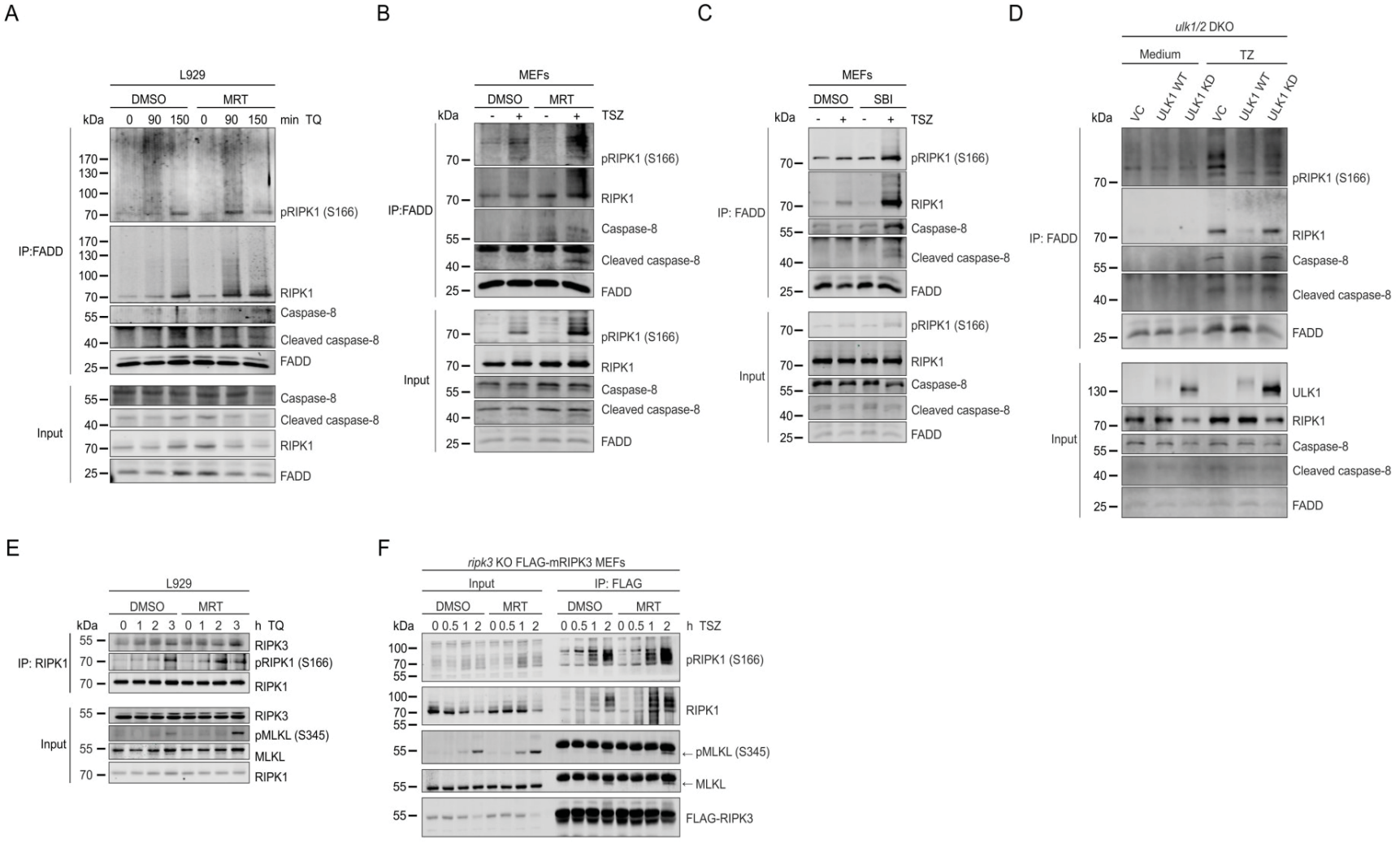
A
L929
DMSO
MRT
kDa
0 90 150 0 90 150 min TQ
IP:FADD
pRIPK1 (S166)
RIPK1
Caspase-8
Cleaved caspase-8
FADD
Input
Caspase-8
Cleaved caspase-8
RIPK1
FADD
B
MEFs
DMSO
MRT
kDa
- + - + TSZ
IP:FADD
pRIPK1 (S166)
RIPK1
Caspase-8
Cleaved caspase-8
FADD
Input
pRIPK1 (S166)
RIPK1
Caspase-8
Cleaved caspase-8
FADD
C
MEFs
DMSO
SBI
kDa
- + - + TSZ
IP: FADD
pRIPK1 (S166)
RIPK1
Caspase-8
Cleaved caspase-8
FADD
Input
pRIPK1 (S166)
RIPK1
Caspase-8
Cleaved caspase-8
FADD
D
ulk1/2 DKO
Medium
TZ
VC
ULK1 WT
ULK1 KD
VC
ULK1 WT
ULK1 KD
kDa
IP: FADD
pRIPK1 (S166)
RIPK1
Caspase-8
Cleaved caspase-8
FADD
Input
ULK1
RIPK1
Caspase-8
Cleaved caspase-8
FADD
E
L929
DMSO
MRT
kDa
0 1 2 3 0 1 2 3 h TQ
IP: RIPK1
RIPK3
pRIPK1 (S166)
RIPK1
Input
RIPK3
pMLKL (S345)
MLKL
RIPK1
F
ripk3 KO FLAG-mRIPK3 MEFs
Input
IP: FLAG
DMSO
MRT
DMSO
MRT
kDa
0 0.5 1 2 0 0.5 1 2 0 0.5 1 2 0 0.5 1 2 h TSZ
pRIPK1 (S166)
RIPK1
← pMLKL (S345)
← MLKL
FLAG-RIPK3

Figure 3

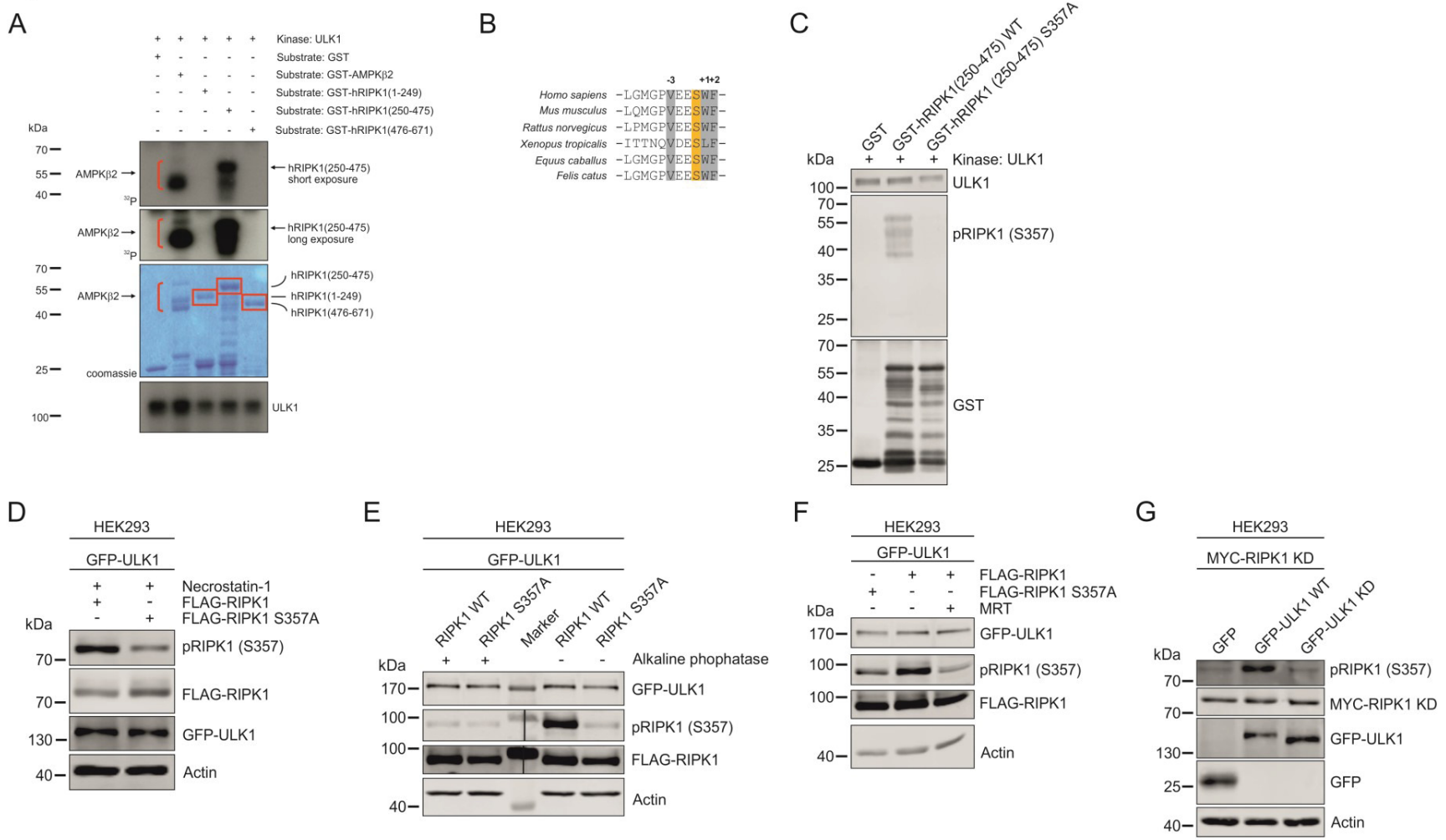
A
Kinase: ULK1
Substrate: GST
Substrate: GST-AMPKβ2
Substrate: GST-hRIPK1(1-249)
Substrate: GST-hRIPK1(250-475)
Substrate: GST-hRIPK1(476-671)
kDa
AMPKβ2
hRIPK1(250-475) short exposure
hRIPK1(250-475) long exposure
hRIPK1(1-249)
hRIPK1(476-671)
coomassie
ULK1
B
-3
+1+2
Homo sapiens -LGMGPVEESWF-
Mus musculus -LQMGPVEESWF-
Rattus norvegicus -LPMGPVEESWF-
Xenopus tropicalis -ITTNQVDESLF-
Equus caballus -LGMGPVEESWF-
Felis catus -LGMGPVEESWF-
C
GST
GST-hRIPK1(250-475) WT
GST-hRIPK1 (250-475) S357A
Kinase: ULK1
ULK1
pRIPK1 (S357)
GST
D
HEK293
GFP-ULK1
Necrostatin-1
FLAG-RIPK1
FLAG-RIPK1 S357A
pRIPK1 (S357)
FLAG-RIPK1
GFP-ULK1
Actin
E
HEK293
GFP-ULK1
RIPK1 WT
RIPK1 S357A
Marker
Alkaline phophatase
GFP-ULK1
pRIPK1 (S357)
FLAG-RIPK1
Actin
F
HEK293
GFP-ULK1
FLAG-RIPK1
FLAG-RIPK1 S357A
MRT
GFP-ULK1
pRIPK1 (S357)
FLAG-RIPK1
Actin
G
HEK293
MYC-RIPK1 KD
GFP
GFP-ULK1 WT
GFP-ULK1 KD
pRIPK1 (S357)
MYC-RIPK1 KD
GFP-ULK1
GFP
Actin

Figure 4

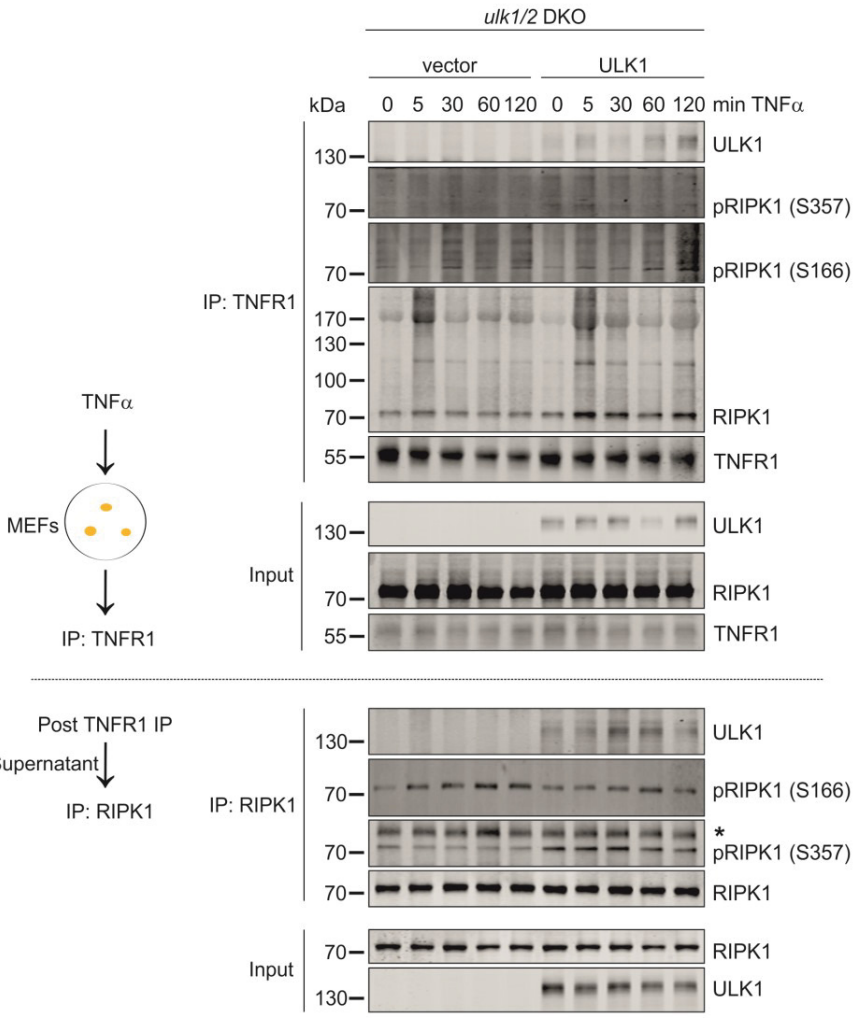
ulk1/2 DKO
vector
ULK1
kDa
0 5 30 60 120 0 5 30 60 120 min TNFα
ULK1
pRIPK1 (S357)
pRIPK1 (S166)
RIPK1
TNFR1
IP: TNFR1
Input
TNFα
MEFs
IP: TNFR1
Post TNFR1 IP
Supernatant
IP: RIPK1
IP: RIPK1
*
130
70
170
100
55

Figure 5

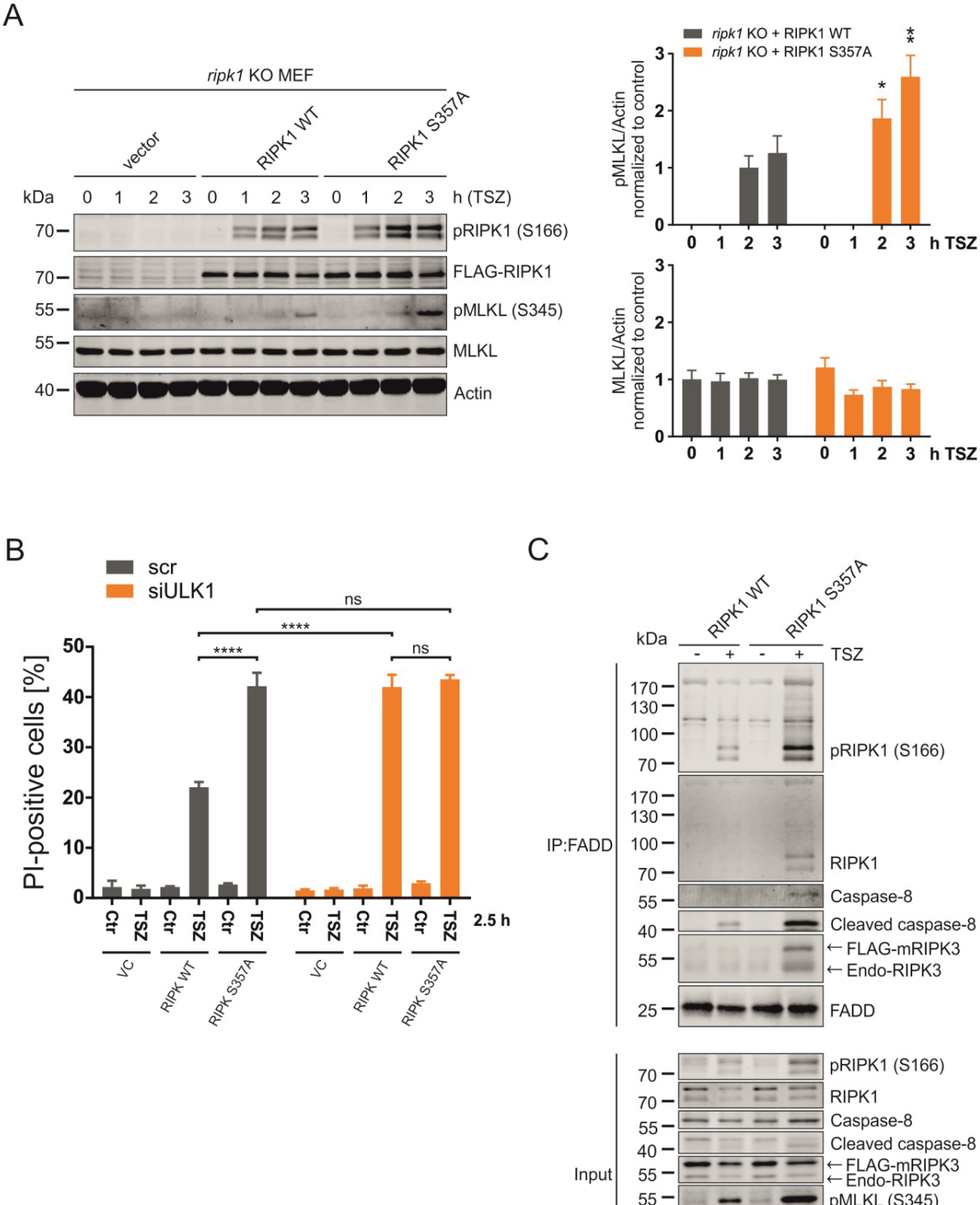
A
ripk1 KO MEF
vector
RIPK1 WT
RIPK1 S357A
kDa
0 1 2 3 0 1 2 3 0 1 2 3 h (TSZ)
70
pRIPK1 (S166)
70
FLAG-RIPK1
55
pMLKL (S345)
55
MLKL
40
Actin
ripk1 KO + RIPK1 WT
ripk1 KO + RIPK1 S357A
pMLKL/Actin normalized to control
MLKL/Actin normalized to control
0 1 2 3 0 1 2 3 h TSZ
B
scr
siULK1
PI-positive cells [%]
ns
****
****
ns
Ctr TSZ Ctr TSZ Ctr TSZ Ctr TSZ Ctr TSZ Ctr TSZ
2.5 h
VC
RIPK WT
RIPK S357A
VC
RIPK WT
RIPK S357A
C
RIPK1 WT
RIPK1 S357A
kDa
- + - + TSZ
pRIPK1 (S166)
IP:FADD
RIPK1
Caspase-8
Cleaved caspase-8
← FLAG-mRIPK3
← Endo-RIPK3
FADD
Input
pRIPK1 (S166)
RIPK1
Caspase-8
Cleaved caspase-8
← FLAG-mRIPK3
← Endo-RIPK3
pMLKL (S345)
MLKL
FADD
Actin

Figure S1

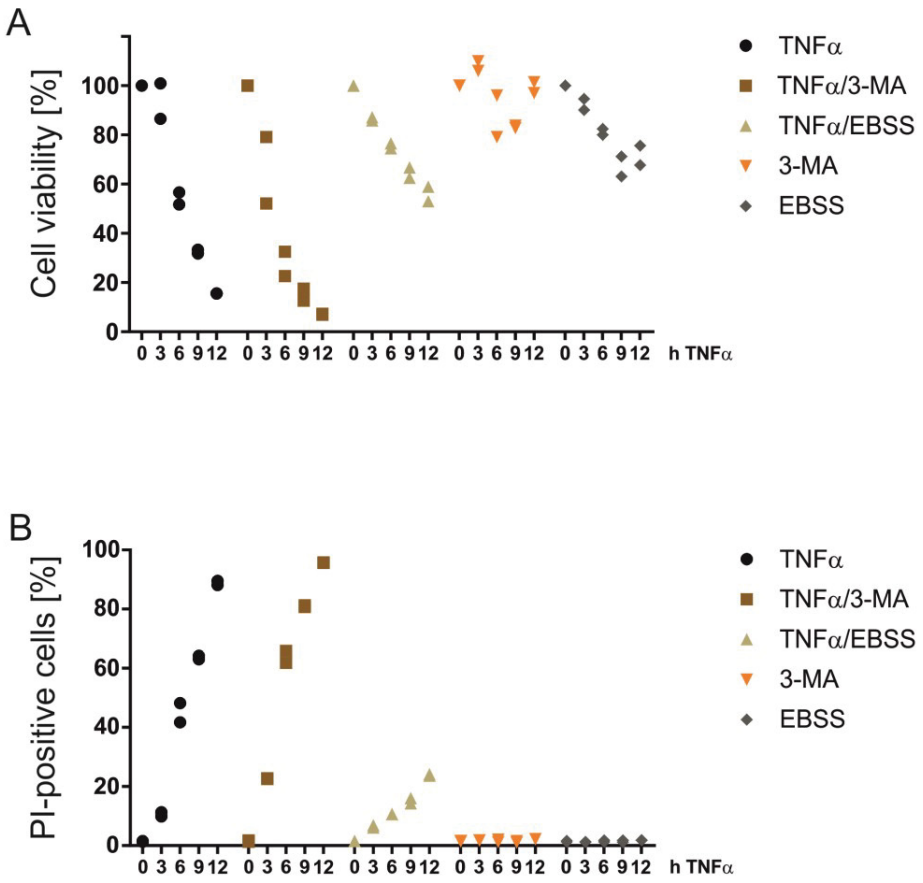
A
Cell viability [%]
100
80
60
40
20
0
0 3 6 9 12 0 3 6 9 12 0 3 6 9 12 0 3 6 9 12 0 3 6 9 12
h TNFα
TNFα
TNFα/3-MA
TNFα/EBSS
3-MA
EBSS
B
PI-positive cells [%]
100
80
60
40
20
0
0 3 6 9 12 0 3 6 9 12 0 3 6 9 12 0 3 6 9 12 0 3 6 9 12
h TNFα
TNFα
TNFα/3-MA
TNFα/EBSS
3-MA
EBSS

Figure S2

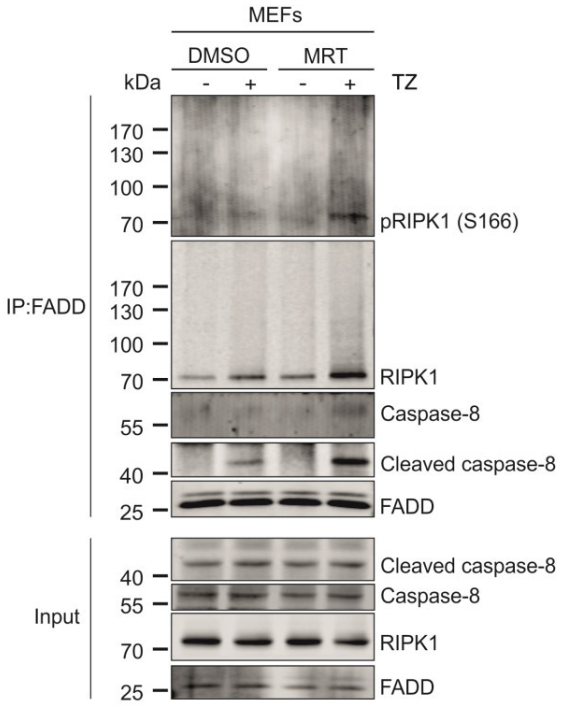
MEFs
DMSO
MRT
kDa
-
+
-
+
TZ
IP:FADD
170
130
100
70
pRIPK1 (S166)
170
130
100
70
RIPK1
55
Caspase-8
40
Cleaved caspase-8
25
FADD
Input
40
Cleaved caspase-8
55
Caspase-8
70
RIPK1
25
FADD

Figure S3

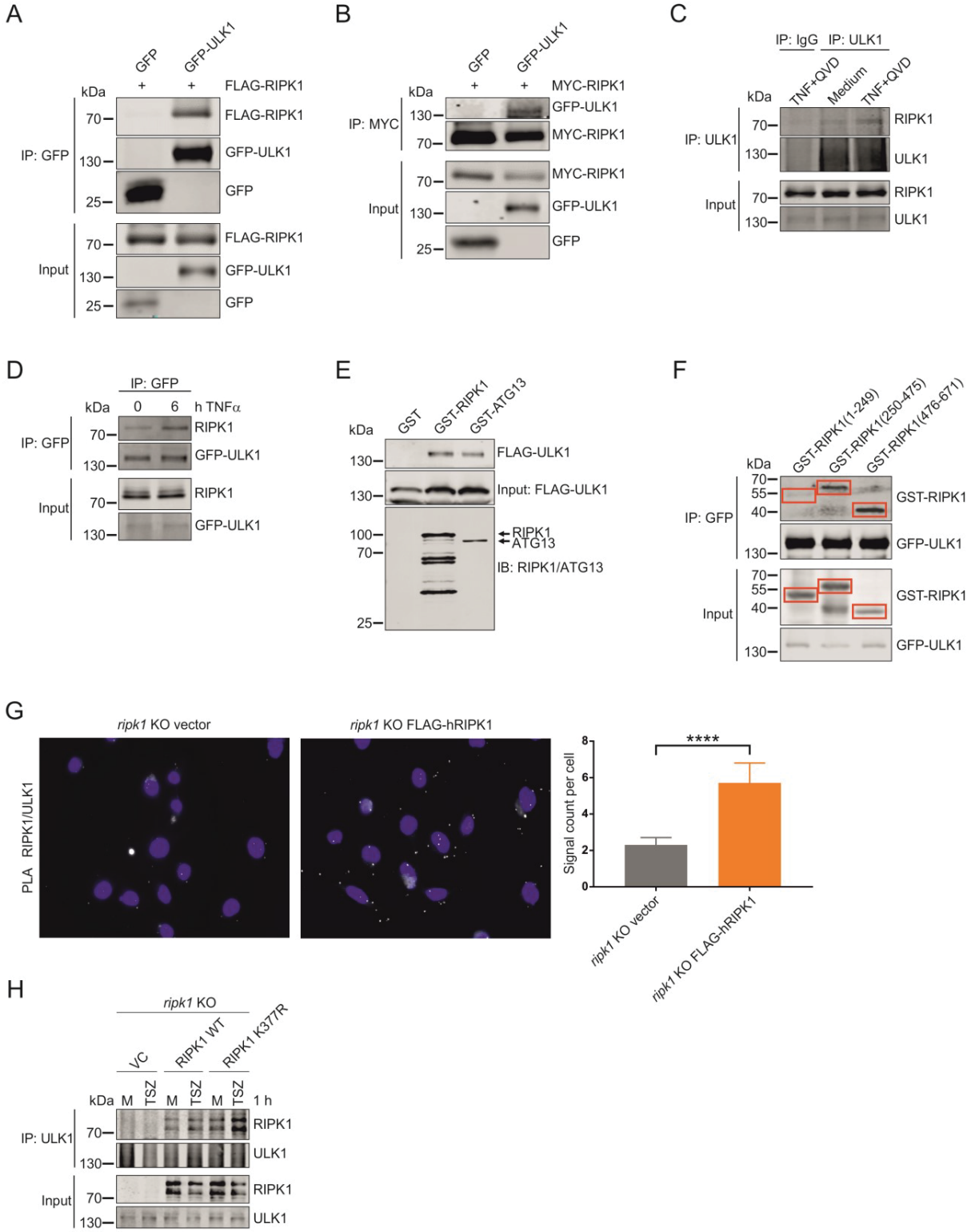
A
GFP
GFP-ULK1
kDa
+
+
FLAG-RIPK1
IP: GFP
70
130
25
FLAG-RIPK1
GFP-ULK1
GFP
Input
70
130
25
FLAG-RIPK1
GFP-ULK1
GFP
B
GFP
GFP-ULK1
kDa
+
+
MYC-RIPK1
IP: MYC
130
70
GFP-ULK1
MYC-RIPK1
Input
70
130
25
MYC-RIPK1
GFP-ULK1
GFP
C
IP: IgG
IP: ULK1
kDa
TNF+QVD
Medium
TNF+QVD
IP: ULK1
70
130
RIPK1
ULK1
Input
70
130
RIPK1
ULK1
D
IP: GFP
kDa
0
6
h TNFα
IP: GFP
70
130
RIPK1
GFP-ULK1
Input
70
130
RIPK1
GFP-ULK1
E
kDa
GST
GST-RIPK1
GST-ATG13
130
130
FLAG-ULK1
Input: FLAG-ULK1
100
70
25
RIPK1
ATG13
IB: RIPK1/ATG13
F
GST-RIPK1(1-249)
GST-RIPK1(250-475)
GST-RIPK1(476-671)
kDa
IP: GFP
70
55
40
130
GST-RIPK1
GFP-ULK1
Input
70
55
40
130
GST-RIPK1
GFP-ULK1
G
ripk1 KO vector
ripk1 KO FLAG-hRIPK1
PLA RIPK1/ULK1
Signal count per cell
8
6
4
2
0
****
ripk1 KO vector
ripk1 KO FLAG-hRIPK1
H
ripk1 KO
VC
RIPK1 WT
RIPK1 K377R
kDa
M
TSZ
M
TSZ
M
TSZ
1 h
IP: ULK1
70
130
RIPK1
ULK1
Input
70
130
RIPK1
ULK1

Figure S4

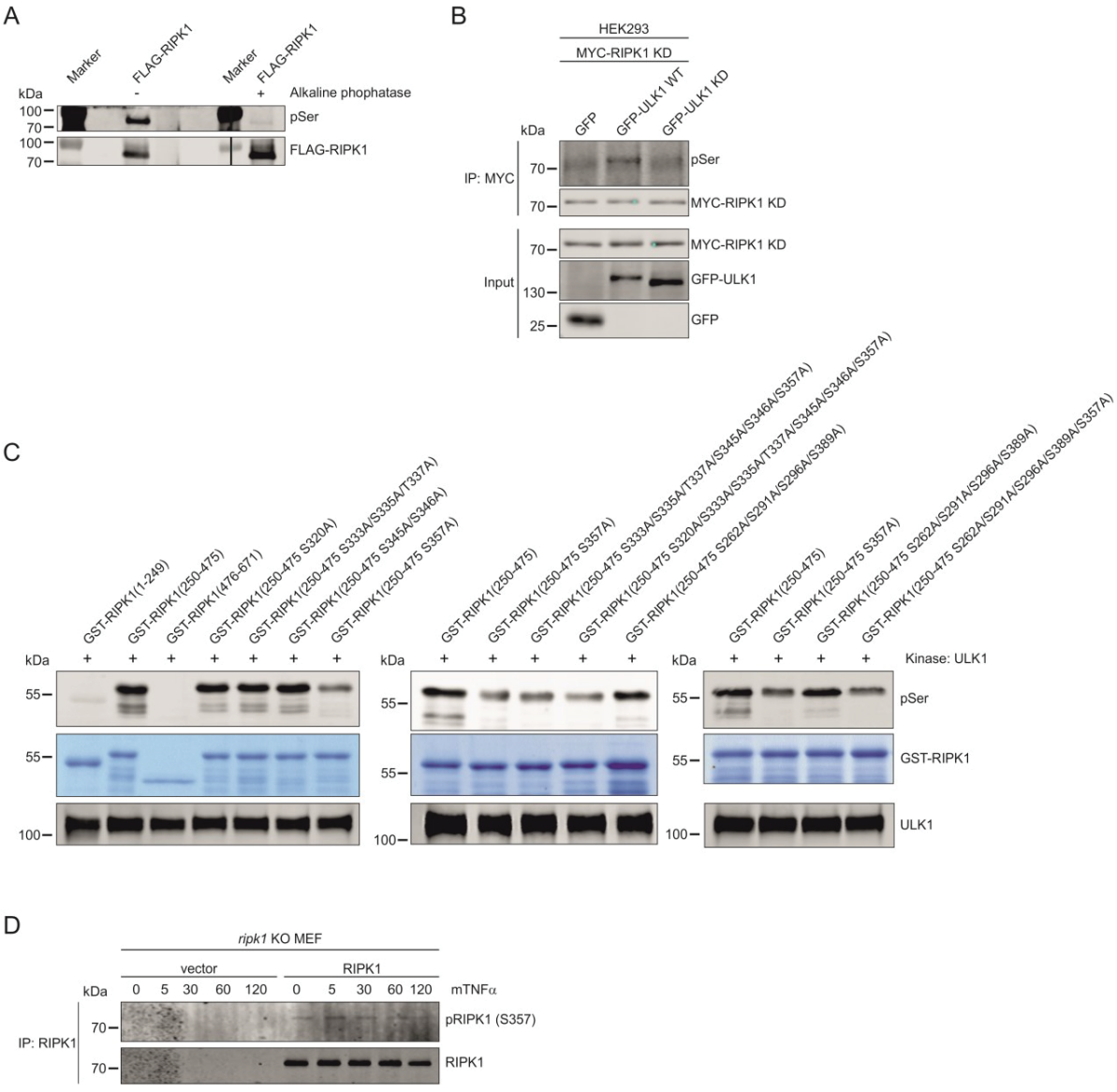
A
Marker
FLAG-RIPK1
Marker
FLAG-RIPK1
kDa
-
+
Alkaline phophatase
100
70
pSer
100
70
FLAG-RIPK1
B
HEK293
MYC-RIPK1 KD
kDa
GFP
GFP-ULK1 WT
GFP-ULK1 KD
IP: MYC
70
pSer
70
MYC-RIPK1 KD
Input
70
MYC-RIPK1 KD
130
GFP-ULK1
25
GFP
C
GST-RIPK1(1-249)
GST-RIPK1(250-475)
GST-RIPK1(476-671)
GST-RIPK1(250-475 S320A)
GST-RIPK1(250-475 S333A/S335A/T337A)
GST-RIPK1(250-475 S345A/S346A)
GST-RIPK1(250-475 S357A)
GST-RIPK1(250-475)
GST-RIPK1(250-475 S357A)
GST-RIPK1(250-475 S333A/S335A/T337A/S345A/S346A/S357A)
GST-RIPK1(250-475 S320A/S333A/S335A/T337A/S345A/S346A/S357A)
GST-RIPK1(250-475 S262A/S291A/S296A/S389A)
GST-RIPK1(250-475)
GST-RIPK1(250-475 S357A)
GST-RIPK1(250-475 S262A/S291A/S296A/S389A)
GST-RIPK1(250-475 S262A/S291A/S296A/S389A/S357A)
kDa
+
Kinase: ULK1
55
pSer
55
GST-RIPK1
100
ULK1
D
ripk1 KO MEF
vector
RIPK1
kDa
0 5 30 60 120 0 5 30 60 120
mTNFα
IP: RIPK1
70
pRIPK1 (S357)
70
RIPK1

Figure S5

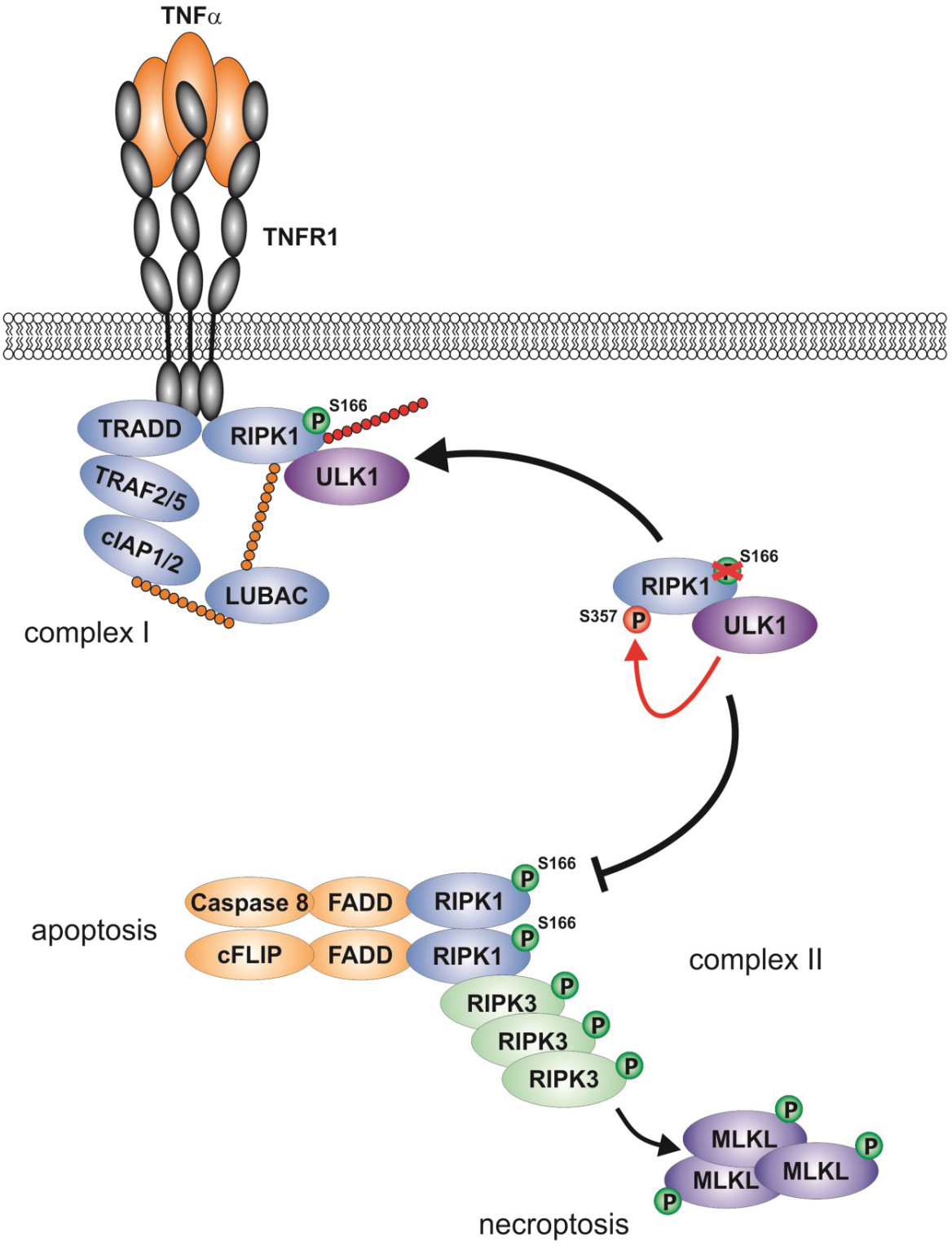
TNFα
TNFR1
TRADD
RIPK1
S166
P
ULK1
TRAF2/5
cIAP1/2
LUBAC
complex I
RIPK1
S166
S357
P
ULK1
Caspase 8
FADD
RIPK1
S166
P
cFLIP
FADD
RIPK1
S166
P
apoptosis
complex II
RIPK3
P
RIPK3
P
RIPK3
P
MLKL
P
MLKL
MLKL
P
P
necroptosis

Manuscript II

Pro-necroptotic RIPK3 controls AMPK activity to regulate autophagy

AUTHORS/AFFILIATIONS

Wenxian Wu[1], Xiaojing Wang[1], Niklas Berleth[1], Jana Deitersen[1], David Schlütermann[1], Fabian Stuhldreier[1], Nora Wallot-Hieke[2], Maria José Mendiburo[1], Christoph Peter[1], Björn Stork[1,*]

[1]*Institute of Molecular Medicine I, Medical Faculty, Heinrich Heine University Düsseldorf, 40225 Düsseldorf, Germany*

[2]*DWI-Leibniz Institute for Interactive Materials, 52074 Aachen, Germany*

CONTACT

*Corresponding author:

Björn Stork, Universitätsstr. 1, Building 23.12, 40225 Düsseldorf, Germany,

Tel.: +49 (0)211 81 11954, Fax: +49 (0)211 81 11611954, E-mail: bjoern.stork@hhu.de

RUNNING TITLE: RIPK3 regulates AMPK activity

KEYWORDS: RIPK3, AMPK, Autophagy, Necroptosis

ABBREVIATIONS: ACACA/ACC, acetyl-CoA carboxylase alpha; AMPK, AMP-activated protein kinase; ATG, autophagy-related; BECN1, beclin 1; CAMKK2, Ca^{2+}/calmodulin dependent protein kinase kinase 2; GFP, green fluorescent protein; EBSS, Earle's Balanced Salt Solution; KO, knockout; LAMP1, lysosomal associated membrane protein 1; MAP1LC3/LC3, microtubule-associated protein 1 light chain 3; MEF, murine embryonic fibroblast; MAP3K7/TAK1, mitogen-activated protein kinase kinase kinase 7; MLKL, mixed-lineage kinase domain-like protein; MTOR, mechanistic target of rapamycin (serine/threonine kinase); NRBF2, nuclear receptor binding factor 2; PIK3C3/VPS34, phosphatidylinositol 3-kinase catalytic subunit type 3; PIK3R4/VPS15, phosphoinositide-3-kinase regulatory subunit 4; PLA, proximity ligation

assay; PRKAA1/2, protein kinase AMP-activated catalytic subunit alpha 1/2; PRKAB1/2, protein kinase AMP-activated non-catalytic subunit beta 1/2; PRKAG1/2/3, protein kinase AMP-activated non-catalytic subunit gamma 1/2/3; PtdIns3K, phosphatidylinositol 3-kinase; PtdIns3P, phosphatidylinositol 3-phosphate; RB1CC1/FIP200, RB1-inducible coiled-coil 1; RHIM, RIPK homotypic interaction motif; RIPK1/3, receptor-interacting kinase 1/3; RPTOR, regulatory associated protein of MTOR complex 1; SQSTM1/p62, sequestosome 1; STK11/LKB1, serine/threonine kinase 11; TNFα, tumor necrosis factor α; ULK1, unc-51 like autophagy activating kinase 1; WIPI2, WD repeat domain, phosphoinositide interacting 2; WT, wild-type.

ABSTRACT

Autophagy and necroptosis represent two opposing cellular stress responses. Whereas autophagy primarily fulfills a cyto-protective function, necroptosis is a form of regulated cell death induced upon stimulation of death receptors. Here, we aimed at investigating the molecular crosstalk between these two stress pathways. We observe that TNFα-induced activation of the necroptosis-mediating RIPK3 (receptor-interacting kinase 3) leads to the induction of early autophagy events but to the blockade of late events. RIPK3 directly associates with AMPK (AMP-activated protein kinase) and phosphorylates its catalytic subunit PRKAA1/2 at Thr183/Thr172. Activated AMPK phosphorylates ULK1 and BECN1 and thus initiates autophagy. However, the lysosomal degradation of autophagosomes appears is blocked by TNFα-induced necroptosis. In summary, we have identified RIPK3 as AMPK-activating kinase and thus a direct link between autophagy- and necroptosis-regulating kinases. Apparently, necroptosis is counterbalanced by the induction of early autophagy events, but supported by the blockade of late autophagy events.

INTRODUCTION

(Macro-)Autophagy is an intracellular recycling process that is characterized by vesicle-mediated transfer of cargo to lysosomes. Several stimuli are able to induce autophagy, e.g. nutrient starvation, hypoxia, protein aggregation, or infection with intracellular pathogens.[1] Upon energy or nutrient deprivation, the energy-sensing AMPK (AMP-activated protein kinase) can be activated by STK11/LKB1 (serine/threonine kinase 11).[2-4] Subsequently, activated AMPK can in turn regulate downstream substrates via phosphorylation, e.g. the autophagy-inducing ULK1 (unc-51 like kinase 1) or MTOR (mechanistic target of rapamycin).[5, 6] The inhibition of MTOR by AMPK can be mediated indirectly by phosphorylating TSC2 (tuberous sclerosis complex subunit 2) at S1387 (human amino acid sequence) or/and directly by phosphorylating RPTOR (regulatory associated protein of MTOR complex 1) at S722 and S792 (human and murine amino acid sequence).[7] MTOR inhibition then results in the dissociation of MTOR from the ULK1 complex, in the dephosphorylation of MTOR-dependent phospho-sites in ULK1 (S638 and S758, human amino acid sequence), and in the activation of ULK1.[5, 8] AMPK can also directly phosphorylate and thus regulate ULK1. AMPK-dependent phospho-sites in ULK1 include S317, S556, and S638 (human amino acid sequence).[8-12] The active ULK1 complex then translocates to specific subdomains of the ER in order to initiate the nucleation of autophagosomes.[1] To date, several subdomains of the ER have been proposed as "hot spots" for autophagosome formation.[13] Subsequently, the class III phosphoinositide 3-kinase (PtdIns3K) is recruited to these subdomains. This lipid kinase complex is composed of the catalytic subunit PIK3C3 (phosphatidylinositol 3-kinase catalytic subunit type 3; alternatively termed vacuolar protein sorting 34, VPS34), and the associated proteins BECN1 (beclin 1), PIK3R4 (phosphoinositide 3-kinase regulatory subunit 4; alternatively termed VPS15), ATG14 and NRBF2 (nuclear receptor binding factor 2).[14] The class III PtdIns3K complex is also regulated by ULK1- and AMPK-dependent phosphorylations of several subunits.[15-19] Activated PtdIns3K produces phosphatidylinositol 3-phosphate (PtdIns3P), leading to the formation of membraneous platforms termed omegasomes/ER cradles that contain the PtdIns3P-binding protein ZFYVE1/DFCP1 (zinc finger FYVE-type containing 1) and that give rise to phagophores.[20-23] This process is supported by the recruitment of further autophagy-specific components, e.g. the PtdIns3P-binding protein WIPI2 (WD repeat domain, phosphoinositide interacting 2) or components of the two autophagy-specific ubiquitin-like conjugation machineries.[1]

In addition to LBK1-mediated AMPK activation, both CaMKK2 (Ca^{2+}-activated Ca^{2+}/calmodulin-dependent protein kinase kinase 2) and MAP3K7/TAK1 (mitogen-activated protein kinase kinase kinase 7) have been shown to activate AMPK, depending on the cytosolic Ca^{2+} level or cytokine treatment, respectively.[24-27] AMPK is composed of a catalytic α-subunit (PRKAA1/AMPKα1 or PRKAA2/AMPKα2), a scaffold β-subunit (PRKAB1/AMPKβ1 or PRKAB2/AMPKβ2) and a regulatory γ-subunit (PRKAG1/AMPKγ1, PRKAG2/AMPKγ2 or PRKAG3/AMPKγ3).[28] All three AMPK-activating kinases phosphorylate the α1-subunit PRKAA1 in the

activation loop at T183, which corresponds to T172 in PRKAA2.[28] Interestingly, Dalle Pezze et al. recently reported that AMPK is not only activated under stress or starvation conditions, but can also positively regulate autophagy under amino acid sufficiency.[29]

In contrast to the cytoprotective function of autophagy, necroptosis represents an inflammatory form of regulated cell death and is characterized by a necrotic morphotype.[30] Although necroptosis can be triggered by several stimuli, induction mediated by death receptors (e.g. TNFR1, tumor necrosis factor receptor 1) is the best characterized form.[31, 32] Auto- and trans-phosphorylation of RIPK1 (receptor-interacting kinase-1) and RIPK3 (receptor-interacting kinase-3) induce the formation of an amyloid-like multiprotein complex termed necrosome. Necroptosis and the assembly of necrosomes can be inhibited by caspase-8-dependent cleavage of RIPK1 or RIPK3.[33-35] When caspase-8 is inhibited by pharmacological compounds (e.g. Q-VD-OPh or z-VAD-FMK) or under certain physiological conditions (e.g. viral infections), necroptosis is initiated.[36-38] Activated RIPK3 recruits and activates MLKL (mixed lineage kinase domain-like), which in turn translocates to the plasma membrane and mediates necrotic membrane disruption.[31, 32, 39]

Both autophagy and necroptosis balance cell death and survival. Although there are some reports indicating a crosstalk between these two stress responses, the mechanistic details remain poorly understood so far. Here, we show that TNFα-induced necroptosis blocks the lysosomal degradation of autophagosomes. In contrast, it appears that early autophagy events are induced under pro-necroptotic conditions and in a RIPK3-dependent manner. We observe that RIPK3 interacts with AMPK and that RIPK3 phosphorylates the catalytic subunit PRKAA1 at T183 in order to activate AMPK. Subsequently, pro-autophagic AMPK substrates such as ULK1 and BECN1 become phosphorylated and activated. Collectively, we have identified RIPK3 as AMPK-activating kinase and thus a molecular crosstalk between the autophagy- and necroptosis-regulating kinases. We speculate that necroptosis is counterbalanced by the induction of early autophagy events, but supported by the blockade of late autophagy events.

RESULTS

Necroptosis induced by TNFα inhibits lysosome-mediated LC3 degradation

To investigate the effect of necroptosis on autophagy, we induced necroptosis by TNFα/QVD treatment in L929 cells (Figure S1A) and monitored levels of (MAP1)LC3-II, which is the phosphatidylethanolamine-conjugated form of LC3 and represents a marker protein for autophagosomes. We observed that LC3-II levels increased with time upon TNFα/QVD treatment (Figure 1A). This phenomenon was significantly reduced when we blocked TNFα/QVD-induced necroptosis by knocking down the necroptosis effector protein RIPK3 in L929 cells. TNFα/QVD-induced LC3-II levels did not further increase with simultaneous bafilomycin A_1 treatment, indicating that lysosomal LC3-II (and thus autophagosome) degradation was rather blocked than induced upon TNFα-induced necroptosis (Figure 1A). In order to confirm our observation by an independent approach, we performed LC3 immunofluorescence in L929 cells. Treatment with TNFα/QVD increased LC3-positive puncta (Figure 1B). Similar to the LC3 turnover analysis by immunoblot, this increase in LC3 puncta was not further increased by parallel bafilomycin A_1 treatment but was reduced by RIPK3 knockdown. To further confirm our observation that the autophagic flux is indeed blocked on the lysosomal level, we analyzed colocalization between exogenously expressed GFP-LC3 and the lysosomal marker protein LAMP1 (lysosomal associated membrane protein 1). Here, we observed strong accumulation of the GFP-LC3 signal in lysosomal compartments upon TNFα/QVD treatment, which was similar to the positive control (EBSS + bafilomycin A_1) (Figure 1C). The TNFα/QVD-induced GFP-LC3 accumulation was blocked by addition of the RIPK3 inhibitor GSK'872 (ref. [40]). In a similar approach, we made use of the mRFP-EGFP-rLC3 tandem construct.[41, 42] The GFP signal is sensitive to the acidic and/or proteolytic environment of lysosomes, whereas the mRFP signal is more stable.[41, 42] We detected a strong accumulation of the tandem fluorescence-tagged LC3 upon TNFα/QVD or medium/bafilomycin A_1 treatment (Figure 1D). Interestingly, there were mRFP-only dots detectable upon TNFα/QVD treatment, which was not the case for bafilomycin A_1, indicating a different mode of lysosomal blockade. Nevertheless, the TNFα/QVD-induced mRFP-EGFP-rLC3 accumulation was reduced upon siRNA-mediated knockdown of RIPK3 (Figure 1D). Finally, we assessed autophagic flux by monitoring mCitrine-LC3 degradation by flow cytometry. Whereas starvation induced a clear reduction of mCitrine-LC3 levels, mCitrine-dependent fluorescence remained unaltered or even increased upon TNFα/QVD treatment (Figure 1E). In order to characterize this lysosomal blockade, we measured CTSB (cathepsin B) and CTSL (cathepsin L) activities. However, we did not detect any differences between TNFα/QVD-treated or control cells, whereas this was clearly the case for bafilomycin A_1 treatment (Figure S2). Taken together, we showed by different assays that TNFα/QVD-induced necroptosis blocks lysosomal autophagosome degradation.

Early autophagy signaling events are activated upon TNFα-induced necroptosis

As described above, we observed lysosomal LC3 accumulation upon TNFα/QVD-induced necroptosis. In the next step, we investigated early autophagy signaling events under these pro-necroptotic conditions. We observed increased activation and activity of AMPK, as detected by immunoblotting for phospho-PRKAA1 (T183), phospho-ACACA (S79), phospho-ULK1 (S555, murine sequence; corresponding to S556 in human ULK1), and phospho-BECN1 (S91, murine sequence; corresponding to S93 in human BECN1) (Figure 2A). These increased phosphorylation events were clearly dependent on RIPK3 signaling, since they were abolished by RIPK3 knockdown. Similar results were obtained when we used a RIPK3 inhibitor (GSK'872) instead of *Ripk3* siRNA (Figure 2B), or when we used *ripk3* KO murine embryonic fibroblasts (MEFs) (Figure 2C). In MEFs, we induced necroptosis by treatment with TNFα in combination with a Smac mimetic (here: Birinapant) and the pan-caspase inhibitor zVAD as previously reported.[37] Generally, AMPK-dependent phosphorylation of ULK1 at S555 (human S556) and of BECN1 at S91 (human S93) have been associated with the induction of autophagy.[10, 16, 43, 44] Accordingly, it appears that initial autophagy signaling is rather activated upon TNFα/QVD-induced necroptosis in a RIPK3-dependent manner. To confirm this observation, we next tested several downstream markers of autophagy, e.g. WIPI2, ZFYVE1, ATG16L1, and ATG14. We observed that GSK'872-mediated inhibition of RIPK3 significantly blocked ATG14 puncta formation upon TFNα/QVD treatment (Figure 2D). Of note, we did not observe any effect on the puncta formation of WIPI2, ZFYVE1, or ATG16L1 (data not shown).

RIPK3 interacts with AMPK

Since we observed that the induction of necroptosis affected AMPK-dependent signaling, we next investigated the crosstalk between AMPK and the pro-necroptotic RIPK3. In a first approach, we performed size exclusion chromatography of S100 lysates derived from MEFs (Figure 3A). We detected the ULK1 complex in high molecular mass fractions of approximately 3 MDa as previously described.[45-47] Of note, AMPK and both RIPK1 and RIPK3 were present in fractions corresponding to a lower molecular mass range of 14-158 kDa (Figure 3A). Since the presence of proteins in the same fractions does not prove a direct interaction, we next performed immunopurification experiments. We focused on RIPK3, since it has previously been reported that RIPK3 positively regulates autophagy.[48] We transiently transfected cDNA encoding FLAG-hRIPK3 into HEK293 cells. Following anti-FLAG immunopurification, we detected co-purification of endogenous AMPK (Figure 3B). In a similar approach, we co-purified FLAG-RIPK3 with purified AMPK (Figure 3C). The direct interaction between RIPK3 and AMPK was confirmed by affinity purification using recombinant proteins (Figure 3D). Finally, we confirmed the interaction between these two kinases on the cellular level by a proximity ligation assay (PLA). In this assay, single protein-protein interactions can be detected using antibody-recognition

combined with exponential signal amplification by PCR. We transfected *ripk3* KO MEFs with cDNA encoding FLAG-mRIPK3. FLAG-RIPK3 was stained with rabbit anti-RIPK3 antibodies and AMPK with mouse anti-PRKAA1/2 antibodies. As control, *ripk3* KO MEFs were transfected with empty vector. Cells reconstituted with FLAG-RIPK3 displayed strong signals with significant difference to control cells (Figure 3E). Collectively, these data indicate that AMPK can associate with RIPK3.

RIPK3 directly phosphorylates PRKAA1 at T183 and thus activates AMPK

Since we observed that RIPK3 interacts with AMPK, we next tested if RIPK3 can phosphorylate AMPK. In a first approach, we used recombinant RIPK3 as kinase and GST-hPRKAA1 (1-278) or GST-hPRKAA1 (279-559) as substrates in an *in vitro* kinase assay. We observed that RIPK3 can phosphorylate both truncated versions of PRKAA1 (Figure 4A). Since we observed that RIPK3 can regulate AMPK activity upon TNFα treatment (Figure 2A-2C), we wondered if RIPK3 could directly phosphorylate PRKAA1 at T183 to regulate AMPK activity. To test this hypothesis, we generated the mutant GST-hPRKAA1 (1-278) T183A and repeated the *in vitro* kinase assay with cold ATP. We performed immunoblotting for phospho-PRKAA1 T183 and observed a specific band for GST-hPRKAA1 (1-278), but not for the GST-hPRKAA1 (1-278) T183A mutant (Figure 4B). This RIPK3-dependent phosphorylation of PRKAA1 at T183 was sensitive to both alkaline phosphatase and RIPK3 inhibitor GSK'872 treatment (Figures 4C and 4D). To test if RIPK3 phosphorylates AMPK in intact cells, we treated HEK293 cells that express either FLAG-hRIPK3 WT or a kinase-dead (KD) variant with TNFα/QVD for 24 h. We observed strong phospho-PRKAA1 T183 signal in HEK293 cells expressing FLAG-hRIPK3 compared to cells expressing kinase-dead FLAG-hRIPK3 (Figure 4E). Using again a proximity ligation assay, we also detected stronger PRKAA phosphorylation in *ripk3* KO MEFs reconstituted with FLAG-mRIPK3 compared to non-reconstituted *ripk3* KO MEFs (Figure 4F). Altogether, our results indicate that RIPK3 phosphorylates PRKAA1 at T183 to regulate AMPK activity upon TNFα-induced necroptosis. This RIPK3-dependent activation of AMPK induces early autophagy events. However, it appears that autophagy is ultimately blocked during the execution of TNFα-induced necroptosis.

DISCUSSION

Autophagy, apoptosis and necroptosis are three main stress responses regulating life and death of a cell. Whereas the crosstalk between autophagy and apoptosis is well established, the relationship between autophagy and necroptosis awaits further clarification. Although recent reports suggest the existence of this crosstalk,[48-50] mechanistic details are rudimentary. Here, we report that necroptosis induced by TNFα blocks late events of the autophagic pathway, i.e. the degradation of autophagosomes by lysosomes. We also find that early events of autophagy—for example AMPK-dependent phosphorylation of ULK1 and BECN1 or formation of ATG14 puncta—are induced upon TNFα treatment. Remarkably, we found that the pro-necroptotic RIPK3 directly phosphorylates PRKAA1/2 at T183/T172 and thus activates it. This is especially noteworthy since only limited examples exist for both RIPK3 substrates and AMPK-activating kinases.

At first glance, the activation of early autophagy events and the simultaneous inhibition of late events appear to be contradictory. We observe that autophagy—specifically the lysosomal degradation of autophagosomes—is blocked upon TNFα treatment and necroptosis induction. However, it still has to be determined how the final steps of autophagy are blocked by the executioners of necroptosis. At least lysosomal cathepsins CTSB and CTSL remain functional upon TNFα treatment, which is not the case for bafilomycin A_1 treatment (Figure S2). Generally, the blockade of cyto-protective pathways upon necroptosis induction is comprehensible and is similar to the crosstalk between apoptosis and autophagy, in which e.g. activated caspases cleave several autophagy-relevant proteins and thus inactivate their autophagic function.[51] In contrast, the induction of early autophagy events upon TNFα treatment is less intuitive. We speculate that this phenomenon might be explained by two hypotheses: 1) an anti-necroptotic and thus cyto-protective function of RIPK3, or 2) a pro-necroptotic function of early autophagy events. In the first scenario, it might be that RIPK3 regulates cyto-protective autophagy independently of its pro-death function during necroptosis. So far, RIPK3 has been attributed a central role in necroptosis signaling, and the best-characterized RIPK3 substrate MLKL is a main executor of necroptosis.[31, 32, 39] A possible role of RIPK3 in the regulation of autophagy has also been suggested by two other groups. Harris et al. suggest RIPK3 positively regulates autophagy since depletion of RIPK3 inhibits autophagic flux and leads to the accumulation of autophagosomes and amphisomes.[48] In contrast, Matsuzawa et al. reported that RIPK3 serves as a negative regulator of selective autophagy by binding to p62/SQSTM1 and thus regulating p62/SQSTM1-LC3 complex formation.[52] We observe that RIPK3 positively regulates AMPK activity. Activated AMPK phosphorylates both ULK1 and BECN1, and these two phosphorylation events have been associated with a positive regulation of autophagy.[10, 16, 43, 44] We also observed increased ATG14 puncta formation in a RIPK3-dependent manner. The RIPK3-dependent induction of early autophagy events might pursue a cyto-protective function and slow down the execution of necroptosis. Along these lines, necroptosis-inhibitory functions have been attributed to

AMPK (ref. [53, 54]) and to ULK1 (unpublished results). Similarly, we observe increased cell death upon TNFα treatment in *ulk1/2* or *prkaa1/2* DKO MEFs compared to wild-type control cells (Figure S3).

In a second and opposing scenario, one might speculate that the induction of early autophagy events supports necroptosis. Goodall et al. reported that inhibition of late stage autophagy enhanced TRAIL-induced cell death. In contrast, genetic or pharmacological inhibition of early/mid-stage autophagy prevented cell death.[50, 55] The authors hypothesized that components of the autophagy machinery mediate cell death by functioning as a scaffold for necrosome formation and activation. Specifically, they propose that the interaction between p62/SQSTM1 and RIPK1 localizes the necrosome on the autophagosome.[50, 55] It is tempting to speculate that RIPK3 itself promotes early autophagy events to support its pro-necroptotic function. Furthermore, Goodall et al. also stated that apparently the turnover of cellular components does not mediate this pro-death function and that they observed necrosome structures on quite mature autophagosomes.[50, 55] Our observed blockade of autophagosome degradation might point toward the same direction. We observed increased LC3-positive structures, which potentially reflect increased necrosome-activating platforms. Additionally, we observed increased ATG14-positive structures, but not increased WIPI2, ZFYVE1 or ATG16L1 structures. ATG14 has been reported to promote membrane tethering and fusion of autophagosomes to endolysosomes.[56] Diao et al. reported that mature LC3-positive autophagosomes accumulated in cells expressing an ATG14 variant that could not homo-oligomerize; however, ATG16L1-positive phagophores did not accumulate in these cells.[56] Collectively, our observations might indicate that RIPK3 "feeds" the autophagic flux via AMPK-dependent activation of ULK1 and BECN1 in order to ensure sufficient autophagosome maturation and accumulation. AMPK becomes activated under stress and starvation conditions, but it has also been shown that AMPK can support autophagy under nutrient sufficiency.[29] Accordingly, it is conceivable that AMPK also supports autophagy induction upon TNFα treatment. Admittedly, our second model is rather speculative and especially kinetic and spatial aspects need further validation. As mentioned above, necroptosis is rather increased in *ulk1/2* or *prkaa1/2* DKO MEFs compared to wild-type control cells, supporting a generally anti-necroptotic function of these two kinases. Both scenarios of TNFα-induced activation of early autophagy events are schematically depicted in Figure S4.

AMPK is the central energy sensor of the cells. To date, three kinases have been shown to phosphorylate and thus activate AMPK, i.e. STK11, CaMKK2, and MAP3K7.[2-4, 24-27] Here, we showed that RIPK3 is another AMPK-activating kinase. However, we do not believe that RIPK3-dependent phosphorylation is the only mechanism to activate AMPK during necroptosis. It has previously been described that the induction of necroptosis results in reduced cellular ATP levels.[57, 58] Accordingly, STK11 likely contributes to AMPK activation during necroptosis. Nevertheless, we think that the RIPK3-dependent activation of AMPK represents another level of crosstalk between necroptosis and autophagy. The ultimate fate of a cell under stress conditions is determined by the integration of different cellular stress responses. Accordingly, a deeper understanding of

the interplay between these stress responses is necessary in order to exploit these pathways for potential therapeutic approaches.

EXPERIMENTAL PROCEDURES

Antibodies and reagents

Anti-mouse RIPK3 (ProSci; 2283), anti-MLKL phospho-Ser345 [EPR9515(2)] (Abcam; ab196436), anti-MLKL (Sigma-Aldrich, SAB1302339), anti-FLAG (Sigma-Aldrich; F3165), anti-ACTB/β-actin (Sigma-Aldrich; A5316), anti-PRKAA1/2 (Cell Signaling Technology; 2793 (clone F6) and 2603 (clone 23A3) for immunoblot, and Santa Cruz; sc-74461 (clone D-6) for immunopurification), anti-PRKAA1/2 phospho-T183/T172 (40H9) (Cell Signaling Technology; 2535), anti-GST (Sigma-Aldrich; G7781), anti-LC3B (Cell Signaling Technology; 2775 for immunoblot [detects endogenous levels of total LC3B protein; cross-reactivity may exist with other LC3 isoforms according to manufacturer specification], and MBL International; PM036 for immunofluorescence [reacts with LC3A/LC3B/LC3C according to manufacturer specification]), anti-BECN1 (H-300) (Santa Cruz; sc-11427), anti-BECN1 phospho-S93 (D9A5G) (Cell Signaling Technology; 14717S), anti-ATG14 (Santa Cruz; sc-164767), anti-ACACA phospho-S79 (Cell Signaling Technology; 3661), anti-ACACA (Cell Signaling Technology; 3662), anti-ULK1 phospho-S555 (Cell Signaling Technology; 5869), anti-ULK1 (Cell Signaling Technology; 8054)), anti-LAMP1 (Developmental Studies Hybridoma Bank, DSHB; DSHB product 1D4B was deposited by August, J.T., Pharmacology & Molecular Sciences, Johns Hopkins School of Medicine). IRDye 800- or IRDye 680-conjugated secondary antibodies were purchased from LI-COR Biosciences (925-32212/13/14, 925-68072/73/74), and Alexa Fluor® 647-conjugated goat anti-mouse IgG (H+L) (715-605-151) and Alexa Fluor® 488-conjugated goat anti-rabbit IgG (H+L) (711-545-152) antibodies from Jackson ImmunoResearch Laboratories. Bafilomycin A_1 (Alfa Aesar; J61835), TNF Recombinant Mouse Protein (Thermo Scientific; PMC3014), active GST-hRIPK3 (Sigma-Aldrich; SRP5316), GSK'872 (Calbiochem; 530389), Alkaline Phosphatase (Thermo Fisher; EF0651), Q-VD-OPh (Selleck Chemicals; S7311), z-VAD-FMK (Selleck Chemicals; S7023), ProLong® Gold Antifade Reagent with DAPI (Cell Signaling Technology; 8961), Lipofectamine™ RNAiMAX Transfection Reagent (Thermo Fisher; 13778150), FuGENE® 6 (Promega; E2692), Magic Red Cathepsin-B/L Assay (ImmunoChemistry Technologies; 937/941). His-AMPK (PRKAA1[11-559] + PRKAB2[1-272] + PRKAG1[1-331]) (catalog number DU32489) was obtained through the MRC PPU Reagents and Services facility (MRC PPU, College of Life Sciences, University of Dundee, Scotland, mrcppureagents.dundee.ac.uk).

Constructs and siRNAs

pBOB-FLAG-mRIPK3 plasmid was kindly provided by Jiahuai Han (School of Life Sciences, Xiamen University, China). pCI-neo-3xFLAG-hRIPK3 was kindly provided by Sudan He (Cyrus Tang Hematology Center, Soochow University, China). pMRX-IP-EGFP1-rLC3-mRFP1-rLC3ΔG was kindly provided by Noboru Mizushima (Department of Biochemistry and Molecular Biology, Graduate School and Faculty of Medicine, The University of Tokyo, Tokyo, Japan) and has been previously described.[59] pMSCVblast-mCitrine-hLC3 and pMSCVblast-mRFP-EGFP-rLC3 were previously described.[45] pCI-neo-3xFLAG-hRIPK3 K50A (kinase dead) plasmid was

generated using one step PCR from pCI-neo-3xFLAG-hRIPK3. cDNA encoding mRIPK3 harboring *XhoI* and *NotI* restriction enzyme sites was amplified from pBOB-FLAG-mRIPK3 plasmid. PCR fragment was inserted into pGEX-5X-3 and generated pGEX-5X-3-mRIPK3. cDNA encoding mRIPK3 harboring *XhoI* and *NotI* restriction enzyme sites amplified from pBOB-FLAG-mRIPK3 plasmid was inserted into pCI-neo-3xFLAG-hRIPK3 vector digested with *XhoI* and *NotI* restriction enzymes to generate pCI-neo-3xFLAG-mRIPK3. cDNA of full length 3xFLAG-mRIPK3 harboring *BglII* and *NotI* restriction enzyme sites amplified from pCI-neo-3xFLAG-mRIPK3 was inserted into pMSCVpuro vector to generate pMSCVpuro-3xFLAG-mRIPK3. cDNA encoding hPRKAA1 was cloned from HEK293 cDNA and inserted into pGEX-5X-3. cDNAs of truncated hPRKAA1 (1-278) and hPRKAA1 (279-559) harboring *XhoI* and *NotI* restriction enzyme sites were amplified from pGEX-5X-3-hPRKAA1 and inserted into pGEX-5X-3. cDNA of GST-hPRKAA1 (1-278) T183A was amplified from GST-hPRKAA1 (1-278) using one-step PCR. Mouse *Ripk3* (ON-TARGETplus siRNA SMARTpool, L-049919-00-0010), and control siRNAs (ON-TARGETplus non-targeting pool, D-001810-10-20) were obtained from Dharmacon (working concentration: 20 nM).

Cell lines

Ripk3 KO MEFs have previously been described and were kindly provided by Jiahuai Han (School of Life Sciences, Xiamen University, China).[60] *Ulk1/2* DKO MEFs have previously been described and were kindly provided by Tullia Lindsten (Memorial Sloan Kettering Cancer Center, New York, USA).[61] *Prkaa1/2* DKO MEFs have previously been described and were kindly provided by Benoit Viollet (Inserm, U1016, Institut Cochin, 75014 Paris, France).[62] For the generation of L929 cells stably expressing EGFP1-rLC3-mRFP1-rLC3ΔG or mRFP-EGFP-rLC3 and *ripk3* KO MEFs stably expressing FLAG-mRIPK3, the vectors pMRX-IP-EGFP1-rLC3-mRFP1-rLC3ΔG, pMSCVblast-mRFP-EGFP-rLC3 or pMSCVpuro-FLAG-mRIPK3 were transfected into Plat-E cells (kindly provided by Toshio Kitamura, Institute of Medical Science, University of Tokyo, Japan) using FuGENE® 6 (Promega; E2692). After 48 h, retroviral supernatant was collected and used for the infection of L929 cells or MEFs in combination with 10 μg/ml polybrene. After 12 h, cells were selected in medium containing puromycin (50 μg/ml for L929 and 2.5 μg/ml for MEFs) or 35 μg/ml blasticidine. MEFs, L929 and Plat-E cell lines were cultured in high D-glucose DMEM (Thermo Fisher; 41965-039) supplemented with 10% FCS (Thermo Fisher; 10270-106), 100 U/ml penicillin and 100 μg/ml streptomycin at 37°C and 5% CO_2. For amino acid starvation, cells were washed once with DPBS (Dulbecco's Phosphate-Buffered Saline, Thermo Fisher, 14190094) and incubated for the indicated time points in EBSS (Earle's Balanced Salt Solution, Thermo Fisher; 24010043).

Immunofluorescence and proximity ligation assay (PLA)

Cells were seeded on glass coverslips overnight and exposed to indicated treatments at the next day. Then, cells were fixed using 4% paraformaldehyde for 10 min at room temperature and after washing three times

with PBS, cells were permeabilized with 50 µg/ml digitonin for 5 min at room temperature. Cells were again washed with PBS three times and incubated with 3% BSA for 30 min at room temperature. The coverslips were transferred to a humidified chamber and incubated with indicated primary antibodies in 3% BSA for 1 h at room temperature. The cells were washed 3 times (3 min each time) with PBS and incubated with indicated secondary antibodies in 3% BSA for 1 h at room temperature in the dark. The cells were washed 3 times (3 min each time) with PBS and mounted on slide glass with ProLong® Gold Antifade Reagent with DAPI after rinsing the coverslips briefly in distilled water. After drying the coverslips, they were stored at 4 ˚C. For proximity ligation assay, fluorescence signals were measured according to Duolink® PLA Fluorescence Protocol (Sigma-Aldrich; DUO82005 [anti-rabbit] and DUO82001 [anti-mouse]). Images were captured by Zeiss Axio Observer 7 (ApoTome extension, Objective Plan-Apochromat 40x/1,4 Oil DIC M27). For all immunofluorescence and PLA analyses, puncta quantification was done using ImageJ software.

Protein expression and purification

pGEX-5X-3-hPRKAA1 variants and pGEX-5X-3-mRIPK3 were transformed into *E. coli* BL21 (DE3). Target protein expression was induced by 0.1-1 mM IPTG for 3-5 h at 30°C. Bacteria were harvested and resuspended in bacterial lysis buffer (300 mM NaCl, 50 mM Tris-HCl (pH 8.0), 5 mM EDTA, 0.01% Igepal, 100 ng/ml lysozyme, 1x protease inhibitor cocktail). After sonification and centrifugation at 10,000 g for 20 min, the supernatant was incubated with glutathione sepharose 4B beads (GE Healthcare; 17-0756-01) overnight. After washing 3 times with lysis buffer, protein bound to beads were stored at -80°C or soluble proteins were obtained by incubation of the beads with elution buffer (50 mM Tris-HCl (pH 8.0), 20 mM glutathione reduced) for 10 min at room temperature (3-5 times). Purified proteins were stored at -80°C.

***In vitro* kinase assay**

For *in vitro* kinase assays, 1-2 µg substrate were incubated with 0.25-0.5 µg activated kinase in kinase buffer (50 mM Tris-Cl pH 7.5, 0.1 mM EGTA, 1 mM DTT, 7.5 mM $Mg(CH_3COO)_2$, 2 µM ATP (non-radioactive) with or without 10 µCi [γ-^{32}P]-ATP) for 45 min at 30°C. The kinase reaction was stopped by adding loading buffer and boiling for 5 min at 95°C. After coomassie staining or immunoblotting, autoradiography was performed or phosphorylation was detected using anti-PRKAA1/2 phospho-T183/T172 antibody.

Protein dephosphorylation assay

Two duplicate samples were separated by the same SDS-PAGE and then transferred to the same PVDF membrane. Following blocking with 5% BSA in TBS-T for 1 h at room temperature, the PVDF membrane was washed with TBS-T twice (5 min each). The membrane was cut into two halves with duplicate samples on each membrane. The two membranes were placed into two tubes with or without 10 U alkaline phosphatase

(2 ml reaction volume) and incubated for 1 h at 37°C with shaking (350 rpm). After washing twice with TBS-T (5 min each), the membranes were incubated with the corresponding primary antibodies at 4°C overnight.

Immunoblotting, immunopurification and size exclusion chromatography

For immunoblotting, cells were lysed in 1% NP-40 lysis buffer (50 mM Tris-Cl pH 7.5, 150 mM NaCl, 1 mM EDTA, 1% NP-40, 10% glycerin, 1 mM Na_3VO_4, 50 mM NaF and protease inhibitor cocktail [Sigma-Aldrich; P2714]). Alternatively, whole cell lysates were prepared by direct addition of sample buffer (125 mM Tris-Cl, pH 6.8, 17.2% glycerol, 4.1% SDS, 0.02% bromophenol blue and 2% β-mercaptoethanol) to the cells and subsequent sonification. An equal amount of protein (30-50 µg) were separated by SDS-PAGE, and then transferred to PVDF membrane (Millipore; IPFL00010). Target proteins were detected by the indicated primary antibodies, followed by the corresponding IRDye®800- or IRDye®680-conjugated secondary antibodies (LI-COR Biosciences). Signals were detected with an Odyssey Infrared Imaging system (LI-COR Biosciences). For immunopurification, cells were lysed in the same lysis buffer for 30 min on ice. After 10,000 g centrifugation for 10 min, the supernatants were incubated with indicated beads [FLAG® M2 Affinity Gel (Sigma-Aldrich; A2220) or Protein A/G PLUS-Agarose (Santa Cruz; sc-2003) conjugated with anti-PRKAA1/2 antibodies (Santa Cruz; sc-74461)] overnight. Thereafter, the beads were washed five times with lysis buffer, and boiled in sample buffer for 5 min at 95°C. Purified proteins were analyzed by immunoblotting. Size exclusion chromatography was performed as described previously.[47]

GST affinity purification

GST fusion proteins were purified from *E. coli* BL21 (DE3) with glutathione sepharose 4B beads (GE Healthcare; 17-0756-01). For GST pulldown, 4 µg of GST fusion protein were incubated with 1 µg His-AMPK (PRKAA1[11-559] + PRKAB2[1-272] + PRKAG1[1-331]) in 0.5% NP-40 lysis buffer (50 mM Tris, pH 8.0, 100 mM NaCl, 6 mM EDTA, 6 mM EGTA, 0.5% Nonidet P-40, 1 mM dithiothreitol supplemented with protease inhibitor cocktail) at 4°C overnight and then washed five times with lysis buffer. The beads were boiled with sample buffer at 95°C for 5 min and purified proteins were analyzed by immunoblotting.

Cell death assay

Total cells treated with indicated stimuli were trypsinized and collected. Cells were then incubated in propidium iodide (PI) solution (5 µg/ml in PBS) at 4°C for 1 h. PI-positive cells were measured by flow cytometry (LSRFortessa™, BD Biosciences).

Statistical analysis

For PI uptake, shown data represent four independent experiments ± SD. Absolute values are shown. For the quantification of immunoblots, the density of each protein band was divided by the average of the density of

all bands from the same protein on the membrane. Subsequently, fold changes were calculated by dividing each normalized ratio (protein to loading control) by the average of the ratios of the control lane (as indicated in the corresponding figure legend). For Figure 1A, statistical analysis was performed using repeated measures two-way ANOVA (corrected by Tukey's multiple comparisons test). For Figure 1E, 2A, and S1, statistical analyses were performed using repeated measures two-way ANOVA (corrected by Sidak's multiple comparisons test). For Figure 2D, statistical analysis was performed using ordinary one-way ANOVA (corrected by Tukey's multiple comparisons test). For Figure 3E, statistical analysis was performed using an unpaired t test with Welch's correction. For Figure 4F and S3, statistical analyses were performed using ordinary two-way ANOVA (corrected by Tukey's multiple comparisons test). Compared treatments or cell lines are indicated in the corresponding bar diagrams. *P* values < 0.05 were considered statistically significant. All statistical data were calculated with GraphPad Prism (version 7.01).

ACKNOWLEDGMENTS

We thank Jiahuai Han (School of Life Sciences, Xiamen University, China) for providing *ripk3* KO MEFs and pBOB-FLAG-mRIPK3 plasmid. We thank Tullia Lindsten (Memorial Sloan Kettering Cancer Center, New York, USA) for providing *ulk1/2* DKO MEFs. We thank Benoit Viollet (Inserm, U1016, Institut Cochin, 75014 Paris, France) for providing *prkaa1/2* DKO MEFs. We thank Sudan He (Cyrus Tang Hematology Center, Soochow University, China) for providing pCI-neo-3xFLAG-hRIPK3. We thank Noboru Mizushima (Department of Biochemistry and Molecular Biology, Graduate School and Faculty of Medicine, The University of Tokyo, Tokyo, Japan) for providing pMRX-IP-EGFP1-rLC3-mRFP1-rLC3ΔG. This work was supported by the Deutsche Forschungsgemeinschaft STO 864/4-1, STO 864/5-1 and GRK 2158 (to BS), and the Düsseldorf School of Oncology (to BS; funded by the Comprehensive Cancer Center Düsseldorf/Deutsche Krebshilfe and the Medical Faculty of the Heinrich-Heine-University Düsseldorf).

CONFLICT OF INTEREST STATEMENT

The authors declare that there are no competing financial interests in relation to the work described.

AUTHOR CONTRIBUTION STATEMENT

WW designed the experiments, performed immunofluorescence, proximity ligation assays, cell death assays, size exclusion chromatography and *in vitro* kinase assays. WW and XW performed immunoblot analyses. XW cloned constructs encoding RIPK3 variants, purified GST fusion proteins. NB and CP supported *in vitro* kinase assays and size exclusion chromatography. JD and MJM gave technical support for immunofluorescence. DS and FS supported cell death assays. NWH gave technical support for proximity ligation assays. WW and BS analyzed and interpreted the data and wrote the manuscript. BS supervised the project. All authors discussed the results and commented on the manuscript.

FIGURE LEGENDS

Figure 1.

Necroptosis inhibits lysosomal LC3 degradation. (**A**) L929 cells were transfected with scramble (scr) or *Ripk3* siRNAs. 48 h post transfection, cells were exposed to 10 ng/ml TNFα and 30 μM QVD with or without 20 nM bafilomycin A_1 (TQ or TQB) for indicated times. Then, cells were lysed and cleared cellular lysates were subjected to SDS-PAGE and immunoblotting for LC3, RIPK3 and ACTB. The density of each protein band was divided by the average of the density of all bands from the same protein on the membrane. Fold changes were calculated by dividing each normalized ratio (protein to loading control) by the average of the ratios of the control lane (scr, 0 h TQ). Results are mean + SD from three independent experiments. Statistical analysis was done by repeated measures two-way ANOVA (corrected by Tukey's multiple comparisons test), **P* < 0.05, ***P* < 0.01, ****P* < 0.001, *****P* < 0.0001. (**B**) L929 cells were transfected with scramble or *Ripk3* siRNAs. 48 h post transfection, cells were exposed to indicated treatments (10 ng/ml TNFα [T], 30 μM QVD [Q], 20 nM bafilomycin A_1 [B]) for 3 h. After that, cells were fixed and subjected to LC3 immunostaining using anti-LC3 antibodies (MBL International; PM036) and Alexa Fluor 488-conjugated goat anti-rabbit second antibodies. Scale bar: 20 μm. (**C**) L929 cells retrovirally transfected with cDNA encoding EGFP1-rLC3-mRFP1-rLC3ΔG were exposed to indicated treatments (10 ng/ml TNFα [T], 30 μM QVD [Q], 5 μM GSK'872, 20 nM bafilomycin A_1 [BafA1]) for 3 h. Then cells were fixed and subjected to LAMP1 immunostaining using anti-LAMP1 antibodies and Alexa Fluor 647-conjugated goat anti-mouse second antibodies. The intensity of colocalization of GFP-LC3 and LAMP1 is shown on the right. Scale bar: 20 μm. (**D**) L929 cells retrovirally transfected with cDNA encoding mRFP-EGFP-rLC3 were transfected with scramble or *Ripk3* siRNAs. 48 h post transfection, cells were exposed to indicated treatments (10 ng/ml TNFα [T], 30 μM QVD [Q], 20 nM bafilomycin A_1 [BafA1]) for 3 h. Then cells were fixed and RFP and GFP fluorescence was analyzed by immunofluorescence microscopy. Scale bar: 20 μm. (**E**) L929 cells were retrovirally transfected with cDNA encoding mCitrine-LC3B. Cells were treated using 10 ng/ml TNFα/30 μM QVD (TQ) or EBSS with or without 20 nM bafilomycin A_1 (B) for indicated times. Cells were collected and mCitrine fluorescence intensity was measured by flow cytometry. The mean of fluorescence intensity for each sample was normalized to cells incubated in growth medium (M). Data represent mean + SD from two independent experiments. Statistical analysis was done by repeated measures two-way ANOVA (corrected by Sidak's multiple comparisons test), ns = not significant, ****P < 0.0001. Statistically significant differences within each treatment compared to the corresponding medium control are depicted directly above the bars.

Figure 2.

TNFα treatment induces activation of AMPK and early autophagy events. (**A**) L929 cells were transfected with scramble or *Ripk3* siRNAs. 48 h post transfection, cells were exposed to 10 ng/ml TNFα and 30 μM QVD (TQ) for indicated times. Then, whole cell lysates were subjected to SDS-PAGE and immunoblotting for indicated proteins. A compilation of representative immunoblots is shown; three ACTB immunblots are shown, but each protein was normalized to its corresponding loading control. The density of each protein band was divided by the average of the density of all bands from the same protein on the membrane. Fold changes were calculated by dividing each normalized ratio (protein to loading control) by the average of the ratios of the control lane (scr, 0 h TQ). Results are mean + SD from at least 3 independent experiments. Statistical analysis was done by repeated measures two-way ANOVA (corrected by Sidak's multiple comparisons test), **P* < 0.05, ***P* < 0.01, ****P* < 0.001, ****P < 0.0001. Statistically significant differences within scramble siRNA-transfected cells (compared to scr, 0 h TQ) are depicted directly above the bars. (**B**) L929 cells were exposed to indicated treatments (10 ng/ml TNFα [T], 30 μM QVD [Q], 5 μM GSK'872 [G]) for 6h. Cells were lysed and cleared cellular lysates were subjected to SDS-PAGE and analyzed by immunoblotting for indicated proteins. (**C**) *Ripk3* WT and KO MEFs were treated with 30 ng/ml TNFα + 100 nM SMAC-mimetic + 20 μM z-VAD (TSZ) for indicated times. Then, cells were lysed and cleared cellular lysates were subjected to SDS-PAGE and analyzed by immunoblotting for indicated proteins. (**D**) L929 cells were exposed to indicated treatments (10 ng/ml TNFα, 30 μM QVD, 5 μM GSK'872) for 3 h. After that, cells were fixed and subjected to ATG14 immunostaining using anti-ATG14 antibodies (Santa Cruz; sc-164767) and IRDye® 680RD Donkey anti-Goat secondary antibodies. Puncta quantification was done using ImageJ software. Data represent mean + SD. A minimum of 120 cells was analyzed. Statistical analysis was performed using ordinary one-way ANOVA (corrected by Tukey's multiple comparisons test), *****P* < 0.0001. Scale bar: 20 μm.

Figure 3.

RIPK3 interacts with AMPK. (**A**) S100 extracts of MEFs were separated by size-exclusion chromatography on a Superose 6 increase column. Fractions were analyzed by immunoblotting for the indicated proteins. The diagram shows protein levels for fractions 16-40 and the density of each protein band was divided by the average of the density of all bands from the same protein on the membrane. **(B)** HEK293 cells were left untransfected or were transfected with a vector encoding FLAG-hRIPK3 for 24 h. Then, cells were lysed and cleared cellular lysates were subjected to immunopurification using anti-FLAG beads. Purified proteins were subjected to SDS-PAGE and analyzed by immunoblotting for FLAG and AMPK. **(C)** HEK293 cells were left untransfected or were transfected with a vector encoding FLAG-hRIPK3 for 24 h. Then, cells were lysed and cleared cellular lysates were subjected to immunopurification using anti-AMPK antibodies. Purified proteins were subjected to SDS-PAGE and analyzed by immunoblotting for FLAG and AMPK. **(D)** GST or GST-mRIPK3

immobilized on glutathione-Sepharose beads was incubated with His-AMPK (PRKAA1[11-559] + PRKAB2[1-272] + PRKAG1[1-331]) overnight. After washing the beads, bound proteins were eluted by boiling for 10 min at 95°C. Proteins were subjected to SDS-PAGE and analyzed by immunoblotting for AMPK and GST. **(E)** *ripk3* KO MEFs were retrovirally transfected with empty vector or cDNA encoding FLAG-mRIPK3. Cells were seeded onto glass coverslips. The next day, cells were fixed and analyzed using proximity ligation assay as described in the material and methods section (anti-RIPK3: Prosci, 2283; anti-PRKAA1/2: Cell Signaling Technology, 2793). Nuclei were stained with DAPI. Signals and nuclei per image were counted and the signal:nuclei ratio was calculated. Data represent mean + SD. A minimum of 216 cells was analyzed. Statistical analysis was performed using an unpaired *t* test with Welch's correction, ****$P < 0.0001$. Scale bar: 20 μm.

Figure 4.

RIPK3 directly phosphorylates PRKAA1 at T183. (**A**) For *in vitro* kinase assay, purified GST, GST-hPRKAA1(1-278) and GST-hPRKAA1(279-559) were incubated with activated RIPK3 and [γ-^{32}P]-ATP. The reactions were subjected to SDS-PAGE. After coomassie staining and drying of the gels, autoradiography was performed. **(B)** GST-hPRKAA1 WT and the T183A mutant were purified and were incubated with activated RIPK3 and cold ATP. The reactions were subjected to SDS-PAGE and analyzed by immunoblotting for phospho-PRKAA1/2 T183/T172 and AMPK. **(C)** GST-hPRKAA1 WT and the T183A mutant were incubated with activated RIPK3 and cold ATP with or without alkaline phosphatase. The reactions were subjected to SDS-PAGE and analyzed by immunoblotting for phospho-PRKAA1/2 T183/T172 and AMPK. **(D)** GST-hPRKAA1 WT was incubated with activated RIPK3 and cold ATP with or without 50 μM GSK'872. The reactions were subjected to SDS-PAGE and analyzed by immunoblotting for phospho-PRKAA1/2 T183/T172 and AMPK. **(E)** HEK293 cells were left untransfected or were transfected with cDNA encoding either FLAG-hRIPK3 WT or FLAG-hRIPK3 kinase-dead (KD) for 24 h. After that, cells were treated with 30 ng/ml TNFα + 30 μM QVD for 24 h. Then, cells were lysed and cleared cellular lysates were subjected to SDS-PAGE and analyzed by immunoblotting for phospho-PRKAA1/2 T183/T172, AMPK, FLAG and ACTB. **(F)** *ripk3* KO MEFs were retrovirally transfected with empty vector or cDNA encoding FLAG-mRIPK3. Cells were seeded onto glass coverslips. The next day, the cells were treated with 30 ng/ml TNFα + 100 nM SMAC-mimetic + 20 μM z-VAD (TSZ) for 3 h. Then cells were fixed and analyzed using proximity ligation assay as described in the material and methods section (anti-phospho-PRKAA1/2 T183/T172: Cell Signaling Technology, 2535; anti-PRKAA1/2: Cell Signaling Technology, 2793). Nuclei were stained with DAPI. Signals and nuclei per image were counted and the signal:nuclei ration was calculated. Data represent mean + SD. A minimum of 107 cells was analyzed. Statistical analysis was performed using ordinary two-way ANOVA (corrected by Tukey's multiple comparisons test), ****$P < 0.0001$. Scale bar: 20 μm.

REFERENCES

1. Mercer TJ, Gubas A, Tooze SA. A molecular perspective of mammalian autophagosome biogenesis. The Journal of biological chemistry 2018; 293:5386-95.
2. Hawley SA, Boudeau J, Reid JL, Mustard KJ, Udd L, Makela TP, et al. Complexes between the LKB1 tumor suppressor, STRAD alpha/beta and MO25 alpha/beta are upstream kinases in the AMP-activated protein kinase cascade. J Biol 2003; 2:28.
3. Shaw RJ, Kosmatka M, Bardeesy N, Hurley RL, Witters LA, DePinho RA, et al. The tumor suppressor LKB1 kinase directly activates AMP-activated kinase and regulates apoptosis in response to energy stress. Proc Natl Acad Sci U S A 2004; 101:3329-35.
4. Woods A, Johnstone SR, Dickerson K, Leiper FC, Fryer LG, Neumann D, et al. LKB1 is the upstream kinase in the AMP-activated protein kinase cascade. Current biology : CB 2003; 13:2004-8.
5. Alers S, Loffler AS, Wesselborg S, Stork B. Role of AMPK-mTOR-Ulk1/2 in the regulation of autophagy: cross talk, shortcuts, and feedbacks. Molecular and cellular biology 2012; 32:2-11.
6. Zhao M, Klionsky DJ. AMPK-dependent phosphorylation of ULK1 induces autophagy. Cell metabolism 2011; 13:119-20.
7. Hindupur SK, Gonzalez A, Hall MN. The opposing actions of target of rapamycin and AMP-activated protein kinase in cell growth control. Cold Spring Harbor perspectives in biology 2015; 7:a019141.
8. Kim J, Kundu M, Viollet B, Guan KL. AMPK and mTOR regulate autophagy through direct phosphorylation of Ulk1. Nature cell biology 2011; 13:132-41.
9. Bach M, Larance M, James DE, Ramm G. The serine/threonine kinase ULK1 is a target of multiple phosphorylation events. Biochem J 2011; 440:283-91.
10. Egan DF, Shackelford DB, Mihaylova MM, Gelino S, Kohnz RA, Mair W, et al. Phosphorylation of ULK1 (hATG1) by AMP-activated protein kinase connects energy sensing to mitophagy. Science 2011; 331:456-61.
11. Mack HI, Zheng B, Asara JM, Thomas SM. AMPK-dependent phosphorylation of ULK1 regulates ATG9 localization. Autophagy 2012; 8:1197-214.
12. Shang L, Chen S, Du F, Li S, Zhao L, Wang X. Nutrient starvation elicits an acute autophagic response mediated by Ulk1 dephosphorylation and its subsequent dissociation from AMPK. Proc Natl Acad Sci U S A 2011; 108:4788-93.
13. Mizushima N. A brief history of autophagy from cell biology to physiology and disease. Nature cell biology 2018; 20:521-7.
14. Hurley JH, Young LN. Mechanisms of Autophagy Initiation. Annu Rev Biochem 2017; 86:225-44.
15. Egan DF, Chun MG, Vamos M, Zou H, Rong J, Miller CJ, et al. Small Molecule Inhibition of the Autophagy Kinase ULK1 and Identification of ULK1 Substrates. Molecular cell 2015; 59:285-97.
16. Kim J, Kim YC, Fang C, Russell RC, Kim JH, Fan W, et al. Differential regulation of distinct Vps34 complexes by AMPK in nutrient stress and autophagy. Cell 2013; 152:290-303.
17. Ma X, Zhang S, He L, Rong Y, Brier LW, Sun Q, et al. MTORC1-mediated NRBF2 phosphorylation functions as a switch for the class III PtdIns3K and autophagy. Autophagy 2017; 13:592-607.
18. Park JM, Jung CH, Seo M, Otto NM, Grunwald D, Kim KH, et al. The ULK1 complex mediates MTORC1 signaling to the autophagy initiation machinery via binding and phosphorylating ATG14. Autophagy 2016; 12:547-64.
19. Russell RC, Tian Y, Yuan H, Park HW, Chang YY, Kim J, et al. ULK1 induces autophagy by phosphorylating Beclin-1 and activating VPS34 lipid kinase. Nature cell biology 2013; 15:741-50.
20. Axe EL, Walker SA, Manifava M, Chandra P, Roderick HL, Habermann A, et al. Autophagosome formation from membrane compartments enriched in phosphatidylinositol 3-phosphate and dynamically connected to the endoplasmic reticulum. The Journal of cell biology 2008; 182:685-701.

21. Hayashi-Nishino M, Fujita N, Noda T, Yamaguchi A, Yoshimori T, Yamamoto A. A subdomain of the endoplasmic reticulum forms a cradle for autophagosome formation. Nature cell biology 2009; 11:1433-7.
22. Uemura T, Yamamoto M, Kametaka A, Sou YS, Yabashi A, Yamada A, et al. A cluster of thin tubular structures mediates transformation of the endoplasmic reticulum to autophagic isolation membrane. Molecular and cellular biology 2014; 34:1695-706.
23. Yla-Anttila P, Vihinen H, Jokitalo E, Eskelinen EL. 3D tomography reveals connections between the phagophore and endoplasmic reticulum. Autophagy 2009; 5:1180-5.
24. Hawley SA, Pan DA, Mustard KJ, Ross L, Bain J, Edelman AM, et al. Calmodulin-dependent protein kinase kinase-beta is an alternative upstream kinase for AMP-activated protein kinase. Cell metabolism 2005; 2:9-19.
25. Hurley RL, Anderson KA, Franzone JM, Kemp BE, Means AR, Witters LA. The Ca2+/calmodulin-dependent protein kinase kinases are AMP-activated protein kinase kinases. The Journal of biological chemistry 2005; 280:29060-6.
26. Momcilovic M, Hong SP, Carlson M. Mammalian TAK1 activates Snf1 protein kinase in yeast and phosphorylates AMP-activated protein kinase in vitro. The Journal of biological chemistry 2006; 281:25336-43.
27. Woods A, Dickerson K, Heath R, Hong SP, Momcilovic M, Johnstone SR, et al. Ca2+/calmodulin-dependent protein kinase kinase-beta acts upstream of AMP-activated protein kinase in mammalian cells. Cell metabolism 2005; 2:21-33.
28. Herzig S, Shaw RJ. AMPK: guardian of metabolism and mitochondrial homeostasis. Nat Rev Mol Cell Biol 2018; 19:121-35.
29. Dalle Pezze P, Ruf S, Sonntag AG, Langelaar-Makkinje M, Hall P, Heberle AM, et al. A systems study reveals concurrent activation of AMPK and mTOR by amino acids. Nature communications 2016; 7:13254.
30. Galluzzi L, Vitale I, Aaronson SA, Abrams JM, Adam D, Agostinis P, et al. Molecular mechanisms of cell death: recommendations of the Nomenclature Committee on Cell Death 2018. Cell Death Differ 2018; 25:486-541.
31. Annibaldi A, Meier P. Checkpoints in TNF-Induced Cell Death: Implications in Inflammation and Cancer. Trends Mol Med 2018; 24:49-65.
32. Grootjans S, Vanden Berghe T, Vandenabeele P. Initiation and execution mechanisms of necroptosis: an overview. Cell Death Differ 2017; 24:1184-95.
33. Feng S, Yang Y, Mei Y, Ma L, Zhu DE, Hoti N, et al. Cleavage of RIP3 inactivates its caspase-independent apoptosis pathway by removal of kinase domain. Cellular signalling 2007; 19:2056-67.
34. Lin Y, Devin A, Rodriguez Y, Liu ZG. Cleavage of the death domain kinase RIP by caspase-8 prompts TNF-induced apoptosis. Genes & development 1999; 13:2514-26.
35. Oberst A, Dillon CP, Weinlich R, McCormick LL, Fitzgerald P, Pop C, et al. Catalytic activity of the caspase-8-FLIP(L) complex inhibits RIPK3-dependent necrosis. Nature 2011; 471:363-7.
36. Cho YS, Challa S, Moquin D, Genga R, Ray TD, Guildford M, et al. Phosphorylation-driven assembly of the RIP1-RIP3 complex regulates programmed necrosis and virus-induced inflammation. Cell 2009; 137:1112-23.
37. He S, Wang L, Miao L, Wang T, Du F, Zhao L, et al. Receptor interacting protein kinase-3 determines cellular necrotic response to TNF-alpha. Cell 2009; 137:1100-11.
38. Vandenabeele P, Vanden Berghe T, Festjens N. Caspase inhibitors promote alternative cell death pathways. Sci STKE 2006; 2006:pe44.
39. Sun L, Wang H, Wang Z, He S, Chen S, Liao D, et al. Mixed lineage kinase domain-like protein mediates necrosis signaling downstream of RIP3 kinase. Cell 2012; 148:213-27.
40. Mandal P, Berger SB, Pillay S, Moriwaki K, Huang C, Guo H, et al. RIP3 induces apoptosis independent of pronecrotic kinase activity. Molecular cell 2014; 56:481-95.

41. Kimura S, Noda T, Yoshimori T. Dissection of the autophagosome maturation process by a novel reporter protein, tandem fluorescent-tagged LC3. Autophagy 2007; 3:452-60.
42. Klionsky DJ, Abdelmohsen K, Abe A, Abedin MJ, Abeliovich H, Acevedo Arozena A, et al. Guidelines for the use and interpretation of assays for monitoring autophagy (3rd edition). Autophagy 2016; 12:1-222.
43. Chauhan S, Mandell MA, Deretic V. IRGM governs the core autophagy machinery to conduct antimicrobial defense. Molecular cell 2015; 58:507-21.
44. Tian W, Li W, Chen Y, Yan Z, Huang X, Zhuang H, et al. Phosphorylation of ULK1 by AMPK regulates translocation of ULK1 to mitochondria and mitophagy. FEBS Lett 2015; 589:1847-54.
45. Hieke N, Loffler AS, Kaizuka T, Berleth N, Bohler P, Driessen S, et al. Expression of a ULK1/2 binding-deficient ATG13 variant can partially restore autophagic activity in ATG13-deficient cells. Autophagy 2015; 11:1471-83.
46. Hosokawa N, Hara T, Kaizuka T, Kishi C, Takamura A, Miura Y, et al. Nutrient-dependent mTORC1 association with the ULK1-Atg13-FIP200 complex required for autophagy. Mol Biol Cell 2009; 20:1981-91.
47. Wallot-Hieke N, Verma N, Schlutermann D, Berleth N, Deitersen J, Bohler P, et al. Systematic analysis of ATG13 domain requirements for autophagy induction. Autophagy 2018; 14:743-63.
48. Harris KG, Morosky SA, Drummond CG, Patel M, Kim C, Stolz DB, et al. RIP3 Regulates Autophagy and Promotes Coxsackievirus B3 Infection of Intestinal Epithelial Cells. Cell host & microbe 2015; 18:221-32.
49. Yonekawa T, Gamez G, Kim J, Tan AC, Thorburn J, Gump J, et al. RIP1 negatively regulates basal autophagic flux through TFEB to control sensitivity to apoptosis. EMBO reports 2015; 16:700-8.
50. Goodall ML, Fitzwalter BE, Zahedi S, Wu M, Rodriguez D, Mulcahy-Levy JM, et al. The Autophagy Machinery Controls Cell Death Switching between Apoptosis and Necroptosis. Developmental cell 2016; 37:337-49.
51. Rubinstein AD, Kimchi A. Life in the balance - a mechanistic view of the crosstalk between autophagy and apoptosis. J Cell Sci 2012; 125:5259-68.
52. Matsuzawa Y, Oshima S, Nibe Y, Kobayashi M, Maeyashiki C, Nemoto Y, et al. RIPK3 regulates p62-LC3 complex formation via the caspase-8-dependent cleavage of p62. Biochemical and biophysical research communications 2015; 456:298-304.
53. Le DT, Jung S, Quynh NTN, Sandag Z, Lee BS, Kim S, et al. Inhibitory role of AMPactivated protein kinase in necroptosis of HCT116 colon cancer cells with p53 null mutation under nutrient starvation. Int J Oncol 2019; 54:702-12.
54. Wang YS, Yu P, Wang Y, Zhang J, Hang W, Yin ZX, et al. AMP-activated protein kinase protects against necroptosis via regulation of Keap1-PGAM5 complex. Int J Cardiol 2018; 259:153-62.
55. Goodall ML, Cramer SD, Thorburn A. Autophagy RIPs into cell death. Cell Cycle 2016; 15:3014-5.
56. Diao J, Liu R, Rong Y, Zhao M, Zhang J, Lai Y, et al. ATG14 promotes membrane tethering and fusion of autophagosomes to endolysosomes. Nature 2015; 520:563-6.
57. Leist M, Single B, Castoldi AF, Kuhnle S, Nicotera P. Intracellular adenosine triphosphate (ATP) concentration: a switch in the decision between apoptosis and necrosis. The Journal of experimental medicine 1997; 185:1481-6.
58. Vandenabeele P, Galluzzi L, Vanden Berghe T, Kroemer G. Molecular mechanisms of necroptosis: an ordered cellular explosion. Nat Rev Mol Cell Biol 2010; 11:700-14.
59. Kaizuka T, Morishita H, Hama Y, Tsukamoto S, Matsui T, Toyota Y, et al. An Autophagic Flux Probe that Releases an Internal Control. Molecular cell 2016; 64:835-49.
60. Zhang DW, Shao J, Lin J, Zhang N, Lu BJ, Lin SC, et al. RIP3, an energy metabolism regulator that switches TNF-induced cell death from apoptosis to necrosis. Science 2009; 325:332-6.

61. Cheong H, Lindsten T, Wu J, Lu C, Thompson CB. Ammonia-induced autophagy is independent of ULK1/ULK2 kinases. Proceedings of the National Academy of Sciences of the United States of America 2011; 108:11121-6.
62. Laderoute KR, Amin K, Calaoagan JM, Knapp M, Le T, Orduna J, et al. 5'-AMP-activated protein kinase (AMPK) is induced by low-oxygen and glucose deprivation conditions found in solid-tumor microenvironments. Molecular and cellular biology 2006; 26:5336-47.

Figure 1

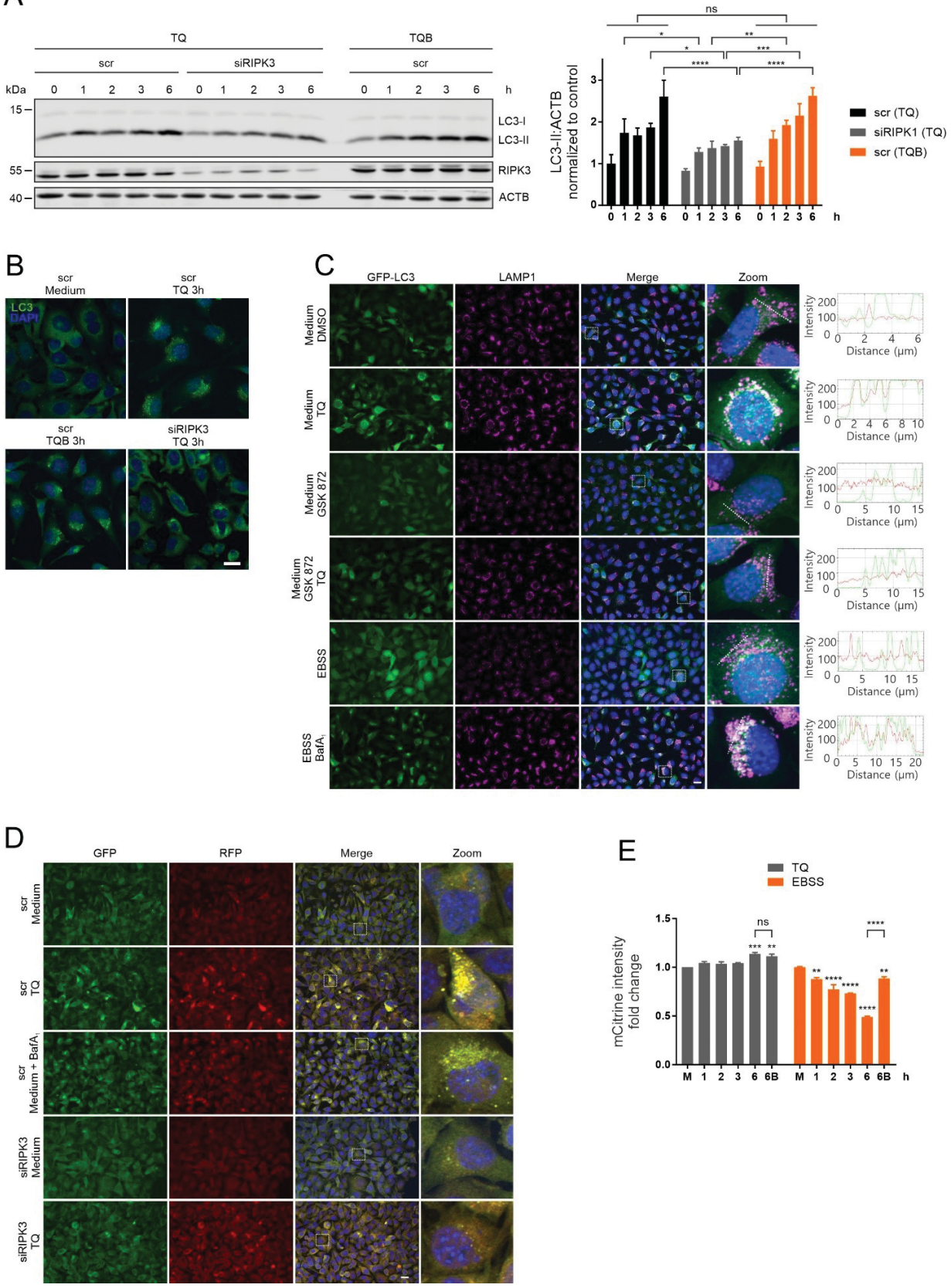
A
TQ
TQB
scr
siRIPK3
scr
kDa
0 1 2 3 6 0 1 2 3 6 0 1 2 3 6 h
15
55
40
LC3-I
LC3-II
RIPK3
ACTB
LC3-II:ACTB normalized to control
ns
*
**
***
****
scr (TQ)
siRIPK1 (TQ)
scr (TQB)
B
scr Medium
scr TQ 3h
scr TQB 3h
siRIPK3 TQ 3h
LC3
DAPI
C
GFP-LC3
LAMP1
Merge
Zoom
Medium DMSO
Medium TQ
Medium GSK 872
Medium GSK 872 TQ
EBSS
EBSS BafA1
Intensity
Distance (μm)
D
GFP
RFP
Merge
Zoom
scr Medium
scr TQ
scr Medium + BafA1
siRIPK3 Medium
siRIPK3 TQ
E
TQ
EBSS
mCitrine intensity fold change
M 1 2 3 6 6B M 1 2 3 6 6B h

Figure 2

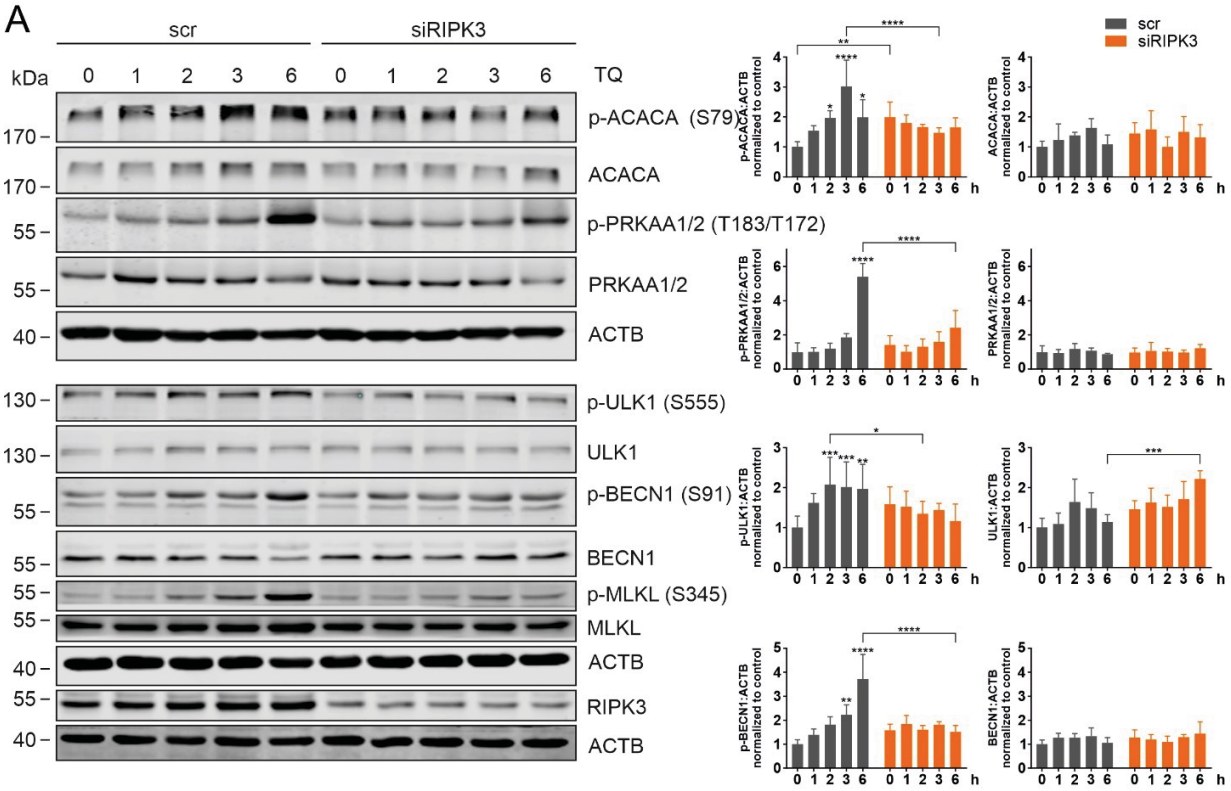
A
scr
siRIPK3
kDa
0 1 2 3 6 0 1 2 3 6
TQ
p-ACACA (S79)
ACACA
p-PRKAA1/2 (T183/T172)
PRKAA1/2
ACTB
p-ULK1 (S555)
ULK1
p-BECN1 (S91)
BECN1
p-MLKL (S345)
MLKL
ACTB
RIPK3
ACTB
170
55
40
130
p-ACACA:ACTB normalized to control
ACACA:ACTB normalized to control
p-PRKAA1/2:ACTB normalized to control
PRKAA1/2:ACTB normalized to control
p-ULK1:ACTB normalized to control
ULK1:ACTB normalized to control
p-BECN1:ACTB normalized to control
BECN1:ACTB normalized to control
0 1 2 3 6 h

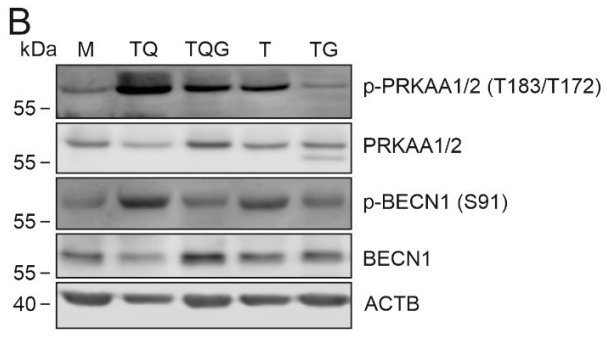
B
kDa
M
TQ
TQG
T
TG
p-PRKAA1/2 (T183/T172)
PRKAA1/2
p-BECN1 (S91)
BECN1
ACTB
55
40

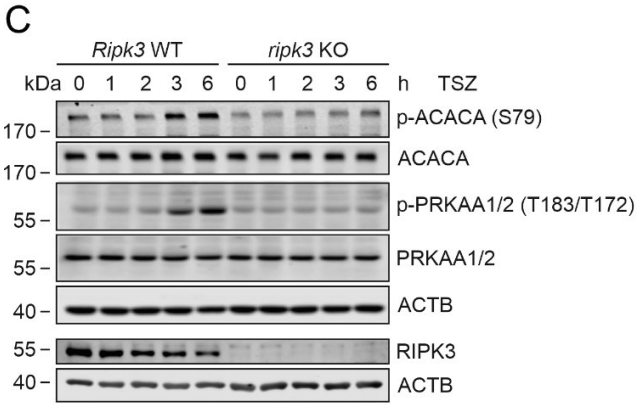
C
Ripk3 WT
ripk3 KO
kDa
0 1 2 3 6 0 1 2 3 6
h
TSZ
p-ACACA (S79)
ACACA
p-PRKAA1/2 (T183/T172)
PRKAA1/2
ACTB
RIPK3
ACTB
170
55
40

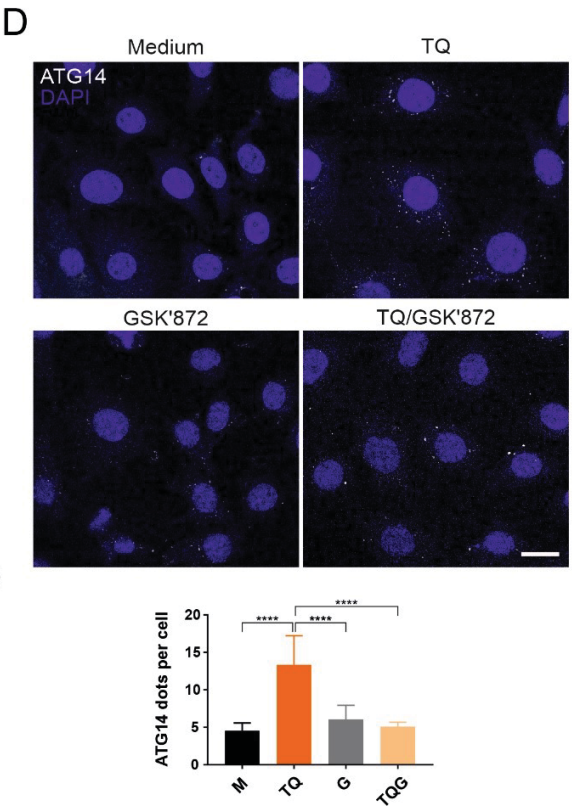
D
Medium
TQ
ATG14
DAPI
GSK'872
TQ/GSK'872
ATG14 dots per cell
M
TQ
G
TQG

Figure 3

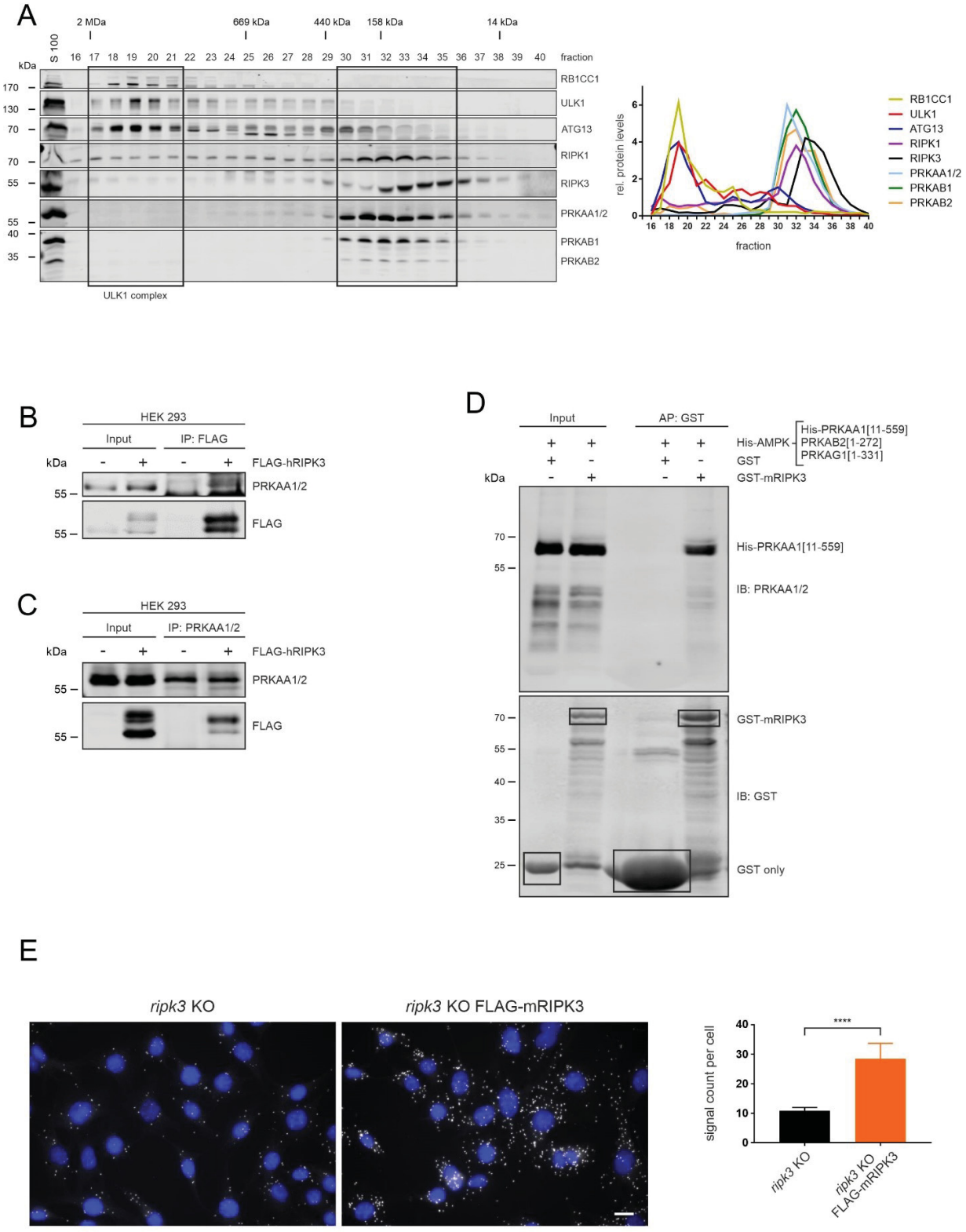
A
2 MDa
669 kDa
440 kDa
158 kDa
14 kDa
S 100
fraction
kDa
RB1CC1
ULK1
ATG13
RIPK1
RIPK3
PRKAA1/2
PRKAB1
PRKAB2
ULK1 complex
rel. protein levels
fraction
B
HEK 293
Input
IP: FLAG
FLAG-hRIPK3
PRKAA1/2
FLAG
C
HEK 293
Input
IP: PRKAA1/2
FLAG-hRIPK3
PRKAA1/2
FLAG
D
Input
AP: GST
His-AMPK
His-PRKAA1[11-559]
PRKAB2[1-272]
PRKAG1[1-331]
GST
GST-mRIPK3
His-PRKAA1[11-559]
IB: PRKAA1/2
GST-mRIPK3
IB: GST
GST only
E
ripk3 KO
ripk3 KO FLAG-mRIPK3
signal count per cell
****
ripk3 KO
ripk3 KO FLAG-mRIPK3

Figure 4

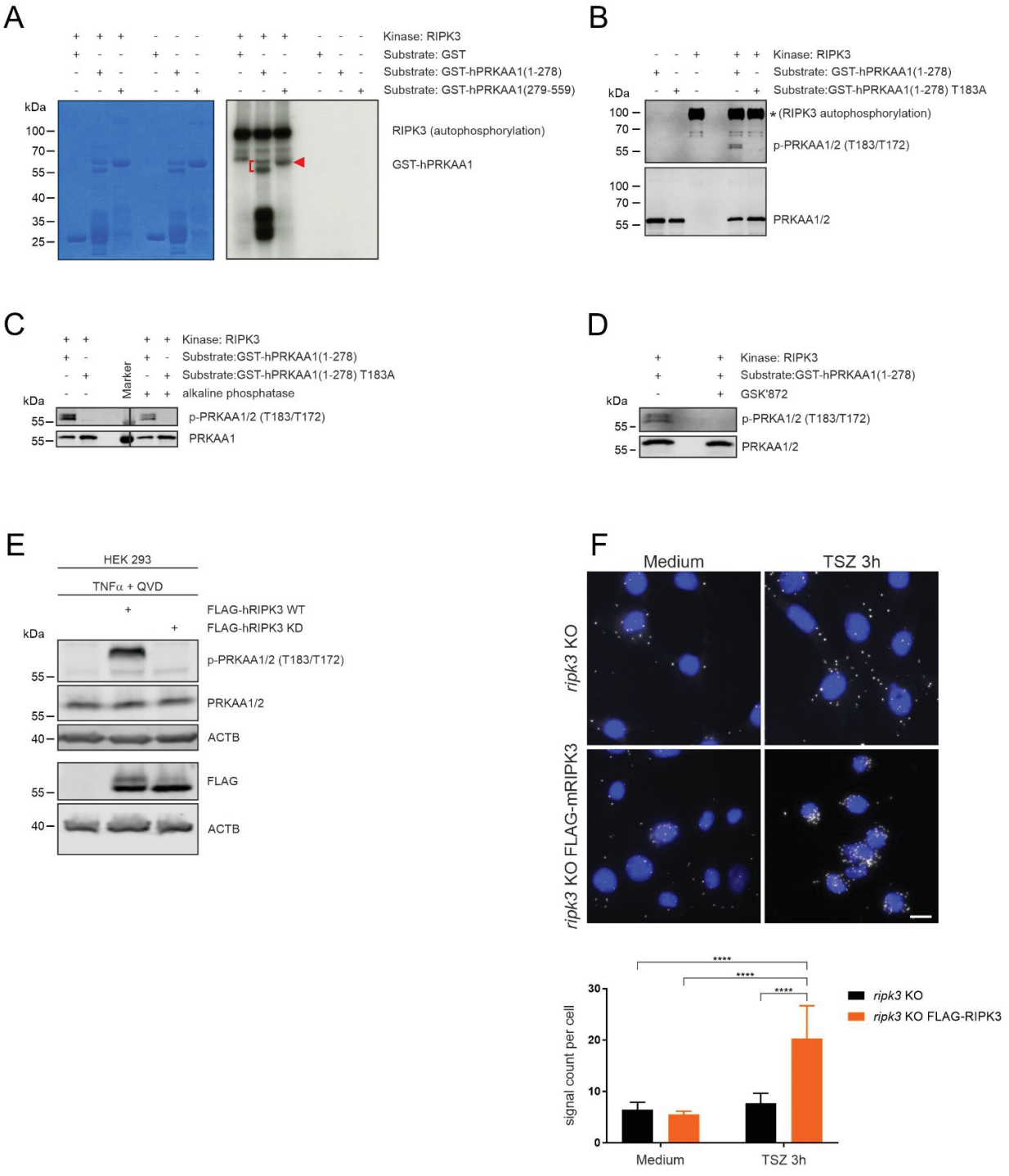
A
Kinase: RIPK3
Substrate: GST
Substrate: GST-hPRKAA1(1-278)
Substrate: GST-hPRKAA1(279-559)
kDa
100
70
55
40
35
25
RIPK3 (autophosphorylation)
GST-hPRKAA1
B
Kinase: RIPK3
Substrate: GST-hPRKAA1(1-278)
Substrate:GST-hPRKAA1(1-278) T183A
kDa
100
70
55
* (RIPK3 autophosphorylation)
p-PRKAA1/2 (T183/T172)
PRKAA1/2
C
Kinase: RIPK3
Substrate:GST-hPRKAA1(1-278)
Substrate:GST-hPRKAA1(1-278) T183A
alkaline phosphatase
Marker
kDa
55
p-PRKAA1/2 (T183/T172)
PRKAA1
D
Kinase: RIPK3
Substrate:GST-hPRKAA1(1-278)
GSK'872
kDa
55
p-PRKA1/2 (T183/T172)
PRKAA1/2
E
HEK 293
TNFα + QVD
FLAG-hRIPK3 WT
FLAG-hRIPK3 KD
kDa
55
p-PRKAA1/2 (T183/T172)
PRKAA1/2
40
ACTB
FLAG
ACTB
F
Medium
TSZ 3h
ripk3 KO
ripk3 KO FLAG-mRIPK3
****
****
****
30
20
10
0
signal count per cell
ripk3 KO
ripk3 KO FLAG-RIPK3
Medium
TSZ 3h

Supplementary Figures

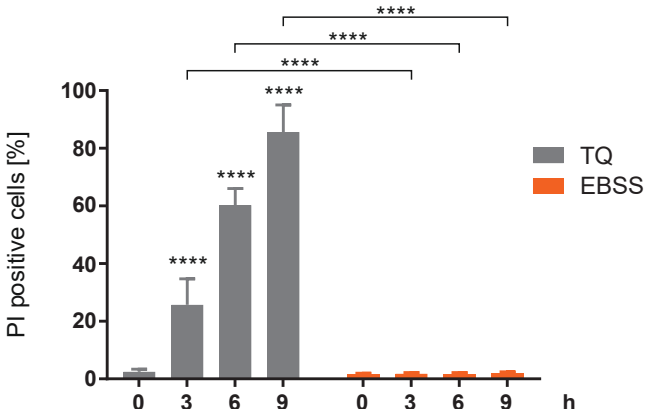

Figure S1.

TNFα/QVD treatment induces cell death in L929 cells. L929 cells were treated with 10 ng/ml TNFα and 30 µM QVD (TQ) for indicated times. Cells were collected and incubated with propidium iodide (PI) for 1 h at 4°C. Then the signal was measured by flow cytometry. Data represent mean + SD. Statistical analysis was performed using repeated measures two-way ANOVA (corrected by Sidak's multiple comparisons test), ****$P < 0.0001$. Statistically significant differences within TQ-treated cells (compared to 0 h TQ) are depicted directly above the bars.

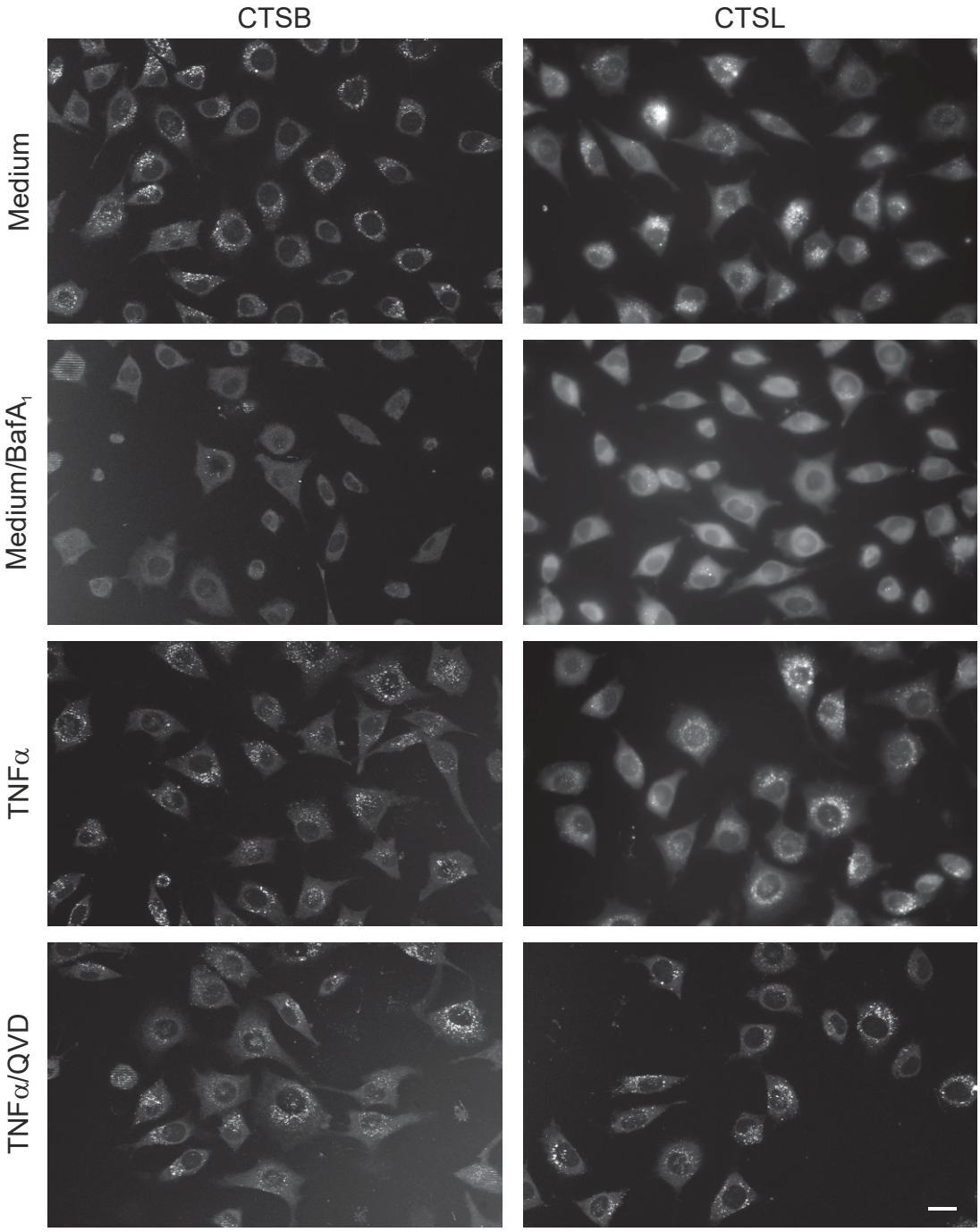

Figure S2.

Necroptosis induced by TNFα does not affect activities of CTSB and CTSL. L929 cells were seeded onto 8 well chambered coverglasses and cultured at 37°C overnight. Next day, cells were exposed to indicated treatments (10 ng/ml TNFα, 30 µM QVD, 20 nM bafilomycin A_1, [BafA1]) for 3 hours. Then, cells were cultured with the magic red bound substrates of CTSB or CTSL for 15 min at 37°C. After washing 5 times with medium preheated to 37°C, cells were analyzed by fluorescence microscopy. Scale bar: 20 µm.

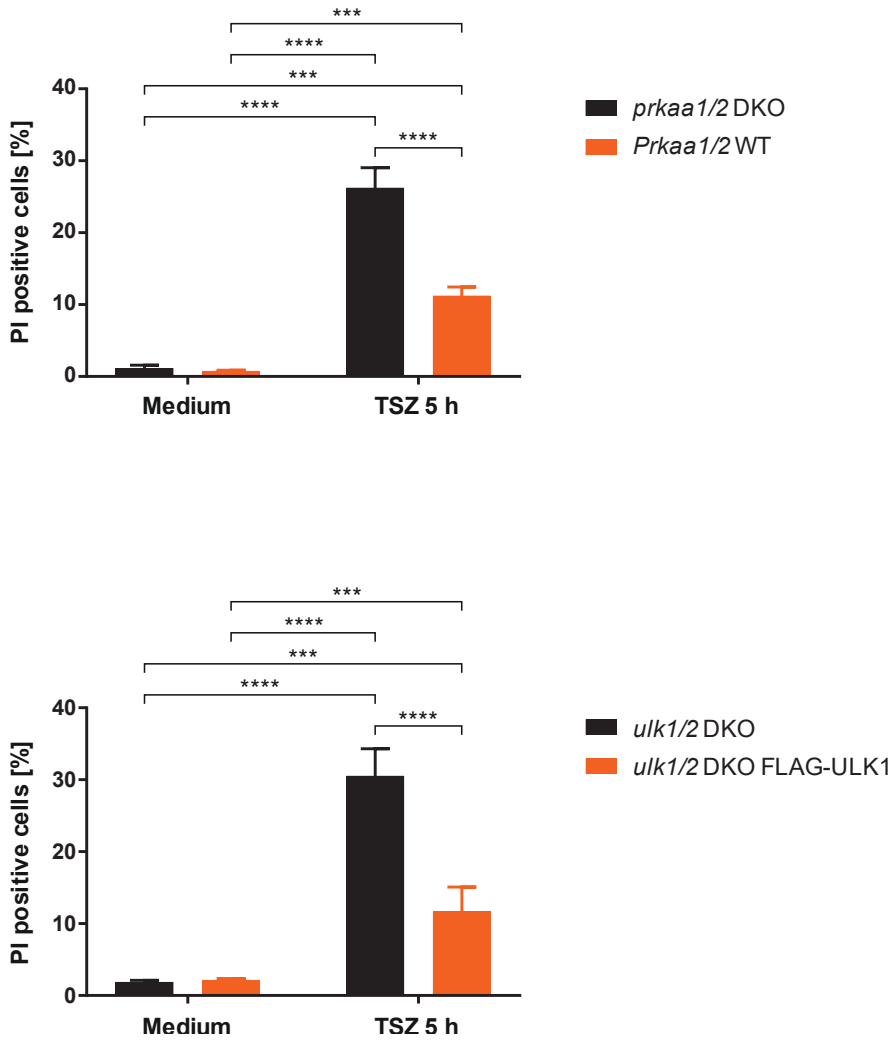

Figure S3.

TNFα-induced necroptosis is reduced in *prkaa1/2* DKO or *ulk1/2* DKO MEFs. (**A** and **B**) *Prkaa1/2* WT and *prkaa1/2* DKO MEFs (A), or *ulk1/2* DKO MEFs and *ulk1/2* DKO MEFs reconstituted with *Ulk1* cDNA (B) were treated with 30 ng/ml TNFα + 100 nM SMAC-mimetic + 20 µM z-VAD (TSZ) for 5 h. Cells were collected and incubated with propidium iodide (PI) for 1 h at 4°C. Then the signal was measured by flow cytometry. Data represent mean + SD from at least three independent experiments. Statistical analysis was performed using ordinary two-way ANOVA (corrected by Tukey's multiple comparisons test), ***$P < 0.001$, ****$P < 0.0001$.

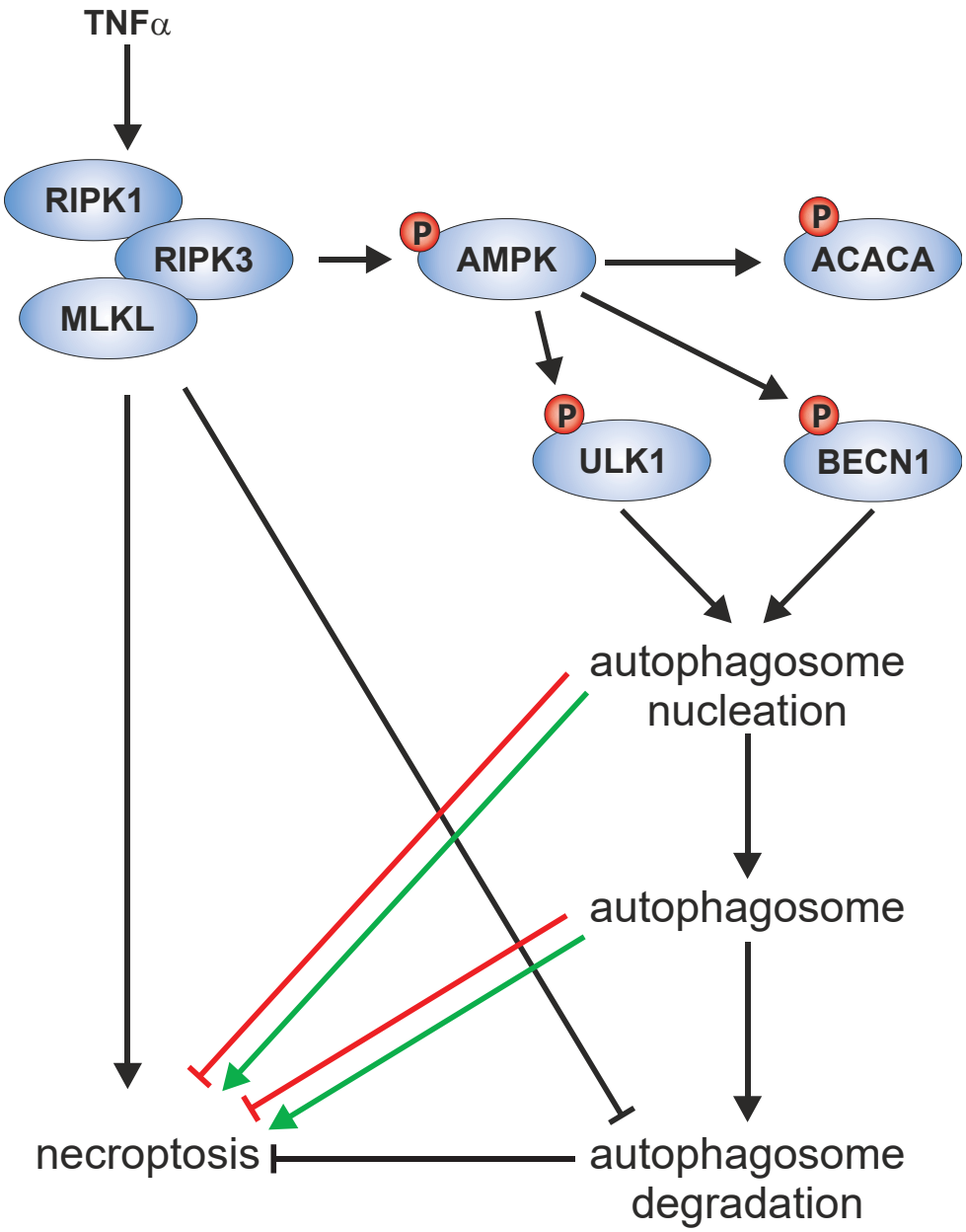

Figure S4.

TNFα-induced necroptosis both supports and inhibits autophagy. Upon TNFα treatment, the pro-necroptotic RIPK3 is activated. RIPK3 itself represents an AMPK-activating kinase. Activation of AMPK in turn induces the phosphorylation and activation of early autophagy mediators, such as ULK1 or BECN1. However, later steps of the autophagy pathway—such as the lysosomal degradation of autophagosomes—are blocked during TNFα-induced necroptosis. We speculate that the RIPK3-dependent phosphorylation of AMPK and the subsequent activation of early autophagy events represent either an anti-necroptotic and thus cyto-protective function of RIPK3 (indicated by red arrows), or 2) a pro-necroptotic function of early autophagy events (indicated by green arrows).